

DAWOOD, SHEEBA, Ph.D. Three-Dimensional Metal Organic Frameworks for Atomic Scale Patterning. (2020)
Directed by Dr. Hemali Rathnayake. 163 pp.

Metal organic frameworks (MOFs) belong to a sub class of coordination polymers in which metal ion nodes are connected with organic ligands to make three-dimensional framework. High porosity of MOFs makes them appealing in real-world applications, such as storage for harmful gasses, drug delivery cargo, and in recently for electronic devices. This dissertation focuses the development of a new synthetic design strategy that offers structural modifications to construct MOFs with tailored optoelectronic and magnetic properties. Combining a solvent driven self-assembly process with a solvothermal method, a series of highly crystalline hierarchical microstructures of isorecticular MOFs, having metal nodes of zinc, manganese, and iron were synthesized and their optoelectronic and magnetic properties were investigated. The synthesis method developed in this research enables tailoring the crystalline structure and its packing pattern, contributing to tailor their properties. The three isorecticular MOFs (IRMOFs) prepared using this novel synthesis method were interpenetrated IRMOF-8 (IRMOF-8A), MIL-88 and Mn-MOF. The structural composition, morphological characterization, and crystalline packing of these MOFs were confirmed. Using this novel synthetic strategy, the crystalline packing pattern and structural orientation of original IRMOF-8 were tailored, yielding its interpenetrating crystal structure with promising optoelectronic properties. Three isorecticular homologous of MIL-88 prepared in same manner by varying the organic linker length using benzene dicarboxylic acid (BDC), naphthalene dicarboxylic acid (NDC), and bi-phenyl dicarboxylic acid (BPDC) as organic linkers,

show magnetic behavior below room temperature. Finally, 3D microstructures of Mn-MOF prepared by coordinating Mn^{+2} with NDC exhibits luminescent behavior, attributing to the ligand emission. The hierarchical structures of isoreticular MOFs developed in this research will contribute to the potential applications in optoelectronic, memory storage, and light harvesting devices, respectively.

THREE-DIMENSIONAL METAL ORGANIC FRAMEWORKS
FOR ATOMIC SCALE PATTERNING

by

Sheeba Dawood

A Dissertation Submitted to
the Faculty of The Graduate School at
The University of North Carolina at Greensboro
in Partial Fulfillment
of the Requirements for the Degree
Doctor of Philosophy

Greensboro
2020

Approved by

Committee Chair

APPROVAL PAGE

This dissertation, written by SHEEBA DAWOOD, has been approved by the following committee of the Faculty of The Graduate School at The University of North Carolina at Greensboro.

Committee Chair _____
Hemali Rathnayake

Committee Members _____
James G. Ryan

Joseph Starobin

Shyam Aravamudhan

June 15, 2020
Date of Acceptance by Committee

June 15, 2020
Date of Final Oral Examination

ACKNOWLEDGMENTS

I would like to thank my advisor Dr. Hemali Rathnayake for the guidance that she has given me over past four years. Without her advice and constant encouragement, I would not come this far in my graduate life. I would also like to express my gratitude to all my committee members: Dr. Shyam, Dr. Joseph Starobin for their input and especially Dr. James Ryan for his dedication and offering precious time to evaluate my research work.

I would like to acknowledge the financial support for my doctoral studies provided by the Joint School of Nanoscience and Nano engineering (JSNN), collaboration between The University of North Carolina Greensboro and North Carolina A&T State University. I extend my sincere thanks to the staff at JSNN for their advice, training, and equipment troubleshooting, particularly Dr. Kristen Dellinger and Kyle Nowlin. I would also like to thank the following peers for both experimental and computational assistance: Klinton Davis and Ryan Yarborough.

I would like to express my gratitude and appreciation to Prof. Dhananjay Kumar and his group member, especially Surabhi Shaji, who collaborated with my work to study the magnetic properties of metal organic framework. I would like to thank Prof. Nathan Hammer and his group member, especially Austin Dorris, who collaborated with my work to study the excited lifetime measurements of metal organic framework. And finally, a huge thanks to god, my parents, and friends. Thank you for all the love and support Thank you for being by my side in my weaker moments and encouraging me.

TABLE OF CONTENTS

	Page
LIST OF TABLES	vii
LIST OF FIGURES	viii
CHAPTER	
I. INTRODUCTION	1
1.1 Metal Organic Frameworks	1
1.2 Metal Organic Frameworks in the Semiconductor Industry	2
1.2.1 Electrically Conductive Metal Organic Frameworks (EMOFs).....	4
1.2.2 Magnetic Metal Organic Frameworks (MMOFs).....	5
1.2.3 Luminescent Metal Organic Frameworks (LMOFs)	7
1.3 Current State of Art.....	8
1.4 General Goals of Research	9
1.5 Dissertation Layout	13
1.6 References	14
II. BACKGROUND	19
2.1 Metal Organic Framework	19
2.1.1 Coordination Polymer	20
2.1.2 Isorecticular Metal Organic Framework.....	22
2.1.3 Types of Isorecticular MOFs	25
2.2 Metal Organic Framework in Electronic Devices	27
2.2.1 Electrically Conductive MOFs	28
2.2.2 Magnetic MOFs	32
2.2.3 Luminescent Metal Organic Framework	38
2.3 References.....	47
III. APPROACH AND METHODS	63
3.1 Methodology	63
3.1.1 Proposed Synthesis Method for Targets IRMOFs	63
3.1.2 Research Aims	65
3.2 Characterization	74
3.2.1 Electrical Properties	74

3.2.2 Magnetic Properties	77
3.2.3 Optical Properties.....	80
3.2.4 Material Composition	81
3.2.5 Morphology and Crystalline Packing	82
3.3 References.....	83
IV. EXPERIMENTAL SECTION.....	91
4.1 Materials	91
4.2 Characterization	91
4.3 Synthesis Procedures	93
4.3.1 Synthesis Procedure for IRMOF-8A	93
4.3.2 Synthesis Procedure for MIL-88B	93
4.3.3 Synthesis Procedure for MIL-88C	94
4.3.4 Synthesis Procedure for MIL-126.....	95
4.3.5 Synthesis Procedure for Mn-MOFs (Mn-NDC)	96
V. RESULTS AND DISCUSSION	97
5.1 Designing and Synthesizing Self-assembled Hierarchical Microstructures of IRMOF-8 to Investigate Optoelectronic Properties of MOF	97
5.1.1 Introduction.....	97
5.1.2 Synthesis and Characterization of IRMOF-8.....	98
5.2 To Investigate the Effect of Different Carboxylate Linkers on Magnetic Properties in Fe-MOFs	110
5.2.1 Introduction.....	110
5.2.2 Synthesis and Characterization of MIL-88 Series	112
5.2.3 Material Characterization of MIL88 Analogues.....	114
5.2.4 Thermal Properties.....	117
5.2.5 Crystalline Structure and Packing.....	118
5.2.6 Morphological Studies of MIL-88 Analogues.....	122
5.2.7 Textural Properties of MIL-88 Analogues.....	124
5.2.8 Magnetic Properties	125
5.2.9 Magnetization vs. Temperature (M-T Curves)	126
5.2.10 Summary	129
5.3 Investigating Luminescence Properties of Mn-MOF	130
5.3.1 Introduction.....	130
5.3.2 Synthesis and Characterization	132
5.4 References.....	145

VI. CONCLUSIONS AND FUTURE DIRECTIONS.....	155
6.1 Conclusions.....	155
6.2 Recommendations for Future Research.....	160
6.2.1 The Electrical Conductivity of INT-IRMOF-8A.....	160
6.2.2 Magnetic Properties of MIL-88 Analogues (MIL-88B, MIL-88C and MIL-126).....	161
6.2.3 Optical Behavior of Mn-NDC.....	162
6.3 References.....	163

LIST OF TABLES

	Page
Table 2.1. The Pore Volume of the MOFs Reported in Literature (1999–2012) Reported from the Origin of MOF-5 (First MOF Reported) [18].....	27
Table 2.2. Significant Progress in the Last Few Years Concerning Electrically Conductive MOFs, Their Pathways Compared with Conventional Metals	30
Table 2.3. Significant Progress in the Last Few Years Concerning Magnetic MOFs and Their Pathways Compared with Conventional Metals	37
Table 2.4. Previously Reported IRMOF-8, MIL-88, and Mn-MOF.....	46
Table 4.1. XPS Data Obtained for IRMOF-8A (Zn-MOFs).....	93
Table 4.2. XPS Data Obtained for MIL-88B (Fe-BDC).....	94
Table 4.3. XPS Data Obtained for MIL-88C (Fe-NDC).....	95
Table 4.4. XPS Data Obtained for MIL-126 (Fe-BPDC)	95
Table 4.5. XPS Data Obtained for Mn-MOF (Mn-NDC).....	96
Table 5.1. Lattice Parameters of MIL-88B, MIL-88C, and MIL-126	122

LIST OF FIGURES

	Page
Figure 2.1. Scheme of a Typical MOF Structure by Connecting the Metal Nodes and Organic Linkers [4]	19
Figure 2.2. Schematic Illustration of 1-2 and Dimensional Coordination Polymer (Left) [9]; Graphical Representation of 1 st , 2 nd , and 3 rd Generation of Coordination Polymer [11]	21
Figure 2.3. Crystal Structures of IRMOFs-n Series [n=1-16]	24
Figure 2.4. Crystal Structure of ZIF-8, MIL-88, and HKUST-1 [18,24,25]	25
Figure 2.5. The Energy Bands of Metals, Semiconductors, and Insulators [38]	28
Figure 2.6. (a) Through-bond Strategy – {[Cu ₂ (6-Hmna) (6-mn)] · NH ₄ } _n [41]; (b) Through Space Strategy – Zn-TTF (Columnar π-Stacking) [42]; (c) Guest Molecule Strategy – NU-901-C ₆₀ ; Blue-C ₆₀ [43]	31
Figure 2.7. Schematic Illustrations of Ferromagnetic, Ferrimagnetic, Paramagnetic, and Diamagnetic [48 a]	32
Figure 2.8. (a) Short Linker; Crystal Structure of Cr ₃ [Cr(CN) ₆] ₂ ·6H ₂ O [35](b) Metallo-Ligand: Brick-Wall Rectangular Layer Architectures of the 2D MOFs from the Self-assembly of Di-copper (II) Metallo-cyclophane Anionic Complexes and Bis (Chelated) Mn(II) Ions- [54]; (c) Radicals: The X-ray Crystal Structure of [Fe ₂ L ₃] ₂ - Viewed Along Crystallographic C Axis [35,55]	35
Figure 2.9. (a) Crystal Structure of Compartmentalized Coordination Polymers of [Fe(btzx) ₃ (ClO ₄) ₂] and [Fe(btzx) ₃ (BF ₄) ₂] [35]; (b) 3D Packing in Planes [Mn[N(CN) ₂] ₆] ⁴⁺ [56]	36
Figure 2.10. Pictorial Representation of the Pathways for the Origin of Luminescence in MOFs [67]	39
Figure 2.11. (Left) The Schematic Representation of MOF-5, MIL-101 (Cr) and UiO-66 with Metal Ions Zn ⁺² , Zr ⁺⁴ , and Cr ⁺³ , Respectively; (Right) Table Shows the Absorption and Emission of the MOF-5, MIL-101, and UiO-66, Terephthalic Acid [69]	40

Figure 2.12. (Left): Pictorial Representation of Antenna Effect in Eu-MOF-L1; (Right): Table Showing the Absorption and Emission of Ligand L1 and Eu-MOF-L1 [70].	41
Figure 2.13. Schematic Representation of Donor-Acceptor Systems Between Coordination Polymer and PAH Guest Molecules [64].	43
Figure 2.14. Various Strategies for the Synthesis of Metal Organic Frameworks [73].	45
Figure 3.1. Reaction Scheme for Synthesis of Isoreticular MOFs	64
Figure 3.2. (a) Monodentate; (b) Bidentate and (C) Tridentate Coordination Modes Adopted by Carboxylate Groups of 2,6 NDC [7,8].	66
Figure 3.3. Structure of (a) IRMOF-8 and (b) Interpenetrated IRMOF-8 Analogue [11].	67
Figure 3.4. Depiction of Linker Replacement Strategy for Computational Prediction of Isoreticular MOF Structures – MIL-88 Family [19].	70
Figure 3.5. (a) Top View Showing 3D Framework Generating 1D Channels Running Along a Direction; (b) Side View Showing That Mn ^{II} 1D Chains are Linked With Each Other Via Naphthalene Rings of NDC.	73
Figure 3.6. Device Scheme for Electrical Measurements: (a) Cu to Cu; (b) Cu to ITO.	75
Figure 3.7. Graphical Representation of (a) Ohmic, (b) Semiconducting Curve [46 b].	76
Figure 3.8. Hysteresis Loop Showing Different Nature of Magnetism [50].	78
Figure 5.1. Synthetic Route of IRMOF-8A.	99
Figure 5.2. (a) FTIR Spectra of IRMOF-8A; (b) XPS of Zn 2P (IRMOF-8A).	100
Figure 5.3. TGA Graph of IRMOF-8A.	101
Figure 5.4. (a) The Powder XRD Spectrum of Microstructures and Simulated Powder XRD Spectra of Original IRMOF-8 and Interpenetrated IRMOF-8A; (b) the Crystal Structure Generated from the Originally Reported Crystal Structures of IRMOF-8; (c) the	

	Crystal Structure Generated from the Crystallography Data of INT-IRMOF 8A.....	102
Figure 5.5.	(a) A View of Two Identical Interpenetrated Network of IRMOF-8A Crystal Structure Units with Off-sets Layer-by-layer Packing Arrangement; (b) The SAED Pattern of Microstructure Taken from the TEM Under Dark Field Diffraction Mode; and (c) A TEM Image of Microstructures of IRMOF-8A	103
Figure 5.6.	SEM and TEM Images of IRMOF-8A	104
Figure 5.7.	SEM and TEM Images of IRMOF-8A in Different Solvents.....	105
Figure 5.8.	(a) UV-Vis Spectra of Microstructures in Solution (Ethanol) and Thin Films; (b) PL Emission Spectra of IRMOF-8A and the Ligand in Solution; (Excitation Wavelength is 292 nm)	107
Figure 5.9.	(a) I-V Curves of IRMOF-8A; (b) Device Fabricated with Casted Thin Film Microstructures	109
Figure 5.10.	Reaction Scheme for MIL-88B.....	113
Figure 5.11.	Reaction Scheme for MIL-88C.....	113
Figure 5.12.	Reaction Scheme for MIL-126	114
Figure 5.13.	(a) FTIR Spectra of MIL-88B; (b) FTIR Spectra of MIL-88C, and (c) FTIR Spectra of MIL-126	115
Figure 5.14.	(a) Fe2p (b) C1s (c) O1s of MIL-88B; (d) Fe 2p (e) C1s (f) O1s of MIL-88C and (g) (h) and (i) of MIL-126	117
Figure 5.15.	TGA of MIL-88B, MIL-88C, and MIL-126.....	118
Figure 5.16.	(a) XRD Spectrum of Fe-BDC MOFs and Simulated Powder XRD Spectra of Original MIL-88B; (b) the Crystal Structure Generated from the Originally Reported Crystal Structure of MIL-88B.....	119
Figure 5.17.	(a) XRD Spectra of Experimental and Simulated MIL-88C; (b) the Crystal Structure of MIL-88C Generated from the Originally Reported Crystal Structure of MIL-88C.....	120

Figure 5.18. (a) XRD Spectrum of Fe-BPDC MOFs and Simulated Powder XRD Spectra of Original MIL-126; (b) the Crystal Structure Generated from the Originally Reported Crystal Structure of MIL-126.....	121
Figure 5.19. SEM and TEM Images of MIL-88B, MIL-88C, and MIL-126.....	123
Figure 5.20. (a) N ₂ Isotherms of MIL-88B, MIL-88C, and MIL-126; (b) BJH Pore Size Distribution of MIL-88B, MIL-88C, and MIL-126.....	125
Figure 5.21. M-H Loops for Samples of MIL-88B, MIL-88C, and MIL-126 at 10 K and 300 K	126
Figure 5.22. Magnetization as a Function of Temperature for MIL-88B, MIL-88C, and MIL-126	127
Figure 5.23. M-H/T Loops for MIL-88B, MIL-88C, and MIL-126 at 10 K and 300 K.....	129
Figure 5.24. Reaction Scheme for the Synthesis of Mn-NDC MOFs.....	132
Figure 5.25. FTIR Spectra of Mn-NDC MOFs	133
Figure 5.26. The XPS Analysis of the Mn-NDC MOFs; (a) XPS Survey; (b) Mn 2p; (c) C1s; (d) O1s	134
Figure 5.27. TGA of Mn-NDC MOF.....	135
Figure 5.28. Left: Powder XRD Spectrum of Mn-NDC MOFs and Simulated Powder XRD Spectra of Original Mn-NDC MOFs; Right: The Crystal Structure Generated from the Originally Reported Crystal Structure	136
Figure 5.29. SEM and TEM Images of Mn-NDC MOFs.....	138
Figure 5.30. (a) N ₂ Isotherms for Mn-NDC MOFs at 77K; (b) BJH Pore Size Distribution of Plots of Mn-NDC MOFs	139
Figure 5.31. (a) UV-Vis Absorption Spectra of 2,6 NDC and Mn-NDC MOFs; (b) PL Spectra of 2,6 NDC and Mn-NDC MOFs.....	140
Figure 5.32. Transient Absorption Data for (a) 2,6 Naphthalene Dicarboxylic Acid; (b) Mn-NDC MOF	142

Figure 5.33. Simulated Crystalline Structure of Mn-NDC MOFs (CCDC-639914)
Showing Electron Densities at the Metal Node.....142

CHAPTER I

INTRODUCTION

1.1 Metal Organic Frameworks

Materials exhibiting electrical, optical, and magnetic properties are currently driving the technology age through revolutions in computing and communication industries[1]. Addressing the current ongoing industry demands, the quest for designing novel materials for specific applications has become a great challenge for current researchers. Hence in this direction, efforts have been undertaken to tailor properties via rational designing and understanding to incorporate superior functionalities. Over the past 50 years , crystalline microporous materials, from zeolites, coordination polymers and metal organic frameworks (MOFs) have gained enormous attention in the scientific community due to their structural versatility and significant features like porosity and surface area [2, 3]. “Metal organic frameworks (MOFs): A new class of crystalline porous materials belonging to a subclass of coordination polymer have evolved in last few years as a revolutionary material that are self-assembled nanostructures[4, 5] built from metal ions and organic ligand. The first MOF, MOF-5 or IRMOF-1 ($Zn_4O(BDC)_3$) reported by Omar M. Yaghi was used in gas adsorption applications accounting to its high surface area about $2900 \text{ m}^2\text{g}^{-1}$ [6, 7]. To date, 80,000 MOFs [8] have been reported owing to its diverse structure, compositions, tunable porosity, specific surface area [9] ease of functionalization, unsaturated metal sites [10] and biocompatibility [11]. As a

result, MOFs were used in a wide range of applications such as gas storage and separation, drug delivery and storage, chemical separation, sensing, catalysis, and bio-imaging[4, 8, 12-14]. In terms of structural orientation, the coordination bonding between a metal ion and organic ligand results in the formation of extended networks of one, two, and three dimensional framework with potential voids [7, 15]. The co-ordination bonding facilitated through a suitable molecular approach (reticular synthesis) provides the flexibility to alter the pore size and structurally transform the nature of the MOFs. Thus, utilizing the advantage of various combinations of metal-ligands and interaction of metal-ligands (reticular synthesis), MOFs could be an ideal candidate in the field of material science offering an attractive property of structural tunability, providing a pathway to introduce and tailor extrinsic characteristics such as optical, electrical, and magnetic properties.

1.2 Metal Organic Frameworks in the Semiconductor Industry

The design and development of new semiconducting materials have been a subject of interest in electronic devices. Recently, there has been a growing interest in studying MOFs as a new type of semiconducting material to meet the current demand in the electronic industry [16]. In particular, the electronic characteristics such as electrical, optical, and magnetic properties of MOFs have become an interesting topic of research attributing to their applications in microelectronic and optical devices. The implementation of MOFs in the electronic industry was first reported by Allendorf and co-workers [17]. MOF-5 with Zn_4O metal nodes and orthogonally interconnected six units of terephthalate is the most-studied MOF as a semiconductor. In 2007, Garcia and

co-workers reported on the semiconducting behavior of MOF-5 synthesized at room temperature, with a bandgap of 3.4 eV [18]. Since then, intense research has been carried out to develop MOFs with semiconducting properties opening new research domains for the scientific community in nanoscience.

The presence of narrow band gap structure either direct or indirect and charge mobility contribute to the semiconducting behavior of MOFs. To design MOFs with semiconducting behavior, significant amount of research is ongoing to identify the general structural requirements for enhancing the orbital overlapping between the building components. The main advantage of MOFs is the ability to tune the crystalline structure and functionality through phenomenal conceptual approaches such as rational designing and synthetic flexibility. In reticular chemistry which is also known as rational designing, the coordination bonding between metal node and organic ligand provides an understanding of atomic positions precisely contributing to determine the fundamental structure-property relationships. Thus, the crystalline structure of MOFs consists of self-assembled ordered nanostructure with defined organized spatial space that is constructed via coordination chemistry between the building components.

Moreover, the sub-angstrom knowledge of atomic positions helps to eliminate any disorder in the structure that contributes to poor mobility in the structure. Considering synthetic flexibility, the electronic properties of MOFs could be tailored resulting in potential applications such as a photovoltaic device tuned for solar cells, electroluminescent devices, field electron transistors, spintronic devices, and sensors.

This development has led many researchers to explore electrical, magnetic, and optical properties of MOFs [16, 19].

1.2.1 Electrically Conductive Metal Organic Frameworks (EMOFs)

The development of electrically conductive MOFs provides direction for the new technologies such as sensors, FETs, energy storage materials, photovoltaics, and thermoelectric[20]. But, the electrical properties of MOFs and integration of them in micro-electronic devices is still at an early stage and remain under research when compared to other types of existing conducting materials[16] [5]. Although MOFs possess the advantageous properties of functioning both as organic and inorganic materials they behave as electrical insulators or poor electrical conductors due to two reasons: 1) Insulating character of organic ligands, and 2) poor overlapping between the π -orbitals and d-orbitals between metal ions and organic ligands[21].

Yet, MOFs serving as an interface between (inorganic) hard and (organic) soft materials provide an opportunity for adapting various structure -property relationships that is related to wide range of parameters such as choice of metal ion, organic linker, and molecular designing approach. In general, the structure-property relationship in MOFs is a consequence of cooperative mechanism i.e. the interaction between the metal and ligand, which could be readily identified by taking advantage of the knowledge of their detailed atomic structure, enabling fine tuning of their functionalities[8, 12]. According to the literature, Bastian Hoppe and his co-workers reported Cu-2, 3, 6, 7, 10, 11-hexahydroxytriphenylene ($\text{Cu}_3\text{hhtp}_2\text{-MOF}$), a copper-based graphene-like framework with inherent electrical conductivity about 0.045 S cm^{-1} [28]. MOFs with electrical

conductivity higher than 0.1 S cm^{-1} was achieved by Talin and co-workers[22]. Thus, the designing of MOFs with conducting or semiconducting properties is necessary to enhance the sensitivity of electrical or demonstrate a sensing concept; but rarely have MOFs been an integral part of actual device [23].

1.2.2 Magnetic Metal Organic Frameworks (MMOFs)

Considering the right approach of molecular designing, MOFs with magnetic order is attainable and is gaining significant interest among researches in the field of magnetism[8, 24]. Magnetic metal organic frameworks (MMOFs) belongs to the class of molecular magnets as the molecular approach in both fields belong to coordination chemistry in which metals are bound through coordination bonding to organic ligands [24, 25]. Despite demonstrating similar synthetic programmability and tunability, MOFs could offer superior potential characteristics such as high operating temperature and fascinating multifunctionalities when compared to molecular-based magnets that are suffering to design high temperature magnets for the last 30 years[26, 27]. The property of magnetism in MOFs can be implemented through three approaches.

- **Intrinsic approach:** The magnetic exchange between the metal nodes and organic linker. This is often achievable in MOFs due to selection of paramagnetic metals, and open shell organic linker. The paramagnetic metal may exist in different oxidation states and organic linker could facilitate the exchange between moment carriers at a distance to render cooperativity phenomenon.

- Extrinsic approach: The magnetic properties can be implemented through incorporation of magnetic guest molecule while the framework is non-magnetic.
- Synergistic approach: Combining above two approaches into one system[26].

Compared to molecular-based magnets, MOFs are found to be an ideal candidate as they offer superior functionalities such as:

1. High temperature magnets: The structure of lattice consists of ordered nanostructures of magnetic entities that could enhance the cooperativity exchange (strong bonding) enabling MOFs to operate at higher temperature
2. Multifunctional properties: The structure of MOFs could show multifunctionalities in which magnetism could co-exist with some of the functional properties such as conductivity, porosity, luminescence, and superconductivity thus broadening the applications in magnetic gas separations, sensing and electronic devices

However, with wide range of molecular approaches, MOFs exhibiting high ordering temperature or incorporation of more than one inimical property (porosity and magnetism) are some of the current challenges in the field of MMOFs. These alarming challenges represent weak magnetic exchange coupling facilitated through linkers which depends on the choice of molecular approaches and building components. Designing and altering the existing molecular approaches with interaction of building components, the addition of porosity to the existing magnetic MOF provides an exciting platform for sensing applications. And the ability to transform structural organization by creating

periodic nanostructures of magnetic centers by keeping them well separated in the space, magnetic MOFs are quickly evolving with potential interest in quantum technologies [26]. Thus, comparing to other functionalities the incorporation of magnetic functionality into a MOF is quite recent and the field must move on to modulating molecular approaches to incorporate multi-functionalities and processing their applications in sensors, electronic devices, magnetic refrigerators and quantum computing [9].

1.2.3 Luminescent Metal Organic Frameworks (LMOFs)

As the research into the electrical and magnetic properties of metal organic frameworks is being intensified, the research on photophysical properties of MOFs have stimulated considerable interest since decades due to wide range of emissive pathways that is facilitated through hybrid nature of the material [28, 29]. The first luminescent MOFs was identified in 2002 [30], since then nearly 1300 different luminescent MOFs have been reported [24, 28, 30] with great potential for use across a broad range of applications such as solid- state lighting, Luminescence-based sensors, and organic emitting diodes[30].

When compared to conventional complexes, the luminescent MOFs provide the flexibility to tune their properties by rational selection of metal ions and organic ligands with judicious combination of molecular approach[30]. The components and pathways that are responsible for luminescent behavior in MOF are based on the following components and mechanisms (1) Ligand- based emission (2) Metal based emission (3) Charge transfer i.e. ligand to metal charge transfer (LMCT) or metal to ligand charge transfer (MLCT) and 4) through incorporation of guest molecule [28, 30]. According to

previous reports, ligand-based emission is mostly noticed in transition-based MOFs unlike MOFs that are developed from lanthanide metals in which metal-based emission is observed due to antenna effect. The charge transfer mechanism that is consequence of cooperative mechanism between ligand and metal depends upon the synergistic approach of efficient molecular designing with suitable choice of metal and ligand combination [31]. Thus, owing to its excellent structural tunability and optical behavior, luminescent MOFs have been implemented extensively in chemical sensing, explosive detection, metal removal, light harvesting sensitizers and light emitting applications [32].

Currently, in OLED industry, the materials that show enhanced fluorescence lifetimes and high quantum efficiencies have gained significant interest in electronic industry that could have an ability to resolve low efficiency issues. The hybrid nature of MOFs, in which the organic linker is rigidified in the structure constructed via self-assembly could be an ideal candidate due to its well-organized spatial arrangements of luminophores. Thus, a molecular approach that enhances the rigidification of organic emissive linker in the MOF structure is required that maintains their geometrical elegance with additional physical functionalities.

1.3 Current State of Art

Currently, wide range of designing strategies have been approached and utilized that enable spontaneous self-assembly of metal and ligand interaction to build MOF lattices [8]. In most of the cases, the self-assembly process between metal ion and organic ligand is either driven by high temperature and pressure i.e. Solvothermal synthesis, choice of solvent i.e. room temperature or through alternative power sources such as

microwave, electrochemical, ultrasonic and mechanochemical, etc. The optimization of interaction between metal and ligand in existing traditional self-assembly strategies enables the structural transformation that provides potential opportunities to incorporate new functionalities and further understand the relationship between structure and properties of obtained MOFs. Modifying synthetic chemistry with proper choice of metal-ligand combinations, electronic characteristics like electrical conductivity magnetic and optical character in MOFs can be introduced [4]. Thus, the goal of this project is to achieve fine control on the structure of MOFs to obtain target physical properties. Herein, we present how the combination of solvent driven self-assembly and solvothermal heating is suitable and highly useful synthetic method to obtain MOFs with semiconducting, magnetic, and optical properties.

1.4 General Goals of Research

Overall dissertation objective:

Designing and developing a new synthetic strategy that enhances the coordination of building components efficiently offering the ability to alter the structural-properties relationship contributing electronic properties (electrical, optical, and magnetic).

Overall dissertation hypothesis:

“A self-assembly driven synthesis process that yields hierarchical structures of isorecticular MOFs may provide the path to tailor optoelectronic, magnetic, and luminescence properties of MOFs.”

Rationale:

In literature, few isorecticular MOFs synthesized using traditional synthetic strategies were reported to exhibit insulating and non-magnetic behavior.

Solvothermal method is used most often to synthesize MOFs. These reactions are carried out in closed vessels under high pressure and heated above the boiling point of the solvent. The most used solvents are dimethyl formamide, acetonitrile, acetone, ethanol, and methanol [10]. However, this synthetic route also has some of the disadvantages such as it requires special equipment like autoclaves to maintain high pressure and temperature, usage of large amounts of solvents and time duration, which takes about 72 hours. As the result, most of the MOFs synthesized using this technique showed high porosity and high surface area, with its potential applications in gas absorption and storage. Thus, many synthetic strategies by tailoring the functionality of organic ligand or changing the metal node were explored to design isorecticular MOFs with semiconducting, luminescence and magnetic properties. However, such systems lack structural rigidity and due to its weak structural interaction between the metal ions and organic ligand in traditional synthetic routes the properties such as electrical, optical, and magnetic were less explored and reported. Thus, there is a need of alternative synthetic method, which is rapid and can induce semiconducting, magnetic and luminescent without the use of any harsh environments [4, 8, 13, 14].

Addressing the overall hypothesis, this research proposes three specific aims:

Aim 1 - Designing and synthesizing Self-assembled Hierarchical Microstructures of IRMOF-8 to investigate optoelectronic properties of MOF.

Hypothesis- A solvent-driven self-assembly approach followed by the solvothermal process may provide a path to tailor optoelectronic properties of IRMOFs.

Rationale: Previously reported IRMOF-8 synthesized by traditional methods like solvothermal method are electrically insulating. Thus, there is a need for an alternative synthetic method, which is rapid and can induce conductivity without the use of any harsh environments.

Expected outcome:

Aim 1 will result in: (1) A novel self-assembly driven synthesis approach to make hierarchical structures of isorecticular MOFs in large scale, (2) Hierarchical nanostructures of IRMOF-8 with tailored optoelectronic properties.

Aim 2 -To Investigate the effect of different carboxylate linkers on magnetic properties in Fe-MOFs.

Hypothesis: The Fe-MOFs developed with different organic linkers may provide a way to tailor magnetic properties of iron-based isorecticular MOFs.

Rationale: MIL-88 (Fe-MOF) synthesized by traditional methods like solvothermal method are reported non- magnetic. Fe-MOFs using different linkers were mostly explored in drug delivery and gas adsorption studies due to its porosity; but very rarely have their magnetic properties were reported. Thus, the

investigation of magnetic properties of Fe-MOFs (MIL-88) is reasonable due to their paramagnetic nature of metal centers.

Expected outcome

Aim 2 will result in: (1) Isoreticular MOFs of MIL-88 series with tailored magnetic properties and porosity approach with substitution of the linker using three different linkers in the structure of MIL-88. (2) Tailoring magnetic properties with the topology of the linker.

Aim 3 – Investigating luminescence properties of Mn-MOF

Hypothesis: Manganese metal with wide variety of oxidation states may provide a pathway to tailor luminescence behavior of manganese-based metal organic framework.

Rationale: The photophysical properties of Mn-MOF developed with 2,6 Naphthalene dicarboxylic acid is less explored. Mostly, the MOFs designed using 2,6 Naphthalene dicarboxylic acid is used for gas adsorption studies. Thus, MOFs with manganese possessing interesting electronic characteristics have rarely been implemented in studying luminescence properties.

Expected outcome:

Aim 3 will result in: (1) Mn-MOFs with tailored optical properties using Mn^{+2} metal precursor in the structure of Mn-MOFs. (2) Mn-MOFs with tailored luminescent and excited lifetime behavior.

1.5 Dissertation Layout

This dissertation has been organized under six chapters. Chapter I begins with an introduction on metal organic frameworks and advances in electronic industry. It also provides the brief background on electrical, magnetic, and optical properties of MOFs as well as emphasis on the goals of the research. In Chapter II, the first section presents a comprehensive theoretical background on the MOFs and reticular chemistry. The second section presents a thorough literature review on metal organic frameworks with electronic characteristics such as electrical, magnetic, and optical properties elucidating their performances. Chapter III presents the approach method for designing MOFs and material selections of specific MOFs for specific applications. The working principle and approach of four-probe I-V system, Vibrating sample magnetometer (VSM) and Transient absorption spectra with UV-Vis and PL spectra used for investigating electrical, magnetic, and optical properties are discussed. Sample preparation and deposition parameters are also explained. This is followed by descriptions of all the characterization techniques used in this research. In Chapter IV, experimental sections of all the materials is discussed. In Chapter V, results, and discussion of all the experimental techniques used in the research work is discussed. Finally, in Chapter VI the conclusion of this research work is discussed with additional potential future experiments and recommendations.

1.6 References

- [1] P. K. JHA, PRATAP, A. AND JANI, A. R, *Condensed matter and materials physics*. 1999.
- [2] E. S. a. F. Zafar, “Metal Organic Frameworks (MOFs).”
- [3] T. Ogawa, K. Iyoki, T. Fukushima, and Y. Kajikawa, “Landscape of Research Areas for Zeolites and Metal-Organic Frameworks Using Computational Classification Based on Citation Networks,” (in eng), *Materials (Basel)*, vol. 10, no. 12, Dec 14 2017.
- [4] H. Furukawa, K. E. Cordova, M. O’Keeffe, and O. M. Yaghi, “The Chemistry and Applications of Metal-Organic Frameworks,” *Science*, vol. 341, no. 6149, p. 1230444, 2013.
- [5] S. Eslava *et al.*, “Metal-Organic Framework ZIF-8 Films As Low- κ Dielectrics in Microelectronics,” *Chemistry of Materials*, vol. 25, no. 1, pp. 27-33, 2013/01/08 2013.
- [6] M. H. Yap, K. L. Fow, and G. Z. Chen, “Synthesis and applications of MOF-derived porous nanostructures,” *Green Energy & Environment*, vol. 2, no. 3, pp. 218-245, 2017/07/01/ 2017.
- [7] N. Zabukovec Logar and V. Kaučič, “Nanoporous Materials: From Catalysis and Hydrogen Storage to Wastewater Treatment,” *Acta Chim. Slov*, vol. 53, pp. 117-135, 01/01 2006.

- [8] G. Mínguez Espallargas and E. Coronado, “Magnetic functionalities in MOFs: from the framework to the pore,” *Chemical Society Reviews*, 10.1039/C7CS00653E vol. 47, no. 2, pp. 533-557, 2018.
- [9] K. Vikrant, V. Kumar, K.-H. Kim, and D. Kukkar, “Metal–organic frameworks (MOFs): potential and challenges for capture and abatement of ammonia,” *Journal of Materials Chemistry A*, 10.1039/C7TA07847A vol. 5, no. 44, pp. 22877-22896, 2017.
- [10] M. Ma, L. Liangyu, H. Li, Y. Xiong, and F. Dong, “Functional Metal Organic Framework/SiO₂ Nanocomposites: From Versatile Synthesis to Advanced Applications,” *Polymers*, vol. 11, p. 1823, 11/06 2019.
- [11] Y. Liu, Y. Zhao, and X. Chen, “Bioengineering of Metal-organic Frameworks for Nanomedicine,” *Theranostics*, Review vol. 9, no. 11, pp. 3122-3133, 2019.
- [12] J. Rowsell and O. Yaghi, “Metal-organic frameworks: A new class of porous materials,” *Microporous and Mesoporous Materials*, vol. 73, pp. 3-14, 08/01 2004.
- [13] M. Kotzabasaki and G. E. Froudakis, “Review of computer simulations on anti-cancer drug delivery in MOFs,” *Inorganic Chemistry Frontiers*, 10.1039/C7QI00645D vol. 5, no. 6, pp. 1255-1272, 2018.
- [14] J. L. C. Rowsell, E. C. Spencer, J. Eckert, J. A. K. Howard, and O. M. Yaghi, “Gas Adsorption Sites in a Large-Pore Metal-Organic Framework,” *Science*, vol. 309, no. 5739, pp. 1350-1354, 2005.
- [15] J. Yang, C. A. Trickett, S. B. Alahmadi, A. S. Alshammari, and O. M. Yaghi, “Calcium L-Lactate Frameworks as Naturally Degradable Carriers for Pesticides,”

- Journal of the American Chemical Society*, vol. 139, no. 24, pp. 8118-8121, 2017/06/21 2017.
- [16] C. G. Silva, A. Corma, and H. García, “Metal–organic frameworks as semiconductors,” *Journal of Materials Chemistry*, 10.1039/B924937K vol. 20, no. 16, pp. 3141-3156, 2010.
- [17] I. Stassen, N. Burch, A. Talin, P. Falcaro, M. Allendorf, and R. Ameloot, “An updated roadmap for the integration of metal–organic frameworks with electronic devices and chemical sensors,” *Chemical Society Reviews*, 10.1039/C7CS00122C vol. 46, no. 11, pp. 3185-3241, 2017.
- [18] M. Usman, S. Mendiratta, and K.-L. Lu, “Semiconductor Metal–Organic Frameworks: Future Low-Bandgap Materials,” *Advanced Materials*, vol. 29, no. 6, p. 1605071, 2017.
- [19] V. Stavila, A. A. Talin, and M. D. Allendorf, “MOF-based electronic and optoelectronic devices,” *Chemical Society Reviews*, 10.1039/C4CS00096J vol. 43, no. 16, pp. 5994-6010, 2014.
- [20] Z. Guo *et al.*, “Lowering Band Gap of an Electroactive Metal–Organic Framework via Complementary Guest Intercalation,” *ACS Applied Materials & Interfaces*, vol. 9, no. 38, pp. 32413-32417, 2017/09/27 2017.
- [21] X. Deng, J. Y. Hu, J. Luo, W. M. Liao, and J. He, “Conductive Metal-Organic Frameworks: Mechanisms, Design Strategies and Recent Advances,” (in eng), *Topics in current chemistry (Cham)*, vol. 378, no. 2, p. 27, Feb 24 2020.

- [22] C. Yang *et al.*, “A semiconducting layered metal-organic framework magnet,” *Nature Communications*, vol. 10, no. 1, p. 3260, 2019/07/22 2019.
- [23] S. Dawood, R. Yarbrough, K. Davis, and H. Rathnayake, “Self-assembly and optoelectronic properties of isorecticular MOF nanocrystals,” *Synthetic Metals*, vol. 252, pp. 107-112, 2019/06/01/ 2019.
- [24] X.-L. Tong, H.-L. Lin, J.-H. Xin, F. Liu, M. Li, and X.-P. Zhu, “Recent Advances as Materials of Functional Metal-Organic Frameworks,” *Journal of Nanomaterials*, vol. 2013, p. 616501, 2013/05/07 2013.
- [25] M. Kurmoo, “Magnetic metal–organic frameworks,” *Chemical Society Reviews*, 10.1039/B804757J vol. 38, no. 5, pp. 1353-1379, 2009.
- [26] E. Coronado, “Molecular magnetism: from chemical design to spin control in molecules, materials and devices,” *Nature Reviews Materials*, vol. 5, no. 2, pp. 87-104, 2020/02/01 2020.
- [27] A. E. Thorarinsdottir and T. D. Harris, “Metal–Organic Framework Magnets,” *Chemical Reviews*, 2020/02/11 2020.
- [28] M. D. Allendorf, C. A. Bauer, R. K. Bhakta, and R. J. T. Houk, “Luminescent metal–organic frameworks,” *Chemical Society Reviews*, 10.1039/B802352M vol. 38, no. 5, pp. 1330-1352, 2009.
- [29] M. Pamei and A. Puzari, “Luminescent transition metal–organic frameworks: An emerging sensor for detecting biologically essential metal ions,” *Nano-Structures & Nano-Objects*, vol. 19, p. 100364, 2019/07/01/ 2019.

- [30] R. Li *et al.*, “An Azole-Based Metal–Organic Framework toward Direct White-Light Emissions by the Synergism of Ligand-Centered Charge Transfer and Interligand π – π Interactions,” *Crystal Growth & Design*, vol. 16, no. 7, pp. 3969–3975, 2016/07/06 2016.
- [31] H. Kaur *et al.*, “Luminescent metal-organic frameworks and their composites: Potential future materials for organic light emitting displays,” *Coordination Chemistry Reviews*, vol. 401, p. 213077, 2019/12/15/ 2019.
- [32] H.-Q. Yin and X.-B. Yin, “Metal–Organic Frameworks with Multiple Luminescence Emissions: Designs and Applications,” *Accounts of Chemical Research*, vol. 53, no. 2, pp. 485–495, 2020/02/18 2020.

CHAPTER II

BACKGROUND

2.1 Metal Organic Framework

Metal organic frameworks (MOFs) are organic and inorganic hybrid systems that are self-assembled from the organic ligand and inorganic metal building blocks as shown in Figure 2.1. These frameworks belong to a subclass of co-ordination network, which is a subset of co-ordination polymer[1]. According to IUPAC, a MOF is a coordination network with organic ligands containing potential voids [2]. In literature, MOFs are referred using several terminologies like metal organic material (MOM), coordination polymer (CP), coordination network (CN), porous coordination polymer (PCP), porous coordination network (PCN), microporous coordination polymer (MCP), and metal organic coordination network (MOCN)[3, 4].

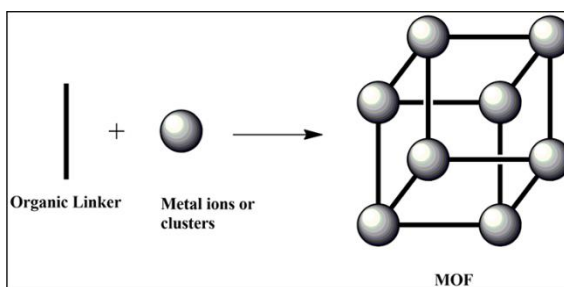


Figure 2.1. Scheme of a Typical MOF Structure by Connecting the Metal Nodes and Organic Linkers [4].

Comparing with the common porous materials such as zeolites and activated carbons, MOFs have emerged as an extensive class of crystalline porous materials owing

to their superior characteristic features such as ultrahigh porosity (up to 90% pore volume [5], high surface area (extending beyond 7000 m²/g)[5] and low density (0.13 g/cm³)[6]. With the variability of organic and inorganic components and their interaction, the freedom of modulating the structure of MOFs into highly ordered hierarchical structures with tunable pore volume and adjustable surface area has become feasible that made MOFs stand out compared to the other porous materials. Taking advantage of one of these hallmarks of MOFs i.e. designing of topologically diverse structures with desirable properties has been explored extensively attracting wide range of applications in gas storage, separation, catalysis, sensing and drug delivery[6]. Thus, since 1990s, this area of chemistry has experienced tremendous growth in the field of material science and modern chemistry [5].

2.1.1 Coordination Polymer

In the vast field of coordination polymer, the Prussian blue compound discovered in the 18th century was considered as one of the first members of this family. Later in the early 1990s, the field of coordination polymer began to grow due to significant contribution by Robson and co-workers [7, 8]. They reported a new porous material that could be engineered as catalyst describing its crystal structures. This led to a significant amount of interest in this field and at last, the coordination polymers (CPs) have emerged as an organic-inorganic hybrid material referring to molecular self-assembly systems. In this system, organic ligands (mono, bi or tri-functional) are coordinately bonded to metal ions or metal clusters forming a coordination network. The energy of such bonding is usually between 50 and 200 KJ mol⁻¹. Apart from strong coordination bonding, weaker

interaction such as hydrogen bonds, van der Waal forces and π - π interactions also influence the formation of coordination polymer. Further, the coordination geometry of metal ions and the functionality of organic ligands classify coordination polymer in different dimensional structures such as one dimensional, two dimensional and three-dimensional crystal structure [9, 10] as shown in Figure 2.2.

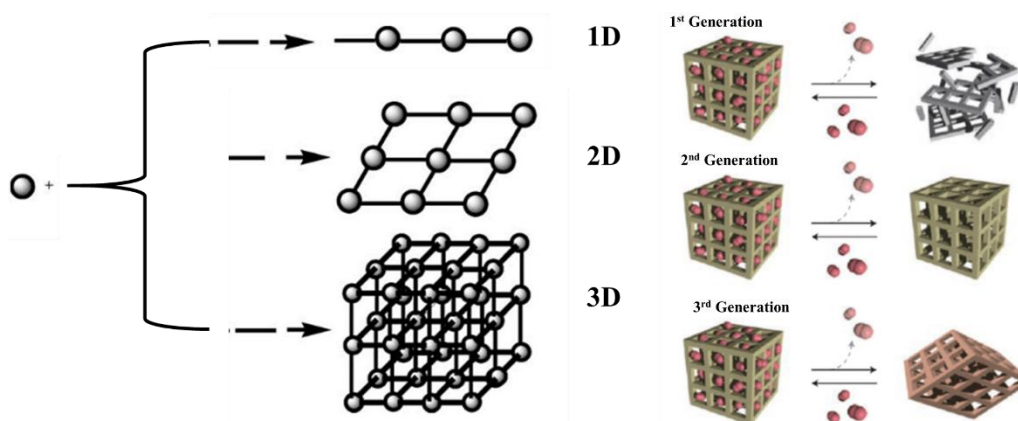


Figure 2.2. Schematic Illustration of 1D and 2D Dimensional Coordination Polymer (Left) [9]; Graphical Representation of 1st, 2nd, and 3rd Generation of Coordination Polymer [11].

The coordination polymer assembled from organic ligand and metal ion into three dimensional hierarchical crystalline structures is often regarded as metal organic framework. Since then, the term coordination polymer and metal organic framework have been used interchangeably. The term MOFs was first coined by Omar Yaghi in 1995 [5, 10]. The framework of MOFs is either porous or non-porous. However, the porosity of MOFs was reported to be reversible due to various environmental factors (temperature, pressure, light intensity) contributing to the weak intermolecular interactions between building components. Thus, efforts have been made to modulate the strong structural

rigidity that could incorporate permanent porosity. Based on this, in 1998 Kitagawa classified MOFs into three categories; 1st, 2nd, and 3rd generation coordinated network. Among three generations of coordinated networks, 3rd generation coordinated networks were defined to have permanent porosity with structural flexibility[11]. This led to numerous amounts of applications and implementation of coordinated networks in the gas storage community. The intermolecular interaction between organic ligand and metal ions, choice of building units, crystallization, environment, and guest molecules determine the crystal structural rigidity and dimensionality of coordination network (MOFs). This major advance in the field of coordination polymer depicted that coordinated networks (MOFs) could be modified and developed in a highly periodic manner, with a defined understanding of the crystalline structure, porosity, and chemical functionality. Thus, the ability to design and control the arrangement of metal ions with extended organic spaces in three-dimensional fashion led to the origin of the term reticular chemistry which was coined by Yaghi and coworkers[5].

2.1.2 Isorecticular Metal Organic Framework

The flexibility with geometry, size, and functionality led to the “design” of a large number of MOFs. The organic units are generally ditopic or polytopic organic carboxylates, linked to metal-containing units, such as Transition metals (e.g., Cu, Zn), alkaline earth elements (e.g. Sr, Ba), p-block elements (e.g. In, Ga), and actinides (e.g. U, Th)[7]. A major advance in the chemistry of MOFs came in 1999 with the invention of two structures i.e. MOF-5 (IRMOF-1) and HKUST-1 [12] reported by Omar et al. and

Chui et al, respectively. Subsequently, in the coming years around 2002, the flexible and non-flexible structures of MIL-88/53 [13] was reported by Ferey et al.

2.1.2.1 Reticular Chemistry

The demand for the synthesis of new materials to perform highly specific and cooperative functions has been increasing rapidly in parallel with advanced technology[14, 15]. Recently, the field of metal organic framework has evolved significantly due to its practical and conceptual approach to design and develop the target material. Intrinsically, the reticular chemistry is described as the process of assembly of molecular building blocks held together by strong bonding that pattern into periodic arrays of the ordered net like structures (Predetermined) [14-17]. Some of the advantages of this approach are listed below.

- **Molecular approach:** It provides the ability to design and control the structure of frameworks [18].
- **Bonding:** The strong bonding between the building blocks could impart superior functionalities like thermal and chemical stability into the framework.
- **Crystalline engineering:** Based on the type of the interactions (intermolecular or intramolecular) design and synthesis could be controlled with desired properties.

2.1.2.2 Isoreticular Series

The synthesis, X-ray single crystal structure determination, and absorption studies were first reported for MOF-5, which consists of Zn_4O units connected by linear 1, 4-benzenedicarboxylate units to form a cubic network[19, 20]. These MOFs showed high

porosity and pore-volume ratio with the pore size that can be used for gas storage. Taking advantage of reticular chemistry that includes reticulating metal ions and organic carboxylate, the group of Omar M. Yaghi synthesized a new class of materials called IRMOFs. Thus, the theory of isorecticular chemistry was established in the year 2002 with the development of IRMOFs. These class of materials were developed to improve the surface area and pore volume by incorporation of different topological linkers. In IRMOF, IR stands for isorecticular, which means it is a series of MOFs with the same topology, but different pore size [15, 21-23]. A series of different IRMOFs share similar pcu topology of IRMOF-n ($n=1-16$). As shown in the figure 2.3, the pore volume and porosity vary with the variation in the organic linker. Applying the concept of isorecticular chemistry, various kinds of MOFs were developed.

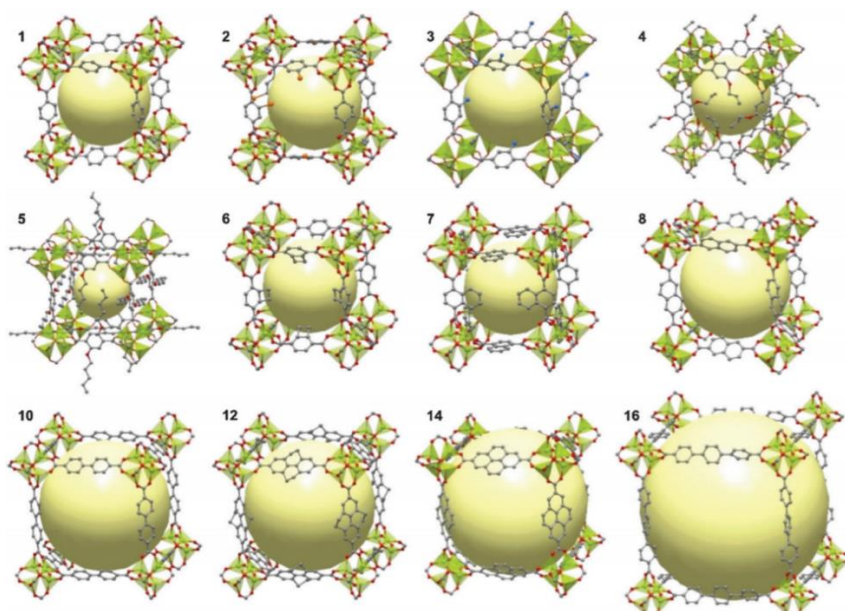


Figure 2.3. Crystal Structures of IRMOFs-n Series [$n=1-16$]. The Non-interpenetrated Structures from ($n=1,2,3,4,5,6,7,8,10,12,14,16$). The Yellow Sphere Represents the Pore Volume. Zn Atoms are in Green, O in Red, C in Grey, Br Atoms in Orange, and Amino Groups in Blue [18].

2.1.3 Types of Isorecticular MOFs

The possibility of tuning the chemical functionality and porosity of MOFs by varying the size and the functionality of linker attracted many physicists and chemists to develop various classes of MOFs using the different combinations of metal ions in the periodic table and organic polycarboxylates. Since then, numerous kinds of MOF families have been reported, of which MOFs such as Zeolitic imidazolate framework (ZIF), materials of Institute Lavoisier (MIL), Hong-Kong University of Science and Technology (HKUST) will be emphasized. shown in the Figure 2.4. [18, 24] due to their significance is gas adsorption studies. The nomenclature of most of the metal organic frameworks is based on either chronological order of discovery, initials of the institution (MIL, HKUST), or by series of isorecticular synthesis (IRMOFs)[18, 25].

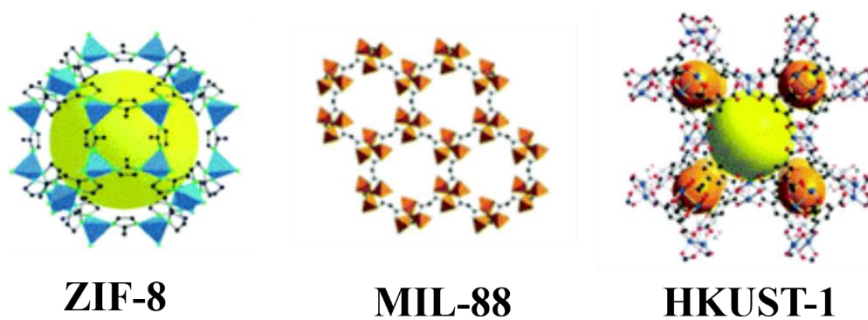


Figure 2.4. Crystal Structure of ZIF-8, MIL-88, and HKUST-1 [18,24,25].

2.1.3.1 Properties and Applications

Zeolitic imidazolate frameworks (**ZIFs**) are three-dimensional crystal porous materials that are constructed from tetrahedral metal ions (e.g. Zn, Co) interconnected through imidazole (Im) linker. The origin of the term zeolitic in ZIF framework is because of the M-Im-M (metal-linker-metal) angle is similar to the Si-O-Si angle in the

zeolites. These materials are one of the best porous materials with chemical and thermal stability. With tetrahedral topologies with well-defined structures porosity in the family of ZIF, a series of ZIF-68, 69, 70, 78, 79,81,82,95 and 100 have found potential application in gas storage and separation applications due to its extraordinary high surface area ($> 3000 \text{ m}^2/\text{g}$)[26, 27].

HKUST-1, also known as MOF-199, is one of the 3D dimensional porous metal organic framework that are known for multi functionalities. These materials are constructed from dimeric units such as Cu_2 paddlewheel units interconnected through 1,3,5 benzene tricarboxylate linkers in cubic topology. These materials were extensively used in gas storage and separation applications due to its high porosity and ultrahigh surface area ($1980 \text{ m}^2/\text{g}$). This metal ion to ligand combination of HKUST-1 containing the highest density of Cu-Cu motifs (coordination sites) with high metal-to unit cell ratio exhibit multifunctionalities such as ionic and electronic characteristics whose properties are being explored. Recently HKUST-1 was also successfully used as biocidal material contributing to the antifungal behavior of the copper ions present in the network[17, 28-30].

MIL-n [88,53]: These are series of Iron based metal organic framework made up of linear dicarboxylate organic ligand and trinuclear metal clusters ($\text{M}=\text{Fe}, \text{Cr}$). These frameworks have been extensively used in biological applications due to their biocompatible and biodegradable nature. Due to the flexible nature of framework with narrow pore sizes, they have limited applications in gas storage though they exhibit high surface area. To modulate these frameworks with structural rigidity and larger pore sizes,

MIL-100(Cr, Fe) and MIL-127 (Fe) were developed that share similar building units as that of MIL-88. Thus, demonstrating significant applications in gas sorption, separation, and drug delivery[31, 32].

Table 2.1

The Pore Volume of the MOFs Reported in Literature (1999–2012) Reported from the Origin of MOF-5 (First MOF Reported) [18]

MOF-5	HKUST-1	MIL-53	MOF-177	MIL-88	MIL-101	IRMOF074-XI
12 Å	Increasing pore volume				34 Å	98 Å
1999						2012

2.2 Metal Organic Framework in Electronic Devices

In the field of modern chemistry, the research for the potential use of MOFs have been significantly influenced due to their structural and chemical diversity. As discussed above, these materials were reportedly trending in the chemical and biomedical industry for their applications in gas storage, drug delivery, gas separation, catalysis, filtration, and sensing[33]. From the physical aspect, these materials possess a rich structural-property relationship that provides crucial intrinsic details necessary to understand their solid-state properties [34, 35]. Based on the structure-property relationship, the superior functionalities such as electrical, magnetic, and optical properties can also be incorporated by judicious choice of metal nodes, organic ligands, the way they interact or by incorporation of guest molecules. The way they interact is the consequence of cooperative phenomena between the metal ions and organic ligands giving rise to

electrical, optical, and magnetic properties with an exception in few classes of magnetic MOFs[36, 37]. Owing to these possibilities significant research towards the application of these materials into a wide span of applications is explored. Addressing the current state of the art, the conductivity in MOFs have been reported but the field is at the initial stage due to its insulating behavior or poor conductivity of the framework. Regarding the luminescent MOFs, this area has been extensively explored and has been successfully implemented in opto-electronic devices. As far as magnetic MOFs are concerned, the field is at infancy with a couple of magnetic MOFs reported [36]. Thus, the pathways to incorporate each of these properties is illustrated and discussed below.

2.2.1 Electrically Conductive MOFs

All the materials that possess electrical conductivity are organized into three categories based on the width of the bandgap Figure 2.5. Any solid material that exhibits bandgap within the electronic spectrum of $\sim 1-3$ eV, with high electrical conductivity owing to the high concentration of free charge carrier (holes or electrons) is considered as a semiconductor material[38].

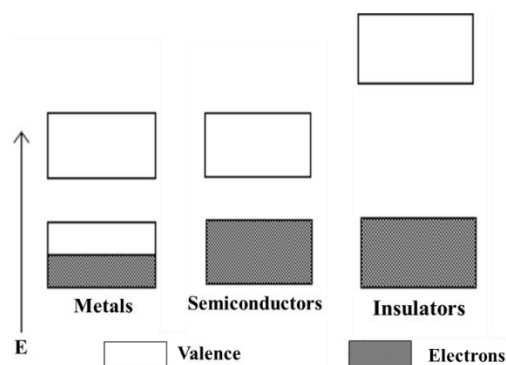


Figure 2.5. The Energy Bands of Metals, Semiconductors, and Insulators [38].

In the modern field of microelectronic and optics, semiconductor materials play a major role. Therefore, metal organic frameworks could be a great choice of materials because of its tunable structural versatility and an ordered structure. To introduce MOFs as semiconductor materials, tuning of band gap such as lowering the bandgap or increasing the charge mobility is required. This tunability is again dependent upon the type of interaction i.e. Intermolecular interaction: metal ion and the organic ligand or Intramolecular interaction - π stacking [33]. The two key factors responsible for poor electrical conductivity in MOFs are: (1) the insulating character of organic ligand and (2) due to poor overlapping between the π -orbitals of organic ligand and d-orbitals of metal ions[39]. The common strategies for constructing MOFs with conductivity involves three possible charge pathways.

Pathway 1: A long range of charge transport in this pathway is facilitated through bonds. This mechanism is promoted by interaction between ligand π and metal d orbital [39]. This mechanism is based on the tunneling of electron between the donor and acceptor portions of the framework. Typically, the electrical conductivity in the range 10^{-7} to 10^{-10} S cm^{-1} is considered as insulator. This is caused due to poor overlapping between the metal ion and organic linker as the electronegative nature of oxygen atom in the carboxylate group of the linker is so high that it requires high voltage for tunneling of the electrons [40]. Various MOFs that exhibit conductivity through this mechanism have been reported, of which $[[\text{Cu}_2(6\text{-Hmna})(6\text{-mn})] \cdot \text{NH}_4]_n$ a copper-sulfur based MOF constructed from 1,6-Hmna=6-mercaptionicotinic acid, 6-mn = 6-mercaptionicotinate shows highest electrical conductivity which is presented in Table 2.2. As Figure 2.6 (a)

indicates, the $(-\text{Cu-S-})_n$ chain within the framework is responsible for charge transfer through the bond approach. The high conductivity is due to the overlapping between the d-orbital of copper and p-orbital of Sulphur atom which results in $(-\text{Cu-S-})_n$ chain and also planes in the structure[41, 42].

Table 2.2

Significant Progress in the Last Few Years Concerning Electrically Conductive MOFs, Their Pathways Compared with Conventional Metals

Materials	Mechanism	Conductivity (S cm^{-1})	Charge carrier	Mobility ($\text{cm}^2 \text{V}^{-1} \text{S}^{-1}$)	Ref.
1. Metals Cu Au Fe	Tunneling	6.5×10^5 4.1×10^5 1.0×10^5	e	46	[43]
2. Organic polymers Polyacetylene Polythiophenes Rubrene	Charge transfer (electron hopping)	10^{-9} 1975	h	1-10 4	[43]
3. TTF-TCNQ Ni_3 (HITP) ₂ Zn_2 (TTFTB)	Through-space	700 40 4.0×10^{-6}	h or e	48.6 0.2	[39, 43, 44]
4. Cu_3 (BTC) ₂ -TCNQ NU-901- C_{60}	Guest molecule	0.07 1×10^{-3}	h		[45, 46]
5. Fe_2 (DSBDC) {[Cu ₂ (6-Hmna) (6- mn)] · NH ₄] _n Cu [Ni(pdt) ₂]	Through-bond	1×10^{-6} 10.96 1×10^{-4}			[33, 37, 42, 47]

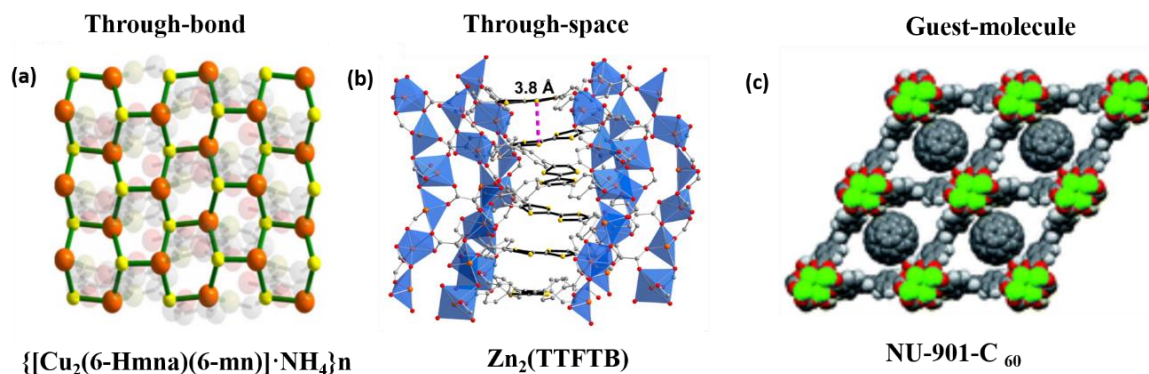


Figure 2.6. (a) Through-bond Strategy – $\{[\text{Cu}_2(6\text{-Hmna})(6\text{-mn})] \cdot \text{NH}_4\}_n$ [41]; (b) Through Space Strategy – Zn-TTF (Columnar π -Stacking) [42]; (c) Guest Molecule Strategy – NU-901- C_{60} ; Blue- C_{60} [43].

Pathway 2: In this pathway, the charge transport is facilitated through space via π stacked aromatic ligands which was proposed as an alternative to through bond strategy. This mechanism typically promotes electron hopping mechanism by employing electroactive molecules [39, 40]. TTF-TCNQ i.e. tetrathiafulvalene- tetracyanoquinomethane is one of the MOFs that demonstrate metallic conductivity (shown in the table.2.2) through-space (π - π stacking) mechanism [41]. Recently, TTF-based ligand consisting of benzoate spacers is used to develop Zn based MOF reported by Dincă et al. These MOFs shows columnar stacks of TTF (3.8\AA) as shown in the Figure 2.6 (b) with the charge mobility of a magnitude that resembles some best conductive organic polymers [42, 43].

Pathway 3: The other alternative strategy to increase the conductivity of MOFs is via incorporating an appropriate guest molecule within the MOF. These molecules can activate long range delocalization either through bonds or through space or that can inject mobile charge carriers by oxidizing or reducing the organic ligand and metal ions [39,

40]. NU-901, a MOF consisting of $Zr_6(\mu_3-O)_4(\mu_3-OH)_4(H_2O)_4(OH)_4$ nodes and tetratopic 1,3,6,8-tetrakis (p- benzoate) pyrene ($TBAPy^{4-}$) linkers Figure 2.6 (c). These materials were chosen for the encapsulation of C_{60} . After installation of C_{60} , the NU-901- C_{60} shows electrical conductivity higher than that of NU-901 (shown in the table 2.2). As per reports, the donor-acceptor interactions between $TBAPy^{4-}/C_{60}$ contribute to the electrical conductivity of the framework[41, 44].

2.2.2 Magnetic MOFs

All the materials that possess magnetic behavior are categorized as diamagnetic, paramagnetic, ferromagnetic, ferrimagnetic and superparamagnetic based on the orientation of spin as shown in Figure 2.7. The basis of magnetic phenomena depends upon the unpaired spin and orientation of the spin in materials. Thus, any material that exhibits magnetization in the absence of magnetic field (H) below critical temperature (T_c) are considered as permanent magnets (ferromagnetism)[48a].

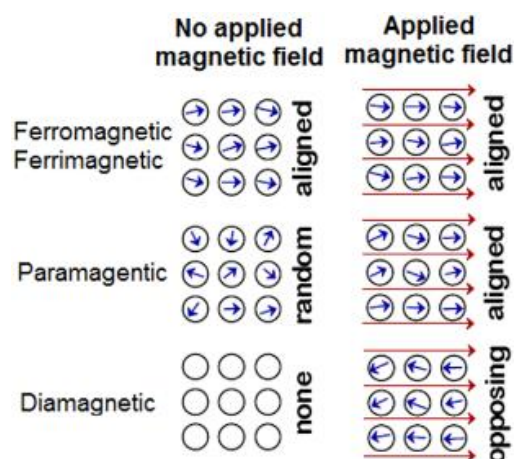


Figure 2.7. Schematic Illustrations of Ferromagnetic, Ferrimagnetic, Paramagnetic, and Diamagnetic [48 a].

Recently permanent magnet technology has been contributing significantly in the field of modern electronic devices and information recording media. Among permanent magnets, the inorganic solids considered as conventional magnets have been potentially applicable due to high temperature magnetic ordering and energy density values. However, these materials impose limitations on their structural tunability and lack of processability. In contrary, the molecular magnets based on coordination chemistry provide structural tunability possessing unique magnetic behavior but cannot operate at higher temperatures[49, 50]. Thus, material that functions at higher temperatures (inorganic solids) with the feasibility of structural tunability (organic solids – molecular magnets) is required. Owing to the requirements, metal organic framework could be suitable candidates due to the synergistic combination of structural tunability via organic ligands and possess magnetic behavior due to metal centers. Magnetism in MOFs can be implemented by incorporating magnetic moment carriers such as paramagnetic metals, open shell organic ligand and both [51-53]. The common strategies for constructing MOFs with magnetism involves three possible pathways which were illustrated in detail in the review paper reported by Eugenio Coronado and his workers.

Pathway 1: First class of Magnetic MOFs. In these frameworks, the property of magnetism is the result of magnetic exchange via ligands. The contribution of organic ligand to the functionality of the MOF can come from their topology, the ability to participate in the interactions and chemical reactivity [54]. Thus, this pathway can be approached using three routes discussed below:

- (a) Using a short linker: Porosity of MOFs requires long linkers in the network but short linkers in MOFs are desirable to maintain the cooperative magnetic exchange between metal centers. The coexistence of magnetic and porosity in one compound is rare or hard to obtain as the two cooperative mechanisms require different topology of the linkers and molecular interactions. MOF exhibiting both magnetism and porosity was first reported by Long and his coworkers in $\text{Co}_3[\text{Co}(\text{CN})_5]_2$ that is constructed using cyanide linkers (Figure 2.8 (a)). In the following years, the related compound $\text{Cr}_3[\text{Cr}(\text{CN})_6]_2 \cdot 6\text{H}_2\text{O}$ showed an increase in the magnetic ordering temperature by absorption of paramagnetic O_2 molecules in the pores of the framework [36, 55].
- (b) Metallo-ligand approach: This approach was successfully demonstrated in magnetic MOFs in which metallo-ligand complexes such as oxamato-based oligonuclear complexes are used. These MOFs were reported by Fernando-Soria in which the oxamato- based dinuclear Cu (II) complexes are coordinated to Mn(II) through free oxygen atom from carboxylate linkers resulting in brick-wall Rectangular layer architecture of the 2D with the chemical formulae $[\text{Mn}_2\text{Cu}_2(\text{Me}_4\text{ppba})_2(\text{H}_2\text{O})_6] \cdot 8\text{H}_2\text{O}$ (Me_4ppba = 2,3,5,6-tetramethyl-N,N'-1,4-phenylenebis (oxamate) [36, 56]. This approach not only contributes to maintaining the topology of the networks but also provides pathways for efficient magnetic interactions as shown In Figure 2.8 (b).
- (c) Radicals used as ligands: In this approach, the radical 2,5- dihydroxy-1,4-benzoquinone is used to coordinate Fe (III) forming a 2D dimensional

honeycomb-like anionic layers Figure 2.8 (c). This radical which is a tetraoxolene ligand possess redox chemistry that could easily stabilize diamagnetic and paramagnetic or semiquinone isomers [55] . Summarizing all the three approaches, each one offers its own set of advantages and disadvantages. Though the short linker approach incorporates magnetism in MOF, porosity is rarely found except in the case reported in the discussion above. These MOFs also show the magnetic temperature at low critical temperature (T_c). Currently, the use of radical ligand is found to be attractive, as the magnetic exchange is possible even at the larger distance between metallic centers. However, the highest concern of this approach is chemical stability. With limitations in these two approaches, the metal-ligand approach is found to be much more favorable due to its ease in designing magnetic MOFs with magnetic ordering at higher temperatures[35].

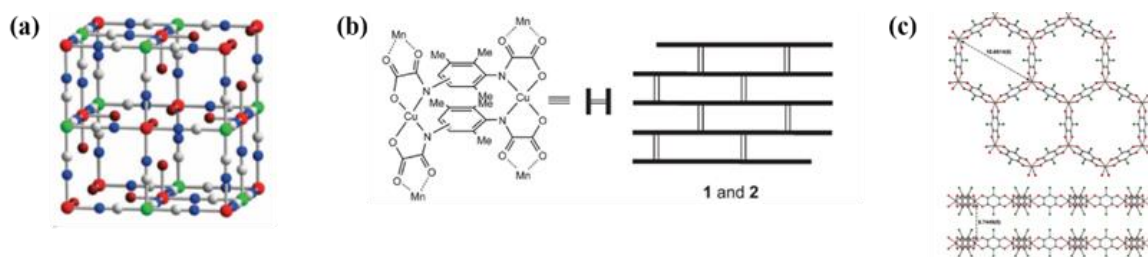


Figure 2.8. (a) Short Linker; Crystal Structure of $\text{Cr}_3[\text{Cr}(\text{CN})_6]_2 \cdot 6\text{H}_2\text{O}$ [35](b) Metallo-Ligand: Brick-Wall Rectangular Layer Architectures of the 2D MOFs from the Self-assembly of Di-copper (II) Metallo-cyclophane Anionic Complexes and Bis (Chelated) Mn(II) Ions-[54]; (c) Radicals: The X-ray Crystal Structure of $[\text{Fe}_2\text{L}_3]^{2-}$ Viewed Along Crystallographic C Axis [35,55].

Pathway 2: Second class of magnetic MOFs. In these frameworks, the origin of magnetism is via spin – crossover complexes in which the spin transition takes place at room temperature[35]. The topology of the linker (short or long) does not matter in this approach as the cooperative mechanism is controlled by elastic forces that are contributed via the polymeric nature of the organic linkers [37,38]. The spin transition takes place due to physical or chemical stimuli such as pressure, light irradiation, temperature, and host-guest interactions [59]. The spin transition temperature that takes place due to the absorption of gas molecules was first reported in two coordination polymers $[\text{Fe}(\text{btzx})_3(\text{ClO}_4)_2]$ and $[\text{Fe}(\text{btzx})_3(\text{BF}_4)_2]$ (btzx=bistetrazole-p-xylene) shown in Figure 2.9 (a). The spin transitions take place differently based on the absorption of different gases such as CO_2 , CH_4 , C_2H_4 , or C_2H_2 due to their difference in interaction[36, 57].

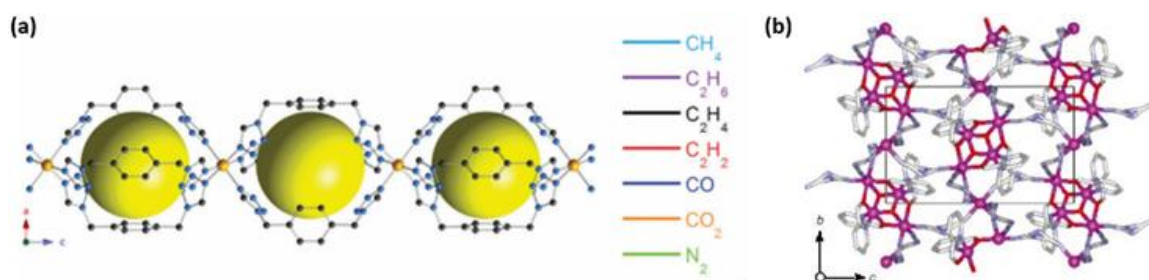


Figure 2.9. (a) Crystal Structure of Compartmentalized Coordination Polymers of $[\text{Fe}(\text{btzx})_3(\text{ClO}_4)_2]$ and $[\text{Fe}(\text{btzx})_3(\text{BF}_4)_2]$ [35]; (b) 3D Packing in Planes $[\text{Mn}[\text{N}(\text{CN})_2]_6]^{4-}$ [56].

Pathway 3: Third class of magnetic MOFs. In these frameworks, the property of magnetism is via magnetic metal clusters that are present at the nodes of the framework which in general behaves as a single molecule magnet (SSM) [36]. The SMMs are magnets that show discrete molecular magnets with potential applications in molecular

spintronics. Thus, this pathway facilitates the design of well-defined magnetic nanostructures with the well-organized spacing of single molecular magnets in the structure of the framework with well insulated magnetic spaces. One more significant feature of SMMs is slow magnetic relaxations at lower temperatures and exhibit magnetic anisotropy with large spin value. Cle'rac and his co-workers reported first 3D coordination network of SMMs composed of units of mixed valence of Mn₄ clusters (SMMs) and M(II) (paramagnetic units) [56] as shown in the Figure 2.9 (b). These building blocks were inter-connected by a dicyanamide bridging. These frameworks incorporated with SMMs at nodes show ferri-magnetic behavior.

Table 2.3

Significant Progress in the Last Few Years Concerning Magnetic MOFs and Their Pathways Compared with Conventional Metals

Materials	Magnetic type	Tc(K)	Mechanism	Ref.
Metals <ul style="list-style-type: none"> • Fe • Co • Ni 	Ferromagnetic	1043 1394 631		[58]
Organic radicals <ul style="list-style-type: none"> • <i>p</i>-nitrophenyl nitronyl nitroxide • p-NPNN (β-phase) • p-NPNN (α-phase) 	Ferromagnetic 3D-F F- dimer	0.60 0.42		[48b]
1. Organic-molecule magnets <ul style="list-style-type: none"> • [Fe^{III}(C₅(Me₅)₂)] [TCNE] • Li [TCNE] 	FO / 0D WF/3D	4.8 21		[59, 60]

Table 2.3

Cont.

Materials	Magnetic type	Tc(K)	Mechanism	Ref.
2. Metal organic framework				
• [M ^{II} (pzdc) ₂] ²⁻ (M= Cu, Co, or Ni) + Ae-O-ae (Ae= Ca, Sr, or Ba)	AF/1D-3D		Metallo-ligand approach	[61]
• MOF (PTC-Fe)	FO/2D			
• [{Ru ₂ (O ₂ CPh- <i>o</i> -Cl) ₄] ₂ TCNQ(MeO) ₂]	AF/2D	20	Short linker	[62]
• M-BHT (M = Cr, Mn, Fe, and Co).	WAF	56	Radical	
• Mn ₁₂ Ac@NU-1000	PM			
			Spin - crossover	[62]
			SMMs	[63, 64]

Note. FO, ferromagnet; FI, ferrimagnet; AF, antiferromagnet, WF, weak ferromagnetic (= canted antiferromagnet).

2.2.3 Luminescent Metal Organic Framework

Any material that absorbs light of longer wavelength and emits light with a shorter wavelength is considered as luminescent material [64-66]. These materials are quite fascinating and are currently employed in a wide range of applications such as light harvesting devices, solar harvesting devices and opto-electronic devices. There are numerous organic and inorganic materials contributing to this field, of which MOFs have been gaining significant attention due to the availability of hybrid-nature with porosity allowing a wide range of emissive phenomena. The first luminescent MOF was reported in the year 2002 and till date about 1337 luminescent MOFs have been reported[5, 67]. The property of luminescence in MOFs causes some of the significant phenomena such as fluorescence, phosphorescence, and scintillations. The choice of luminescent building component in the structure of MOFs is central for achieving Luminescent metal organic

frameworks (LMOFs). Thus, the origin of this mechanism is based upon the choice of metal nodes, organic ligand and the interaction between the metal nodes and organic ligand. Thus, the common strategies for constructing MOFs with luminescence involves three possible pathways[67, 68].

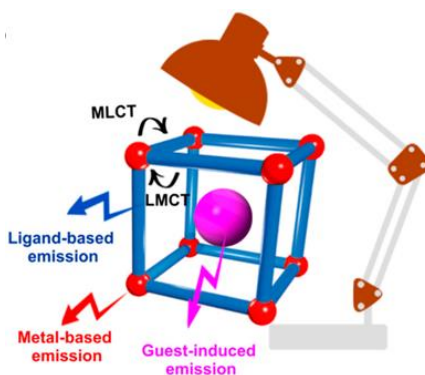
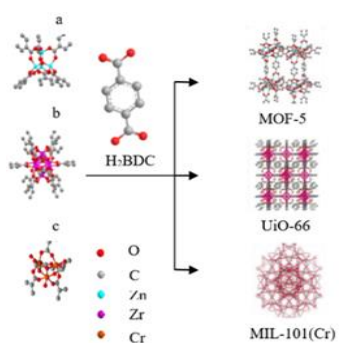


Figure 2.10. Pictorial Representation of the Pathways for the Origin of Luminescence in MOFs [67].

2.2.3.1 Pathway 1: Ligand Centered Emission

The origin of luminescence in MOFs is a molecular phenomenon and often the organic linker is the source of the emission. Linker based emission is the most common type which is further categorized into three subtypes: (a) Linker emission: Generally, MOFs built from the transition metal ions interconnected via organic linkers show linker-based emission due to completely filled d orbitals (d^{10} configuration) of metal ions where d-d transitions are not possible. Thus, organic linkers consisting of rigid aromatic or π -conjugated backbones contributes to the linker-based emission upon irradiation eliminating the chances of charge transfer and quenching. The following mechanisms are based on charge transfer pathway which is dependent upon the coordination geometry of

the metal nodes[68]. (b) Ligand to metal charge transfer (LMCT) and Ligand to ligand charge transfer (LLCT): LMCT shows charge transfer from organic linker to metal centered orbital. This mechanism was very well illustrated by Fang-Chang Tsai and his co-workers in transition based (Zn, Zr, Cr) MOFs built using terephthalic acid. Though all the three metal ions were coordinated to similar organic linker, the pathway of emission showed different mechanism due to difference in the coordination environment of metal ions shown in Figure 2.11 with table.



Compounds	Absorption peak	Emission peak	Mechanism
Terephthalic acid	200–350 nm	-	-
MOF-5	200–400 nm	440 nm	LLCT
UiO-66	200–400 nm	398 nm	LMCT
MIL-101 (Cr)	200–700 nm	485 nm, 525 nm, 580 nm	LMCT

Figure 2.11. (Left) The Schematic Representation of MOF-5, MIL-101 (Cr) and UiO-66 with Metal Ions Zn⁺², Zr⁺⁴, and Cr⁺³, Respectively; (Right) Table Shows the Absorption and Emission of the MOF-5, MIL-101, and UiO-66, Terephthalic Acid [69].

The Zn (II) and Zr (II) ions in MOF-5 and UiO-66 respectively, do not undergo any d-d transitions due to stable d^{10} and d^0 configuration. The emission of MOF-5 and UiO-66 at 440nm and 398 nm accounts to ligand to ligand charge transfer ($\pi-\pi^*$ transitions), as the terephthalic acid did not show any emission. The LMCT transfer was very evident in MIL-101 attributing to the unstable d^3 orbital confirming the strong coordination between the ligand and metal ($\pi-d$) conjugation [69]. (c) Metal to ligand charge transfer (MLCT): In this mechanism the charge transfer takes place from metal to

the organic linker if the; MOFs are composed of metals with electrons in valence orbitals as in the case of Cu (I) and Ag(I) MOFs; and reduced ligands reported in the case of Zn (II) MOFs constructed with rigid 3,5-di(3,5- dicarboxylphenyl) nitrobenzne ligand[64, 68, 70].

2.2.3.2 Pathway 2: Metal Centered Emission

This mechanism is mostly observed in the luminescent metal organic framework that are constructed using transition metal with unpaired electrons as discussed in case of MLCT and more prominently in lanthanide metal ions. The lanthanide ions that are incorporated in the framework of MOFs via organic linkers (chromophores) are sensitized through antenna effects. Taking advantage of antenna effect, in which the organic ligand is connected to lanthanide ions absorbs photon and sensitizes the metal ions resulting brighter emission when compared to free ions. This phenomenon was reported in various MOFs that were built from lanthanide-based metal ions. Example: As shown in Figure 2.12.

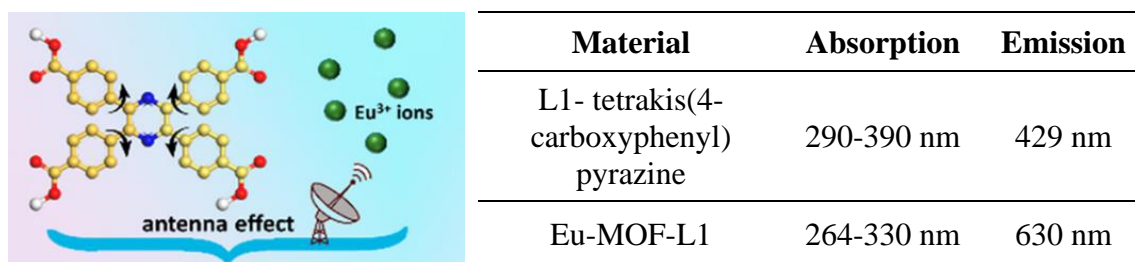


Figure 2.12. (Left): Pictorial Representation of Antenna Effect in Eu-MOF-L1; (Right): Table Showing the Absorption and Emission of Ligand L1 and Eu-MOF-L1 [70].

MOFs composed of Eu⁺³ metal ions and tetrakis(4-carboxyphenyl) pyrazine-L1 were reported by Yin et al showed metal centered emission. The absorption and emission

spectra (excitation spectra 240 – 440 nm) obtained for the free ligand and Eu-MOFs are listed below in the table of Figure 2.12. Thus, L1 is excited and sensitizes the metal causing emission at 630 nm [64, 68-72].

2.2.3.3 Pathway 3: Through Incorporation of Guest Molecule

In this mechanism, the luminescence is incorporated by the incorporation of guest functional molecule in the pores of the well-defined metal organic framework. These luminophores are bounded to the MOF surfaces. This is one of the alternative pathways that is beneficial to incorporate multifunctionality in the MOF structure. In literature, there are a wide range of MOFs in which the luminescence properties of the framework with non-emissive behavior is transformed into a luminescent metal organic framework by incorporation of the guest molecule. Example: As shown in the Figure 2.13. Using electron rich PAH (polycyclic aromatic hydrocarbons) molecules such as coronene, perylene and triphenylene as guest molecules, the coordination polymers of $[Cd_2(tpt)_2(CBA)_2(H_2O)_2]$ composed of cd (II) and tpt (2,4,6-tri (pyridine-4-yl)-1,3,5-triazine) $H_2CBA = 4-$ (carboxymethyl) benzoic acid, shows enhanced emission which was reported by Liu et al. The incorporation of guest molecule in these coordination systems creates a donor acceptor zone and the overlapping between acceptor tpt and donor guest may have caused the emission[64, 73].

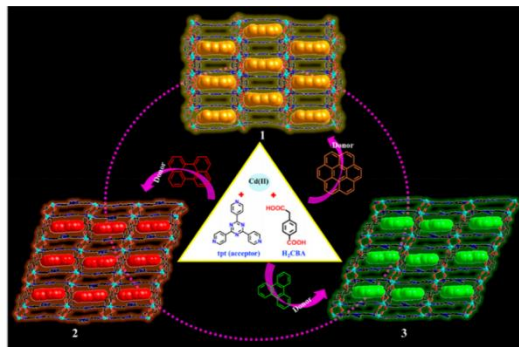


Figure 2.13. Schematic Representation of Donor-Acceptor Systems Between Coordination Polymer and PAH Guest Molecules [64].

2.2.3.4 Synthetic Strategies

The synthesis of MOFs is often regarded as “design” which implies to construct, built, execute, or create according to the target material. The chemistry of MOFs is based on the molecular approach in which the building units are self- assembled spontaneously or via external parameters (energy). One such spontaneous reaction is slow evaporation, in which the separate salts of metal ion and organic ligand are mixed in a solvent. This reaction is carried out at room temperature in a liquid phase without the use of external energy [74]. The major disadvantage of this technique is that it takes about several days to months. Thus, to rapid the synthesis method several forms of energy were proposed by researchers to develop MOF crystals within a short duration of time. Some of the external parameters implemented to develop MOFs include the use of high temperature and pressure (solvothermal), Microwave energy (Microwave synthesis), Ultrasonic waves (Sonochemical synthesis), Mechanical energy (Mechano-chemical synthesis) and electrical energy (Electrochemical synthesis) shown in the Figure 2.14 [18].

Traditionally, the most used synthetic-strategy is solvothermal method, in which high crystalline products of MOFs are obtained within 72 hours. This reaction is performed under high temperatures and pressure in a closed autoclave container. However, limitations such as the requirement of autoclaves to maintain high temperature and pressure; large amounts of solvent; and time duration, (about several weeks to months) led to the development of new alternative synthetic strategies [75, 76]. The novel synthetic strategies like microwave synthesis, electrochemical synthesis, mechanochemical synthesis, and sonochemical synthesis offer advantages such as rapid reaction; requires a minimal amount of solvent or no solvent; and does not require harsh conditions. [77-85]. The microwave synthesis involves heating of solution for a few minutes to an hour [10], resulting in MOF crystals with high yield and purity [88].

Electrochemical synthesis, being one of the mild and quick synthetic procedures, requires metal ions but not metal salts for the production of MOF crystals, thereby, offering advantages such as shorter synthesis time and the ability to have control over synthesis procedure[10, 17, 21, 22]. In the sonochemical reaction, due to intensive ultrasonic radiation (20kHz-10MHz), the reaction mixture undergoes a chemical or physical change. This synthetic route is carried out at a temperature and is known to synthesize MOFs rapidly under mild conditions such as solvent free conditions[80, 84, 85]. Mechanochemical synthesis is a solvent free chemical reaction that takes place by applying mechanical force [86]. Currently, all these synthetic strategies are still at an early stage and further research is required to understand various synthetic parameters and its limitations[77]. Thus, the knowledge of building units and the synthesis procedure

is very important in the chemistry of MOFs for the development of isorecticular network with different topologies

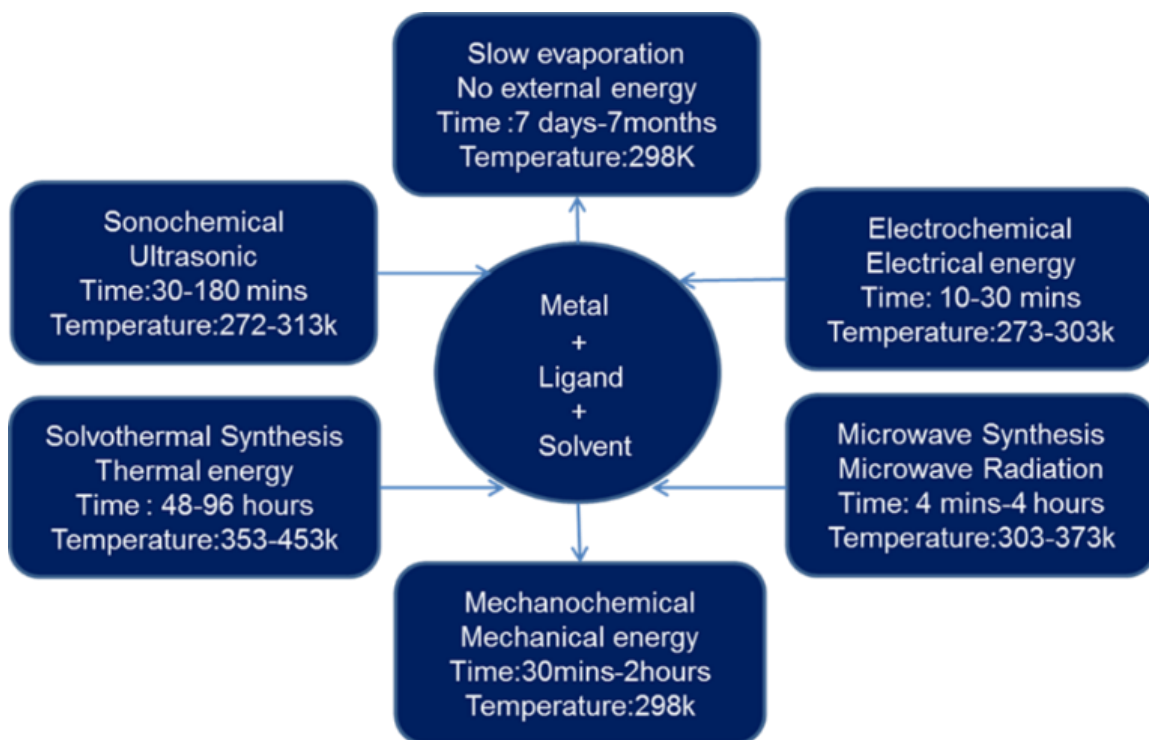


Figure 2.14. Various Strategies for the Synthesis of Metal Organic Frameworks [73].

Table 2.4 illustrates the properties and synthesis methods reported previously. The justification for the choice of these types of metal organic framework to study electrical, magnetic, and optical properties is detailed in Chapter III.

Table 2.4

Previously Reported IRMOF-8, MIL-88, and Mn-MOF

Compound	Isorecticular family	Synthesis	Properties
IRMOF-8A	IRMOFs series- isorecticular metal organic framework. IRMOF-1 (parent compound) to 16 IRMOF-8 which is non-interpenetrated consists of Interpenetrated – IRMOF-8A	Solvothermal Room temperature	High surface area and porosity[22, 23, 86-88]
MIL-88	MILL series – Materiaux de l’Institut Lavoisier. (MIL-53, MIL-126, MIL-88,) MILL-88 A (parent compound) MILL-B, C and MIL- 126 (MILL-D) analogues.	Solvothermal Microwave	Biocompatible, Biodegradable, Antibacterial, Semiconducting [13, 89-98]
Mn-MOF	Mn-MOF from 2,6 Naphthalene dicarboxylic acid following the chemical formulae (Mg ₃ (NDC) ₃)	Solvothermal Micro-wave	Surface area and porosity [99-103][118-122]

2.3 References

- [1] M. Kotzabasaki and G. E. Froudakis, "Review of computer simulations on anti-cancer drug delivery in MOFs," *Inorganic Chemistry Frontiers*, 10.1039/C7QI00645D vol. 5, no. 6, pp. 1255-1272, 2018.
- [2] N. R. C. Stuart R. Batten¹, Xiao-Ming Chen³, Javier Garcia-Martinez⁴, Susumu Kitagawa⁵, Lars Öhrström^{6*}, Michael O'Keeffe⁷, Myunghyun Paik Suh⁸ and Jan Reedijk⁹, "Terminology of metal–organic frameworks and coordination polymers," *Pure and Applied chemistry*, vol. 85, pp. 1715-1724, 2013.
- [3] S. Seth and A. J. Matzger, "Metal–Organic Frameworks: Examples, Counterexamples, and an Actionable Definition," *Crystal Growth & Design*, vol. 17, no. 8, pp. 4043-4048, 2017/08/02 2017.
- [4] E. Sharmin and F. Zafar, "Introductory Chapter: Metal Organic Frameworks (MOFs)," 2016.
- [5] "Introduction to Metal–Organic Frameworks," *Chemical Reviews*, vol. 112, no. 2, pp. 673-674, 2012/02/08 2012.
- [6] J. Liu, "Electronic and Optical Properties of Surface-Anchored Metal-Organic Frameworks," 2015.
- [7] S. R. Batten and N. R. Champness, "Coordination polymers and metal–organic frameworks: materials by design," *Philosophical Transactions of the Royal Society*

- A: Mathematical, Physical and Engineering Sciences*, vol. 375, no. 2084, p. 20160032, 2017/01/13 2017.
- [8] X.-M. Chen, "Assembly Chemistry of Coordination Polymers," 2011, pp. 207-225.
- [9] B.-H. Ye, M.-L. Tong, and X.-M. Chen, "Metal-organic molecular architectures with 2,2'-bipyridyl-like and carboxylate ligands," *Coordination Chemistry Reviews*, vol. 249, pp. 545-565, 03/01 2005.
- [10] N. F. Sunday, "Emerging Trends in Coordination Polymers and Metal-Organic Frameworks: Perspectives, Synthesis, Properties and Applications," *Archives of Organic and Inorganic Chemical Sciences*, vol. 1, no. 2, 2018/01/29 2018.
- [11] J. H. Lee, S. Jeoung, Y. G. Chung, and H. R. Moon, "Elucidation of flexible metal-organic frameworks: Research progresses and recent developments," *Coordination Chemistry Reviews*, vol. 389, pp. 161-188, 2019/06/15/ 2019.
- [12] Y. Chen, X. Mu, E. Lester, and T. Wu, "High efficiency synthesis of HKUST-1 under mild conditions with high BET surface area and CO₂ uptake capacity," *Progress in Natural Science: Materials International*, vol. 28, no. 5, pp. 584-589, 2018/10/01/ 2018.
- [13] S. Surblé, C. Serre, C. Mellot-Draznieks, F. Millange, and G. Férey, "A new isorecticular class of metal-organic-frameworks with the MIL-88 topology," *Chemical Communications*, 10.1039/B512169H no. 3, pp. 284-286, 2006.
- [14] O. M. Yaghi, "Reticular Chemistry in All Dimensions," *ACS Central Science*, vol. 5, no. 8, pp. 1295-1300, 2019/08/28 2019.

- [15] K. E. Cordova and O. M. Yaghi, "The 'folklore' and reality of reticular chemistry," *Materials Chemistry Frontiers*, 10.1039/C7QM00144D vol. 1, no. 7, pp. 1304-1309, 2017.
- [16] O. Yaghi, M. O'Keeffe, N. Ockwig, H. Chae, M. Eddaoudi, and J. Kim, "Reticular Synthesis and the Design of New Materials," *Nature*, vol. 423, pp. 705-714, 06/12 2003.
- [17] C. Janiak and J. K. Vieth, "MOFs, MILs and more: concepts, properties and applications for porous coordination networks (PCNs)," *New Journal of Chemistry*, 10.1039/C0NJ00275E vol. 34, no. 11, pp. 2366-2388, 2010.
- [18] P. Silva, S. M. F. Vilela, J. P. C. Tomé, and F. A. Almeida Paz, "Multifunctional metal-organic frameworks: from academia to industrial applications," *Chemical Society Reviews*, 10.1039/C5CS00307E vol. 44, no. 19, pp. 6774-6803, 2015.
- [19] C. S. Diercks, Y. Liu, K. E. Cordova, and O. M. Yaghi, "The role of reticular chemistry in the design of CO(2) reduction catalysts," (in eng), *Nature materials*, vol. 17, no. 4, pp. 301-307, Apr 2018.
- [20] K. M. Thomas, "Adsorption and desorption of hydrogen on metal-organic framework materials for storage applications: comparison with other nanoporous materials," *Dalton Transactions*, 10.1039/B815583F no. 9, pp. 1487-1505, 2009.
- [21] M. Eddaoudi *et al.*, "Modular Chemistry: Secondary Building Units as a Basis for the Design of Highly Porous and Robust Metal-Organic Carboxylate Frameworks," *Accounts of Chemical Research*, vol. 34, no. 4, pp. 319-330, 2001/04/01 2001.

- [22] D. J. Tranchemontagne, J. R. Hunt, and O. M. Yaghi, "Room temperature synthesis of metal-organic frameworks: MOF-5, MOF-74, MOF-177, MOF-199, and IRMOF-0," *Tetrahedron*, vol. 64, no. 36, pp. 8553-8557, 2008/09/01/ 2008.
- [23] J. I. Feldblyum, A. G. Wong-Foy, and A. J. Matzger, "Non-interpenetrated IRMOF-8: synthesis, activation, and gas sorption," *Chemical Communications*, 10.1039/C2CC34689C vol. 48, no. 79, pp. 9828-9830, 2012.
- [24] Z. Mai and D. Liu, "Synthesis and Applications of Isorecticular Metal-Organic Frameworks IRMOFs-n (n = 1, 3, 6, 8)," *Crystal Growth & Design*, vol. 19, no. 12, pp. 7439-7462, 2019/12/04 2019.
- [25] A. Ebelegi, A. Nimibofa, A. Inengite, and W. Donbebe, "Metal-organic Frameworks as Novel Adsorbents: A Preview," *American Journal of Environmental Protection*, vol. 5, pp. 61-67, 08/28 2017.
- [26] A. Phan, C. J. Doonan, F. J. Uribe-Romo, C. B. Knobler, M. O'Keeffe, and O. M. Yaghi, "Synthesis, Structure, and Carbon Dioxide Capture Properties of Zeolitic Imidazolate Frameworks," *Accounts of Chemical Research*, vol. 43, no. 1, pp. 58-67, 2010/01/19 2010.
- [27] J.-P. Zhang, Y.-B. Zhang, J.-B. Lin, and X.-M. Chen, "Metal Azolate Frameworks: From Crystal Engineering to Functional Materials," *Chemical Reviews*, vol. 112, no. 2, pp. 1001-1033, 2012/02/08 2012.
- [28] A. Sakhivel *et al.*, "Replication of Mesoporous Aluminosilicate Molecular Sieves (RMMs) with Zeolite Framework from Mesoporous Carbons (CMKs)," *Chemistry of Materials*, vol. 16, no. 16, pp. 3168-3175, 2004/08/01 2004.

- [29] C. H. Hendon and A. Walsh, "Chemical principles underpinning the performance of the metal–organic framework HKUST-1," *Chemical Science*, 10.1039/C5SC01489A vol. 6, no. 7, pp. 3674-3683, 2015.
- [30] M. Todaro *et al.*, "Decomposition Process of Carboxylate MOF HKUST-1 Unveiled at the Atomic Scale Level," *The Journal of Physical Chemistry C*, vol. 120, no. 23, pp. 12879-12889, 2016/06/16 2016.
- [31] J. F. Eubank *et al.*, "Porous, rigid metal(III)-carboxylate metal-organic frameworks for the delivery of nitric oxide," *APL Materials*, vol. 2, no. 12, p. 124112, 2014/12/01 2014.
- [32] L. R. Redfern and O. K. Farha, "Mechanical properties of metal–organic frameworks," *Chemical Science*, 10.1039/C9SC04249K vol. 10, no. 46, pp. 10666-10679, 2019.
- [33] V. Stavila, A. A. Talin, and M. D. Allendorf, "MOF-based electronic and optoelectronic devices," *Chemical Society Reviews*, 10.1039/C4CS00096J vol. 43, no. 16, pp. 5994-6010, 2014.
- [34] K. T. Butler, C. H. Hendon, and A. Walsh, "Electronic Structure Modulation of Metal–Organic Frameworks for Hybrid Devices," *ACS Applied Materials & Interfaces*, vol. 6, no. 24, pp. 22044-22050, 2014/12/24 2014.
- [35] G. Mínguez Espallargas and E. Coronado, "Magnetic functionalities in MOFs: from the framework to the pore," *Chemical Society Reviews*, 10.1039/C7CS00653E vol. 47, no. 2, pp. 533-557, 2018.

- [36] J. Wu *et al.*, “Metal–Organic Framework for Transparent Electronics,” *Advanced Science*, vol. 7, no. 8, p. 1903003, 2020.
- [37] G. Wu, J. Huang, Y. Zang, J. He, and G. Xu, “Porous Field-Effect Transistors Based on a Semiconductive Metal–Organic Framework,” *Journal of the American Chemical Society*, vol. 139, no. 4, pp. 1360-1363, 2017/02/01 2017.
- [38] J. A. Lewis. *Conductors, Insulators, and Semiconductors:*
<http://matse1.matse.illinois.edu/sc/prin.html>.
- [39] I. Stassen, N. Burtch, A. Talin, P. Falcaro, M. Allendorf, and R. Ameloot, “An updated roadmap for the integration of metal–organic frameworks with electronic devices and chemical sensors,” *Chemical Society Reviews*, 10.1039/C7CS00122C vol. 46, no. 11, pp. 3185-3241, 2017.
- [40] C.-W. Kung, P.-C. Han, C.-H. Chuang, and K. C. W. Wu, “Electronically conductive metal–organic framework-based materials,” *APL Materials*, vol. 7, no. 11, p. 110902, 2019/11/01 2019.
- [41] A. Pathak *et al.*, “Integration of a (–Cu–S–)n plane in a metal–organic framework affords high electrical conductivity,” *Nature Communications*, vol. 10, no. 1, p. 1721, 2019/04/12 2019.
- [42] T. C. Narayan, T. Miyakai, S. Seki, and M. Dincă, “High Charge Mobility in a Tetrathiafulvalene-Based Microporous Metal–Organic Framework,” *Journal of the American Chemical Society*, vol. 134, no. 31, pp. 12932-12935, 2012/08/08 2012.

- [43] S. Goswami *et al.*, “A porous, electrically conductive hexa-zirconium(iv) metal–organic framework,” *Chemical Science*, 10.1039/C8SC00961A vol. 9, no. 19, pp. 4477-4482, 2018.
- [44] L. Sun, C. H. Hendon, M. A. Minier, A. Walsh, and M. Dincă, “Million-Fold Electrical Conductivity Enhancement in Fe₂(DEBDC) versus Mn₂(DEBDC) (E = S, O),” *Journal of the American Chemical Society*, vol. 137, no. 19, pp. 6164-6167, 2015/05/20 2015.
- [45] A. Talin *et al.*, “Tunable Electrical Conductivity in Metal-Organic Framework Thin-Film Devices,” *Science (New York, N.Y.)*, vol. 343, 12/05 2013.
- [46] A. K. T. S. Banerjee, *Functional Materials: Preparation, Processing and Applications*.
- [47] Y. Kobayashi, B. Jacobs, M. D. Allendorf, and J. R. Long, “Conductivity, Doping, and Redox Chemistry of a Microporous Dithiolene-Based Metal–Organic Framework,” *Chemistry of Materials*, vol. 22, no. 14, pp. 4120-4122, 2010/07/27 2010.
- [48] (a) Sinatra, F. L. (2010). Understanding the interaction between blood flow and an applied magnetic field. (b) J. S. Miller, “Organic- and molecule-based magnets,” *Materials*, vol. 17, no. 5, pp. 224-235, 2014/06/01/ 2014.
- [49] E. Coronado, “Molecular magnetism: from chemical design to spin control in molecules, materials and devices,” *Nature Reviews Materials*, vol. 5, pp. 1-18, 10/01 2019.

- [50] X.-L. Tong, H.-L. Lin, J.-H. Xin, F. Liu, M. Li, and X.-P. Zhu, "Recent Advances as Materials of Functional Metal-Organic Frameworks," *Journal of Nanomaterials*, vol. 2013, p. 616501, 2013/05/07 2013.
- [51] M. Kurmoo, "Magnetic metal-organic frameworks," *Chemical Society Reviews*, 10.1039/B804757J vol. 38, no. 5, pp. 1353-1379, 2009.
- [52] A. Schneemann, V. Bon, I. Schwedler, I. Senkovska, S. Kaskel, and R. A. Fischer, "Flexible metal-organic frameworks," *Chemical Society Reviews*, 10.1039/C4CS00101J vol. 43, no. 16, pp. 6062-6096, 2014.
- [53] L. G. Beauvais and J. R. Long, "Co₃[Co(CN)₅]₂: A Microporous Magnet with an Ordering Temperature of 38 K," *Journal of the American Chemical Society*, vol. 124, no. 41, pp. 12096-12097, 2002/10/01 2002.
- [54] J. Ferrando-Soria *et al.*, "Spin Control in Oxamate-Based Manganese(II)-Copper(II) Coordination Polymers with Brick-Wall Layer Architectures," *Inorganic Chemistry*, vol. 50, no. 18, pp. 8694-8696, 2011/09/19 2011.
- [55] I.-R. Jeon, B. Negru, R. P. Van Duyne, and T. D. Harris, "A 2D Semiquinone Radical-Containing Microporous Magnet with Solvent-Induced Switching from T_c = 26 to 80 K," *Journal of the American Chemical Society*, vol. 137, no. 50, pp. 15699-15702, 2015/12/23 2015.
- [56] H. Miyasaka, K. Nakata, K. Sugiura, M. Yamashita, and R. Clérac, "A three-dimensional ferrimagnet composed of mixed-valence Mn⁴ clusters linked by an [Mn[N(CN)₂]₆]₄- unit," (in eng), *Angewandte Chemie (International ed. in English)*, vol. 43, no. 6, pp. 707-11, Jan 30 2004.

- [57] Y. Mnyukh, "Paramagnetic State and Phase Transitions," *American Journal of Condensed Matter Physics*, vol. 5, pp. 56-59, 06/15 2015.
- [58] M. Sorai, Y. Nakazawa, M. Nakano, and Y. Miyazaki, "Update 1 of: Calorimetric Investigation of Phase Transitions Occurring in Molecule-Based Magnets," *Chemical Reviews*, vol. 113, no. 1, pp. PR41-PR122, 2013/01/09 2013.
- [59] S. Zhang, X. Liu, Q. Yang, Q. Wei, G. Xie, and S. Chen, "Mixed-metal-organic frameworks (M'MOFs) from 1D to 3D based on the "organic" connectivity and the inorganic connectivity: syntheses, structures and magnetic properties," *CrystEngComm*, 10.1039/C5CE00126A vol. 17, no. 17, pp. 3312-3324, 2015.
- [60] N. Motokawa, S. Matsunaga, S. Takaishi, H. Miyasaka, M. Yamashita, and K. R. Dunbar, "Reversible Magnetism between an Antiferromagnet and a Ferromagnet Related to Solvation/Desolvation in a Robust Layered [Ru₂]2TCNQ Charge-Transfer System," *Journal of the American Chemical Society*, vol. 132, no. 34, pp. 11943-11951, 2010/09/01 2010.
- [61] R. Dong *et al.*, "A coronene-based semiconducting two-dimensional metal-organic framework with ferromagnetic behavior," (in eng), *Nat Commun*, vol. 9, no. 1, p. 2637, Jul 6 2018.
- [62] C. Chakravarty, B. Mandal, and P. Sarkar, "Bis(dithioline)-Based Metal-Organic Frameworks with Superior Electronic and Magnetic Properties: Spin Frustration to Spintronics and Gas Sensing," *The Journal of Physical Chemistry C*, vol. 120, no. 49, pp. 28307-28319, 2016/12/15 2016.

- [63] D. Aulakh *et al.*, “Direct Imaging of Isolated Single-Molecule Magnets in Metal–Organic Frameworks,” *Journal of the American Chemical Society*, vol. 141, no. 7, pp. 2997-3005, 2019/02/20 2019.
- [64] M. Pamei and A. Puzari, “Luminescent transition metal–organic frameworks: An emerging sensor for detecting biologically essential metal ions,” *Nano-Structures & Nano-Objects*, vol. 19, p. 100364, 2019/07/01/ 2019.
- [65] J. Zhu, S. Shaikh, N. Mayhall, and A. Morris, “Energy Transfer in Metal-Organic Frameworks,” 2018, pp. 581-654.
- [66] Y. Zhang, S. Yuan, G. Day, X. Wang, X. Yang, and H.-C. Zhou, “Luminescent sensors based on metal-organic frameworks,” *Coordination Chemistry Reviews*, vol. 354, pp. 28-45, 2018/01/01/ 2018.
- [67] G. Mercuri, G. Giambastiani, and A. Rossin, “Thiazole- and Thiadiazole-Based Metal–Organic Frameworks and Coordination Polymers for Luminescent Applications,” *Inorganics*, vol. 7, p. 144, 12/14 2019.
- [68] M. D. Allendorf, C. A. Bauer, R. K. Bhakta, and R. J. T. Houk, “Luminescent metal–organic frameworks,” *Chemical Society Reviews*, 10.1039/B802352M vol. 38, no. 5, pp. 1330-1352, 2009.
- [69] B. Ruan, H. Liu, X.-Q. Zhan, H. Ding, L. Xie, and F.-C. Tsai, “Effect of transition metal ions on luminescence of MOFs,” *MATEC Web of Conferences*, vol. 238, p. 05004, 01/01 2018.

- [70] H.-Q. Yin, X.-Y. Wang, and X.-B. Yin, "Rotation Restricted Emission and Antenna Effect in Single Metal–Organic Frameworks," *Journal of the American Chemical Society*, vol. 141, no. 38, pp. 15166-15173, 2019/09/25 2019.
- [71] D. Yang *et al.*, "A Series of Lanthanide-Based Metal–Organic Frameworks: Synthesis, Structures, and Multicolor Tuning of Single Component," *Inorganic Chemistry*, vol. 56, no. 4, pp. 2345-2353, 2017/02/20 2017.
- [72] X.-T. Liu *et al.*, "Structure and Emission Modulation of a Series of Cd(II) Luminescent Coordination Polymers through Guest Dependent Donor–Acceptor Interaction," *Crystal Growth & Design*, vol. 19, no. 2, pp. 1391-1398, 2019/02/06 2019.
- [73] C. Dey, T. Kundu, B. P. Biswal, A. Mallick, and R. Banerjee, "Crystalline metal-organic frameworks (MOFs): synthesis, structure and function," (in eng), *Acta crystallographica Section B, Structural science, crystal engineering and materials*, vol. 70, no. Pt 1, pp. 3-10, Feb 2014.
- [74] P. Pachfule, R. Das, P. Poddar, and R. Banerjee, "Solvothermal Synthesis, Structure, and Properties of Metal Organic Framework Isomers Derived from a Partially Fluorinated Link," *Crystal Growth & Design*, vol. 11, no. 4, pp. 1215-1222, 2011/04/06 2011.
- [75] C. McKinstry, R. J. Cathcart, E. J. Cussen, A. J. Fletcher, S. V. Patwardhan, and J. Sefcik, "Scalable continuous solvothermal synthesis of metal organic framework (MOF-5) crystals," *Chemical Engineering Journal*, vol. 285, pp. 718-725, 2016/02/01/ 2016.

- [76] Y. Sun and H. C. Zhou, "Recent progress in the synthesis of metal-organic frameworks," (in eng), *Science and technology of advanced materials*, vol. 16, no. 5, p. 054202, Oct 2015.
- [77] N. Stock and S. Biswas, "Synthesis of Metal-Organic Frameworks (MOFs): Routes to Various MOF Topologies, Morphologies, and Composites," *Chemical Reviews*, vol. 112, no. 2, pp. 933-969, 2012/02/08 2012.
- [78] M. Rubio-Martinez, C. Avci-Camur, A. W. Thornton, I. Imaz, D. MasPOCH, and M. R. Hill, "New synthetic routes towards MOF production at scale," *Chemical Society Reviews*, 10.1039/C7CS00109F vol. 46, no. 11, pp. 3453-3480, 2017.
- [79] K. M. L. Taylor-Pashow, J. Della Rocca, Z. Xie, S. Tran, and W. Lin, "Postsynthetic Modifications of Iron-Carboxylate Nanoscale Metal–Organic Frameworks for Imaging and Drug Delivery," *Journal of the American Chemical Society*, vol. 131, no. 40, pp. 14261-14263, 2009/10/14 2009.
- [80] S. Khazalpour, V. Safarifard, A. Morsali, and D. Nematollahi, "Electrochemical synthesis of pillared layer mixed ligand metal–organic framework: DMOF-1–Zn," *RSC Advances*, 10.1039/C5RA04446D vol. 5, no. 46, pp. 36547-36551, 2015.
- [81] A. Bétard and R. A. Fischer, "Metal–Organic Framework Thin Films: From Fundamentals to Applications," *Chemical Reviews*, vol. 112, no. 2, pp. 1055-1083, 2012/02/08 2012.
- [82] Z. Ni and R. I. Masel, "Rapid Production of Metal–Organic Frameworks via Microwave-Assisted Solvothermal Synthesis," *Journal of the American Chemical Society*, vol. 128, no. 38, pp. 12394-12395, 2006/09/01 2006.

- [83] A. Martinez Joaristi, J. Juan-Alcañiz, P. Serra-Crespo, F. Kapteijn, and J. Gascon, “Electrochemical Synthesis of Some Archetypical Zn²⁺, Cu²⁺, and Al³⁺ Metal Organic Frameworks,” *Crystal Growth & Design*, vol. 12, no. 7, pp. 3489-3498, 2012/07/03 2012.
- [84] C. G. Carson, A. J. Brown, D. S. Sholl, and S. Nair, “Sonochemical Synthesis and Characterization of Submicrometer Crystals of the Metal–Organic Framework Cu[(hfpbb)(H₂hfpbb)_{0.5}],” *Crystal Growth & Design*, vol. 11, no. 10, pp. 4505-4510, 2011/10/05 2011.
- [85] Y.-R. Lee, J. Kim, and W.-S. Ahn, “Synthesis of metal-organic frameworks: A mini review,” *Korean Journal of Chemical Engineering*, vol. 30, no. 9, pp. 1667-1680, 2013/09/01 2013.
- [86] Z.-L. Chen *et al.*, “A novel coordination polymer based on 2,6-naphthalenedicarboxylic acid: synthesis, crystal structure and luminescence sensing,” *Transition Metal Chemistry*, vol. 45, 02/01 2020.
- [87] N. Saffon-Merceron, A. Vigroux, and P. Hoffmann, “Crystal structure of a two-dimensional coordination polymer of formula [Zn(NDC)(DEF)] (H₂ NDC is naphthalene-2,6-dicarboxylic acid and DEF is N , N -diethylformamide),” *Acta Crystallographica Section E Crystallographic Communications*, vol. 75, pp. 1759-1762, 11/01 2019.
- [88] R. S. Pillai, M. L. Pinto, J. Pires, M. Jorge, and J. R. B. Gomes, “Understanding Gas Adsorption Selectivity in IRMOF-8 Using Molecular Simulation,” *ACS Applied Materials & Interfaces*, vol. 7, no. 1, pp. 624-637, 2015/01/14 2015.

- [89] Y. Li *et al.*, “TiO₂ Nanoparticles Anchored onto the Metal–Organic Framework NH₂-MIL-88B(Fe) as an Adsorptive Photocatalyst with Enhanced Fenton-like Degradation of Organic Pollutants under Visible Light Irradiation,” *ACS Sustainable Chemistry & Engineering*, vol. 6, no. 12, pp. 16186-16197, 2018/12/03 2018.
- [90] H. T. Vu, L. T. Tran, G. H. Le, Q. K. Nguyen, T. M. Vu, and T. A. Vu, “Synthesis and application of novel Fe-MIL-53/GO nanocomposite for photocatalytic degradation of reactive dye from aqueous solution,” *Vietnam Journal of Chemistry*, vol. 57, no. 6, pp. 681-685, 2019/12/01 2019.
- [91] W.-T. Xu *et al.*, “Metal–organic frameworks MIL-88A hexagonal microrods as a new photocatalyst for efficient decolorization of methylene blue dye,” *Dalton Transactions*, 10.1039/C3DT52574K vol. 43, no. 9, pp. 3792-3798, 2014.
- [92] B. Xu, H. Yang, Y. Cai, H. Yang, and C. Li, “Preparation and photocatalytic property of spindle-like MIL-88B(Fe) nanoparticles,” *Inorganic Chemistry Communications*, vol. 67, pp. 29-31, 2016/05/01/ 2016.
- [93] M. Shen *et al.*, “Antibacterial applications of metal–organic frameworks and their composites,” *Comprehensive Reviews in Food Science and Food Safety*, vol. n/a, no. n/a, 2020/01/07 2020.
- [94] A. Guo, M. Durymanov, A. Permyakova, S. Sene, C. Serre, and J. Reineke, “Metal Organic Framework (MOF) Particles as Potential Bacteria-Mimicking Delivery Systems for Infectious Diseases: Characterization and Cellular Internalization in

- Alveolar Macrophages,” (in eng), *Pharmaceutical research*, vol. 36, no. 4, p. 53, Feb 21 2019.
- [95] G. Wyszogrodzka, B. Marszałek, B. Gil, and P. Dorożyński, “Metal-organic frameworks: mechanisms of antibacterial action and potential applications,” *Drug Discovery Today*, vol. 21, no. 6, pp. 1009-1018, 2016/06/01/ 2016.
- [96] D. Xie *et al.*, “Bifunctional NH₂-MIL-88(Fe) metal–organic framework nanooctahedra for highly sensitive detection and efficient removal of arsenate in aqueous media,” *Journal of Materials Chemistry A*, 10.1039/C7TA07934F vol. 5, no. 45, pp. 23794-23804, 2017.
- [97] H. Pham *et al.*, “Tuning Crystal Structures of Iron-Based Metal-Organic Frameworks for Drug Delivery Applications,” (in eng), *ACS omega*, vol. 5, no. 7, pp. 3418-3427, Feb 25 2020.
- [98] A. Laurikėnas, J. Barkauskas, J. Reklaitis, G. Niaura, D. Baltrūnas, and A. Kareiva, “Formation peculiarities of iron (III) acetate: Potential precursor for iron metal-organic frameworks (MOFs),” *Lithuanian Journal of Physics*, vol. 56, 04/26 2016.
- [99] Y.-P. Zhao, H. Yang, F. Wang, and Z.-Y. Du, “A microporous manganese-based metal–organic framework for gas sorption and separation,” *Journal of Molecular Structure*, vol. 1074, pp. 19-21, 2014/09/25/ 2014.
- [100] K. M. L. Taylor, W. J. Rieter, and W. Lin, “Manganese-Based Nanoscale Metal–Organic Frameworks for Magnetic Resonance Imaging,” *Journal of the American Chemical Society*, vol. 130, no. 44, pp. 14358-14359, 2008/11/05 2008.

- [101] M. Karthikeyan, B. Bhagyaraju, C. R. Mariappan, S. M. Mobin, and B. Manimaran, "Novel semiconducting metal-organic framework: Synthesis, structural characterisation and electrical conductivity studies of manganese based two dimensional coordination polymer," *Inorganic Chemistry Communications*, vol. 20, pp. 269-272, 2012/06/01/ 2012.
- [102] T. Ladrak, S. Smulders, O. Roubeau, S. J. Teat, P. Gamez, and J. Reedijk, "Manganese-Based Metal–Organic Frameworks as Heterogeneous Catalysts for the Cyanosilylation of Acetaldehyde," *European Journal of Inorganic Chemistry*, vol. 2010, no. 24, pp. 3804-3812, 2010/08/01 2010.
- [103] Y. Li *et al.*, "A manganese-based metal-organic framework electrochemical sensor for highly sensitive cadmium ions detection," *Journal of Solid State Chemistry*, vol. 275, pp. 38-42, 2019/07/01/ 2019.

CHAPTER III

APPROACH AND METHODS

This chapter details three aims with three different systems of MOF for specific applications is elaborated. The chapter is divided into two sections; the first section discusses about the synthesis approach for designing metal organic framework with electrical, optical, and magnetic properties. Later, the choice of material approach (MOF systems) to investigate electrical, optical, and magnetic properties is discussed. Likewise, the second section explains all the characterization techniques used in investigating electrical, magnetic, and optical properties of developed MOF systems. All the samples once synthesized were dried in vacuum until characterization was carried out.

3.1 Methodology

3.1.1 Proposed Synthesis Method for Targets IRMOFs

When developing a novel creative synthetic strategy, it is always important to keep an account of parameters such as availability and cost of the reactants/precursors, synthesis conditions (like low temperature, ambient pressure), workup procedure, and activation process, necessity of obtaining high yields, avoiding large amount of impurities, and using only small amounts of solvents. In this research, a new method is proposed by modifying solvothermal method that is followed by solvent driven self-assembly process to synthesize a MOF with enhanced optoelectronic or magnetic properties. This method offers advantages such as low use of solvent, high yield, less

time consumption and does not require any special reaction apparatus and is carried out at an atmospheric pressure.

3.1.1.1 Synthesis Method Discussion

In the proposed method, a rapid and self-assembly driven solvothermal synthesis method is developed in which three different microstructures of Isorecticular MOFs-nanocrystals are prepared from solutions of organic linkers and metal precursors (Zn^{+2} , Mn^{+2} , Fe^{+3}). Solvents are chosen according to the solubility of the organic ligand and metal precursor. In this case, dimethylformamide (DMF) is used as a solvent. Initially, the organic ligand and metal precursor are dissolved in solvent using stirring at room temperature and then followed by subjecting the reaction to solvothermal heating at a temperature above the boiling point of solvent for time span of 7 minutes. After the completion of the reaction, the resulting powder is washed with cold DMF, followed by acetone, and collected to yield pure crystalline product. Figure 3.1. summarizes the self-assembly synthetic path used to make microstructures of three different Isorecticular MOFs.

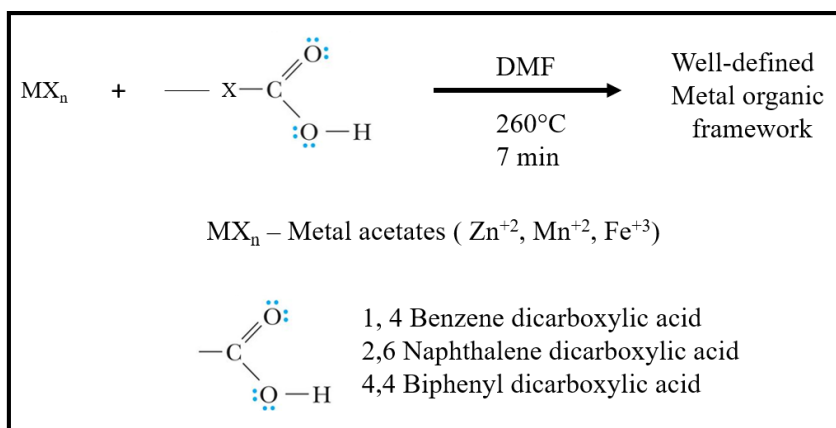


Figure 3.1. Reaction Scheme for Synthesis of Isorecticular MOFs.

As mentioned above, three different systems of isoreticular MOFs i.e. IRMOF-8, MIL-88 and Mn-MOF are developed using proposed synthetic strategy and approach to the material selection is discussed further in the research aims.

3.1.2 Research Aims

a) Aim 1: Designing and synthesizing Self-assembled Hierarchical Microstructures of IRMOF-8 to investigate optoelectronic properties of MOF.

Hypothesis: A solvent-driven self-assembly approach followed by the solvothermal process may provide a path to tailor optoelectronic properties of IRMOFs.

3.1.2.1 Material Selection Approach to Semiconducting – IRMOF-8

MOFs with semiconducting behavior could be possible using three different approaches: (1) through-bond approach and (2) through-space approach and (3) Guest molecules. The process of charge mobility could originate either from interaction between metal ions and the organic ligands (Through bond approach) or through interaction between organic ligands i.e. π - π stacking (Through space approach) [1]. To facilitate interaction, the presence of high energy free electrons or holes in metal ions and unpaired electrons in organic ligands is required[2]. Addressing the Aim 1 of this project, a well-modulated synthetic molecular approach with appropriate choice of metal and ligand combination is designed to meet the general structural requirements essential for developing MOFs with semiconducting behavior.

Likewise, the semiconducting behavior in the MOFs is determined based on the effective overlapping between the orbitals of metals and organic linkers that precisely outline the requirements of metals and linkers assisting in the design of MOFs as

semiconductors [3, 4]. Transition metals are well suitable for this purpose, due to the presence of localized d orbital. Zinc (Zn^{+2}) is chosen as metal node which have filled, core like d-orbitals, thus avoiding d-d transitions states [4, 5]. The Charge transport mechanism in MOFs is closely related to the aromaticity of the linkers, where the conjugation of π bonds could render efficient transport of electrons. Considering electron rich organic network of aromatic linkers[2, 3] 2,6 Naphthalene dicarboxylic acid is considered as it has been used as an excellent linker for constructing frameworks previously. The anionic nature of 2,6 NDC offers structural predictability with their wide range of coordination modes [6-8] (Figure 3.2).

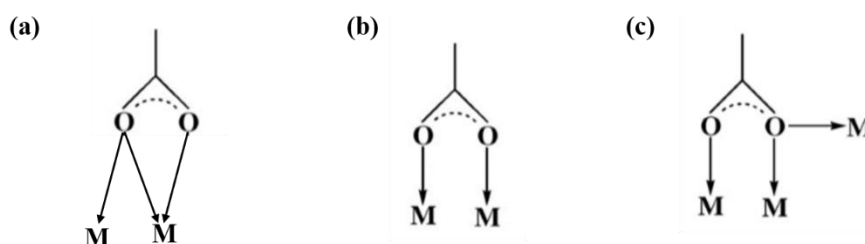


Figure 3.2. (a) Monodentate; (b) Bidentate and (C) Tridentate Coordination Modes Adopted by Carboxylate Groups of 2,6 NDC [7,8].

In the literature, MOFs developed from Zn^{+2} metal precursor and 2,6 naphthalene dicarboxylic acid is denoted as IRMOF-8 shown in Figure 3.3. These MOFs belongs to the family of IRMOF i.e. Isoreticular metal organic framework (IRMOF-1-16) which are series of MOFs that owns similar network topology (discussed in Background) [9-11]. With the replacement of organic unit in IRMOF-1 (MOF-5), other IRMOFs have been obtained with superior functionalities. Following the topology of MOF-5, IRMOF-8 has a cubic structure with extremely high surface area and porosity which led to H_2 storage

applications. However, the surface area of these MOFs exceeded when compared to IRMOFs that was developed using a longer linker (IRMOF-20) than that of 2,6 NDC. This odd behavior of IRMOF-8 was scrutinized by many researchers, which has finally led to number of reasons such as extra-framework zinc species, incomplete activation and interpenetration in IRMOF-8 [12-14].

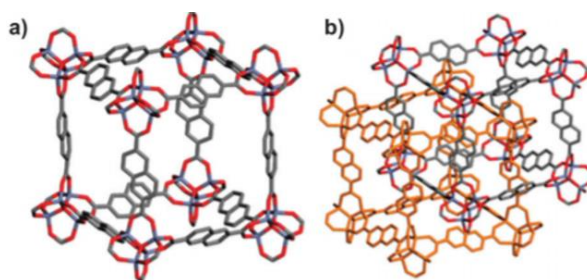


Figure 3.3. Structure of (a) IRMOF-8 and (b) Interpenetrated IRMOF-8 Analogue [11].

Taking advantage of its structural versatility, in this aim, IRMOF-8 is chosen to provide experimental evidence supporting the behavior as semiconductor among wide range of IRMOFs ($n = 1-16$) considering two important factors:

- 1) **Structural orientation:** The Zinc metal cluster is coordinated to six naphthalene centers forming a network. The oxygen atom of the Zn_4O lies at the center of the cluster with the tetrahedral coordination of four Zn atoms [12, 13]. The coordination bonding between metal and ligand may provide a pathway for charge carrier transport.
- 2) **Analogue of IRMOF-8:** Interpenetrated networks are reported in very few classes of IRMOFs as reported in the case of IRMOF-8 which is an interwoven identical network structure arising from Zn_4O nodes [14]. The

extended ligands in the network may result in π - π stacking resulting in charge transport.

To complete the Aim 1, this research targets the following three research tasks.

Task 1: Synthesis and characterization of MOF (**Zn-MOF**).

Proposed synthetic strategy

Characterization: FTIR, XPS, TGA, XRD

Task 2: Investigate morphology using solvent driven self-assembly

Characterization: SEM and TEM.

Task 3: Investigate opto-electronic properties of synthesized MOFs

Characterization: UV-Vis, Fluorescence and two probe I-V test system

b) Aim 2 -To Investigate the effect of different carboxylate linkers on magnetic properties in Fe-MOFs.

Hypothesis: The Fe-MOFs developed with different organic linkers may provide a way to tailor magnetic properties of iron-based isorecticular MOFs.

3.1.2.2 Material Selection Approach to Magnetic – MIL-88

MOFs with magnetism could be designed using three different approaches: (1) Bond (intrinsically); (2) Space (extrinsically) and (3) Synergistic approach (Extrinsically and intrinsically). The choice of moment carriers (metals), interaction (molecular approach) and interacting distance (length of the linker) are some of the deciding factors in implementing magnetism in MOFs [15, 16]. Addressing the Aim 2 of this project, synthetic strategy proposed in this research with appropriate choice of metal and different length linkers is used for developing MOFs with tailored-made magnetic behavior.

Considering the requirements, transition metals especially those containing paramagnetic centers in particular first row transition metals (V, Mn, Fe, Co, Ni, Cr and Cu) are well suitable as moment carriers. These metals offer advantage of existing in different oxidation states allowing possibility of spin quantum number and magnetic anisotropy [16-18]. The exchange between the moment carriers requires a certain range of distance which can often be achieved in MOFs depending upon the topology of organic ligand chosen. Aromatic linkers with different topology such as 1,4-benzene dicarboxylic acid (1,4 BDC), 2,6-naphthalene dicarboxylic acid (2,6 NDC) and Biphenyl-4,4'-dicarboxylic acid (4,4 BPDC) are considered to investigate and tailor the magnetic properties. These organic linkers were extensively used to develop rigid frameworks taking advantage of various modes of coordination [7, 8].

Among various transition metals, a trinuclear Fe^{+3} is chosen as metal nodes or metal cluster due to its paramagnetic nature and mixed valency that could account for unsaturated metal centers while developing MOFs. In the literature, microstructures of MOFs developed from trimeric metallic centers with dicarboxylate ligands has led to the formation of new structural type iron (III) dicarboxylate MIL-88 (MIL = Matériaux de l'Institut Lavoisier/ Materials from the Lavoisier Institute). In this isoreticular series, MOFs consisting of Fe (III) – μ_3 – oxo clusters linked together through organic linkers exhibit great variety of topology, pore size and properties [19, 20]. According to previous reports, the isoreticular series of MOFs with MIL-88 topology were used in variety of applications such as photocatalytic activity [21-24], antibacterial properties [25-28], sensing [29, 30] and drug delivery [31, 32]. However, in this work, MIL-88 are chosen to

provide experimental evidence supporting the behavior as magnetic material that is designed using proposed method in the research. In this aim 2, MIL-88 is chosen considering two important factors:

- 1) **Structural orientation:** The Fe metal centers are equivalent, in which they are octahedrally bound to six oxygen ligands with additional triple bridging oxide at the center of the equilateral triangle. These trinuclear building units remains intact while exchange of acetate cations with the dicarboxylates [33].
- 2) **Ligand replacement strategy:** Previously, considering the structure of parent MOF i.e. MIL-88 (Figure 3.4), various structures of possible isorecticular analogues were predicted using computational modelling by replacing the linker. Taking advantage of the strategy, magnetic properties of MOFs could be investigated and tailored by replacing the linker [19].

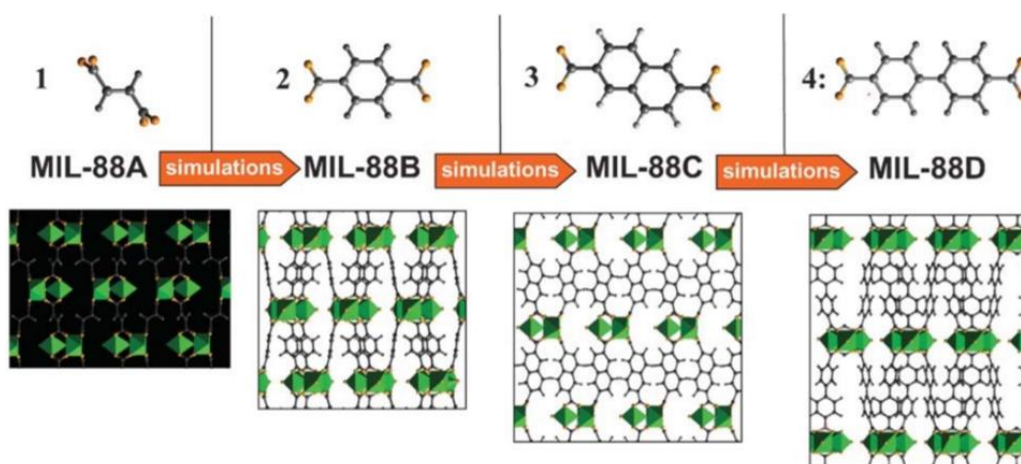


Figure 3.4. Depiction of Linker Replacement Strategy for Computational Prediction of Isorecticular MOF Structures – MIL-88 Family [19].

To complete the Aim 2, this research targets following three tasks:

Task 1

- a) Synthesis of MOF using Iron acetate (III) and 1,4-benzene dicarboxylic acid.
- b) Synthesis of MOF using Iron acetate (III) and 2,6-naphthalene dicarboxylic acid.
- c) Synthesis of MOF using Iron acetate (III) and Biphenyl-4,4'-dicarboxylic acid.

Characterization: Material composition – FTIR, XPS, and XRD,

Morphological studies – SEM, TEM.

Task 2: Investigate the magnetic behavior and textural properties with respect to length of the linker.

Characterization: M-H and M-T curves (PPMS), BET analysis and TGA.

(c) Aim 3: Investigating luminescence properties of Mn-MOF.

Hypothesis: Manganese metal with wide variety of oxidation states may provide a pathway to tailor luminescence behavior of manganese-based metal organic framework.

3.1.2.3 Material Selection Approach to Magnetic – Mn-MOF

The origin of luminosity in MOFs is based on the following four mechanisms (1) Ligand based emission; (2) Metal based emission; (3) Charge transfer process – Ligand to metal charge transfer (LMCT) and Metal to ligand charge transfer (MLCT); and (4) Guest molecule (incorporation)[3]. Based on the previous reports in literature, MOFs containing transition metal ions shows emission centered on the ligand while MOFs containing lanthanide ions exhibit metal centered emission. The choice of metal precursor

and its coordination environment provide solid rationale in determining the pathway of luminescence mechanism and provide flexibility to tailor its optical properties [34-36]. Thus, considering the MOF structure in aim1, 2,6-naphthalene dicarboxylic acid is used as a linker while substituting Zinc metal precursor with Manganese to develop Mn-MOFs with tailorable luminescence. However, combination of metal- ligand, interaction between metal and ligand, and interaction between ligands are some of the deciding factors in incorporating luminescence in MOFs.

Considering the requirements, transition metals especially first row transition metals are well suitable as they consist of more than one oxidation state. Among various transition metals, Mn^{+2} is chosen as metal nodes or metal cluster as it is one of the elements with a very rich variety of electronic properties with multi-electron redox-active center [37-39]. As mentioned above, 2,6-naphthalene dicarboxylic acid as an organic linker is chosen due to the presence of π - π conjugated systems that facilitate the inter/intra-ligand charge transfer in the MOFs. To date, MOFs developed from 2,6-naphthalene dicarboxylic acid like (1) $Zn_4O(NDC)_3$ and (2) $Mg_3(NDC)_3$ were used in gas adsorption studies due to their high surface area[6, 40, 41]. In order to design MOFs with higher surface area, the metal precursor was replaced with Mn^{+2} in the previously reported MOFs. The structural confirmation of Mn-MOF developed from 2,6-naphthalene dicarboxylic acid was similar to $Mg_3(NDC)_3$ which is reportedly applicable for gas adsorption studies. Thus, the structural characteristics, coordination geometry and variation of MOF geometry can potentially enable a pathway to tailor the functionalities and obtain MOFs with superior functionalities. In this case the absorbance and emission

with excited lifetime behavior is explored [7, 42, 43]. In this work, Mn-MOFs are chosen to provide experimental evidence supporting the behavior as luminescent material that is designed using proposed method in the research. In this Aim 3, Mn-MOF is chosen considering two important factors:

- 1) **Structural orientation:** The trimeric Mn_3 metal clusters are coordinated via six carboxylate units of NDC ligands to form three-dimensional (3D) network of Mn-MOFs. The carboxylate units of 2,6-naphthalene dicarboxylic acid follow either bidentate or tridentate coordination modes to form 3D network [7] offering flexibility to alter the structural characteristics which in turn having a profound influence on origin of luminescence.
- 2) **Time resolved emission measurements:** Excited lifetime behavior of designed Mn-MOFs also used to understand the local environment and rigidity of 2,6-naphthalene dicarboxylic acid in MOF structures.

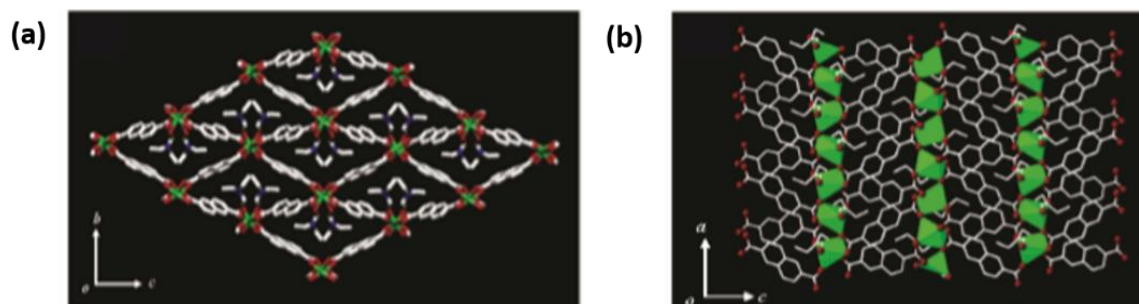


Figure 3.5. (a) Top View Showing 3D Framework Generating 1D Channels Running Along a Direction; (b) Side View Showing That Mn^{II} 1D Chains are Linked With Each Other Via Naphthalene Rings of NDC. Color Code: Mn, Green; C, White; O, Red; N, Blue [37].

To complete the Aim 3, this research targets following three tasks:

Task 1: Synthesis and characterization of Mn-MOF, Proposed synthetic strategy

Characterization: FTIR, XPS, TGA, XRD.

Task 2: Investigate optical and excited lifetime behavior of Mn-MOFs

Characterization: UV-Vis spectroscopy, Fluorescence, and transient absorption spectroscopy.

3.2 Characterization

3.2.1 Electrical Properties

The mechanism of charge transport in metal organic framework is evaluated using techniques like Hall effect measurements, field effect transistors (FETs) and diode conductivity measurements. In this case, two probe method is used to evaluate the conductivity of the samples.

3.2.1.1 Sample Preparation

The sample preparation for electrical conductivities was measured using ITO substrates. Before thin film deposition, the substrates were washed with dichloromethane in an ultrasonic bath for ten minutes, followed by washing with soap solution. Then the substrates were rinsed in deionized water and treated with mixture of ammonium hydroxide and hydrogen peroxide for 15 min at 50-70°C. Then the substrates were again rinsed with deionized water in an ultrasonication for 15 min and blown dry with dry argon. Then the cleaned ITO substrates were subject to UV cleaning for 35 min prior to deposition of the sample. For the MOF solution, 25 mg into 500 μ L DMF was spin coated

on the substrate at the rate of 1000 rpm for 60s followed by vacuum drying under nitrogen atmosphere [44].

3.2.1.2 Device Fabrication

Electrical conductivities of all test devices were measured using either ITO as a counter anode and copper as a counter cathode or copper as a common electrode using two-probe method. For this purpose, spin-coated thin films of microstructures only devices were fabricated. For device fabrication, the films of the materials are deposited on the ITO substrates, and then the proper electrodes like Cu or Ag to make ohmic contacts are deposited using E-beam physical vapor deposition[45, 46], which is shown in Figure 3.6.

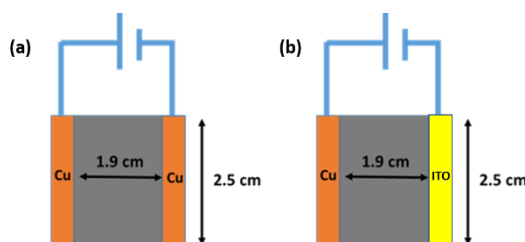


Figure 3.6. Device Scheme for Electrical Measurements: (a) Cu to Cu; (b) Cu to ITO.

3.2.1.3 Electrical Measurements

It is basically conducted on thin films using two-point probe resistivity method [41]. The resistivity and conductivity of materials can be obtained from the current-voltage curve using Equation (3.1). The current-voltage relationship i.e. I-V curves gives the graphical representation of the relationship between the voltage applied across an electrical device and the current flowing through it. The important properties of the electronic device can be understood from the shape and details of the curve, enabling

greater insight into their operation shown in Figure 3.7. Conductance of the samples is calculated from the slope of the ohmic region of I–V curves and conductivities are obtained from Equation (3.1):

$$\rho = \frac{Gl}{a}, \quad (\text{Eq. 3.1})$$

where ρ is conductivity, G is conductance, and l and a are channel length and area, respectively. Each sample is tested multiple times to ensure reproducibility of the results.

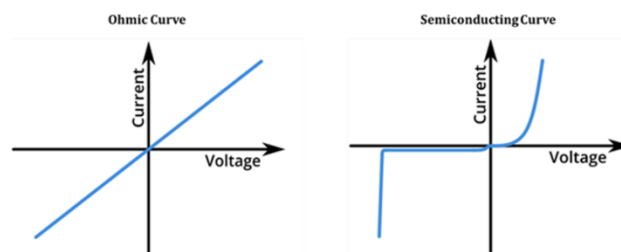


Figure 3.7. Graphical Representation of (a) Ohmic, (b) Semiconducting Curve [46 b].

The mechanism of electrical conductivity in MOFs is accomplished by charge hopping within the framework. However, only handful of well characterized electrically conductive have been reported. The primary objective of this work is to synthesize MOFs, which inherently show semiconducting behavior by using modified conventional method. Generally, in solid state semiconductor, the approach to impart tunable conductivity is achieved using atomic dopants that can create free electrons or holes. In a way, the dopant atoms serve as guest molecule. Therefore, guest molecules that possess necessary electronic properties will be incorporated onto MOF surface to have semiconductor behavior[45, 46a].

3.2.2 Magnetic Properties

3.2.2.1 Sample Preparation

Magnetic measurements are performed on powdered samples of synthesized Fe-MOFs using vibrating sample magnetometer (VSM) attached to a Quantum Design Physical Property Measurements System (PPMS). Samples were washed prior to the measurements, with DMF followed by acetone and dried in vacuum for 24 hours.

3.2.2.2 Magnetic Measurements

It is generally measured on thin films or powdered samples, and in this case, a known weight of the sample powder is carefully loaded in the opening of the powder sample. Then it is sealed as the second piece compresses the sample in brass half tube followed by placing it at the center of the mounting station [47]. The vibrating sample magnetometer feature in Quantum Design Physical Property Measurements system (PPMS) is used to measure magnetization as a function of magnetic field (H) and temperature (T) to determine the coercivity and blocking temperature, respectively. Two important key features of ferromagnetic material are spontaneous magnetization and the existence of magnetic ordering temperature. Thus, M-H and M-T studies are performed to determine the magnetic nature of the material.

3.2.2.3 M-H Measurements

The hysteresis loop is a function of variation in magnetization (M) and magnetic field strength (H) which describes the magnetic response of the sample when exposed to a magnetic field. For hysteresis loop measurement, the point of saturation is achieved by applying a DC (H_{\max}) magnetic field strong enough and then followed by decreasing step

by step to $-H_{\max}$. Similarly, the applied field changes from $-H_{\max}$ to H_{\max} for reverse direction. At each step, the magnetic moment is measured, and hysteresis loop is obtained [47]. In this project, The M-H measurements were carried out at multiple temperatures ranging from 10 K to 300 K. The shape of hysteresis loop obtained will demonstrate the type of the magnetism acquired by the sample shown in Figure 3.8. The demanding parameters of loop are the remanence (M_r), the intrinsic coercivity (H_c) and the saturation magnetization (M_s) which determines the nature of the magnetic material.

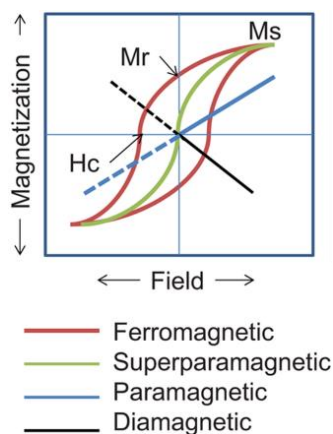


Figure 3.8. Hysteresis Loop Showing Different Nature of Magnetism [50].

3.2.2.4 M-T Measurements

Curie temperature in principle helps in determining the intrinsic property of the material. It is measured and identified using the typical plot between magnetization and temperature. Even though electronic exchange forces in ferromagnets are very large, thermal energy eventually overcomes the exchange and produces a randomizing effect [48-50]. All ferromagnets have a maximum temperature where the ferromagnetic property disappears as a result of thermal agitation. In this project, The M-T

measurements entailed zero field cooled (ZFC) process where the sample is cooled from room temperature to 10 K in zero field and then a magnetic field of 200 G is applied. The magnetization is recorded while warming up the samples from 10 K to 300 K.

3.2.2.5 Vibrating Sample Magnetometer (VSM)

The working principle of VSM is based upon Faraday's law which states that an emf. is induced in a conductor as the magnetic field changing is proportional to the rate of change of flux. With respect to stationary pick up coils, a sample magnetized by a homogenous magnetic field vibrates sinusoidally at small fixed amplitude. With the moment of the sample, the magnetic field, which is proportional to magnetic moment, M , adjust the magnetic flux through coils. This induces a voltage across the terminals of the pick-up coils. Thus, the voltage is proportional to the magnetization of the sample by the following relationship.

$$V(t) = C \frac{df_i(t)}{dt}, \quad (\text{Eq. 3.2})$$

where $f_i(t)$ represents the (changing) flux in the pick-up coils caused by the moving magnetic sample. Thereafter, the coil output voltage is combined with the output from the displacement transducer to produce a magnetization signal. Variations in vibration amplitude and frequency are then cancelled out. The signal is then detected by a high gain but narrow bandwidth "lock-in amplifier" and fed along with the applied field signal to an x-y plotter to generate a hysteresis loop [47].

3.2.3 Optical Properties

In order to investigate the origin of MOFs luminosity, absorbance, and emission studies of MOFs in both solution and thin film were studied using UV-Vis spectra and photoluminescence spectroscopy. The on-set wavelengths of the thin films UV-Vis spectra were used to calculate the optical band gaps and band gap energy was calculated from Equation (3.3).

$$E = \frac{hc}{\lambda} \quad (\text{Eq. 3.3})$$

Here, h is Planck's constant, c is the speed of light, and λ is the on-set wavelength. In future, excited state lifetime measurements will be conducted to study the luminescence properties.

3.2.3.1 Experimental Approach

Absorption and emission studies were conducted in solution and thin film. In the current study, ethanol was used as a solvent, as it provides better solubility. For solution analysis, a MOFs sample (~ 1 mg) were dissolved in ethanol solution (Stock solution- 1mg/1mL) followed by ~ 500 μ L of solution (Stock solution) is taken and mixed with ethanol solution (~1 mL). It was then transferred to UV-vis cell and collected the spectra. Also, emission spectra were collected in solution. For thin film analysis: ITO substrates were washed and cleaned. After drying, 5mg/1mL sample was spin coated on the ITO substrate (1000rpm, 60sec). Once thin film was deposited, the samples were investigated using UV-Vis spectra [44].

3.2.3.2 Transient Absorption Spectra

Excited state lifetime measurements were conducted by our collaborator, Dr. Hammer at University of Mississippi. Excited state fluorescence lifetimes were obtained in 70% ethanol solution in a quartz cuvette. The 800 nm output from a Coherent Astrella fs amplifier laser was used to pump a Light Conversion optically parametric oscillator (OPO) laser to generate 340 nm laser light with a bandwidth less than 100 fs. Fluorescence emission was collected at 90 degrees from the excited sample using an Electro-Optics Technology, Inc ET-2000 silicon photodiode detector with a rise time of less than 350 ps. The instrument response function was obtained by detection of excitation laser light. Scattering by the solvent solution alone was also recorded for comparison. The excited state lifetime was fit to a single exponential.

3.2.4 Material Composition

1. The chemical composition and functional groups of synthesized MOFs were analyzed using Fourier transform infrared spectroscopy (FTIR-Varian 670-IR spectrometer).
2. Thermal stability of microstructures was analyzed using the thermogravimetric analyzer (Q500).
3. Textural properties such as high surface area and porosity was analyzed using Brunauer- Emmett-Teller (BET).
4. The elemental composition and oxidation state of the MOF elements were obtained from an elemental composition analyzer and X-ray photon spectroscopy (XPS-Escalab Xi+-Thermo Scientific) respectively.

3.2.4.1 Sample Preparation

Samples were heated up to 700 °C at the rate of 10 °C/min in the flow of nitrogen. The samples (MOFs) for FTIR, XPS and TGA were analyzed in powder form, which were obtained after washing and drying in vacuum for 24 hours. For BET analysis, the samples obtained were activated by soaking the samples in chloroform for three consecutive days and replacing with fresh chloroform for every 6 hours. Prior to measurements the samples were dried under vacuum at 80°C for 3 hours followed by degassing of samples at 150°C for 12 hours.

3.2.5 Morphology and Crystalline Packing

The morphology and the size of the MOFs were analyzed using transmission electron microscopy (TEM Carl Zeiss Libra 120) at 120 keV and scanning electron microscopy (Zeiss Auriga FIB/FESEM). The crystalline packing was investigated using powder XRD analysis Cu Ka radiation (40 kV, 40 mA, $k = 1.540 \text{ \AA}$) with a speed of 60 s on the X-ray diffractometer (XRD, Agilent technologies Gemini) and selective area electron diffraction (SAED) pattern was also obtained from the TEM under dark field diffraction mode. The experimental XRD data obtained for MOFs was compared to simulated data generated from the acquired crystal structures from either Crystallographic Open Data Center (CODC) or Cambridge Crystallographic Data Center (CCDC)[51].

3.3 References

- [1] L. S. Xie, G. Skorupskii, and M. Dincă, “Electrically Conductive Metal–Organic Frameworks,” *Chemical Reviews*, 2020/04/10 2020.
- [2] X. Deng, J.-Y. Hu, J. Luo, W.-M. Liao, and J. He, “Conductive Metal–Organic Frameworks: Mechanisms, Design Strategies and Recent Advances,” *Topics in Current Chemistry*, vol. 378, no. 2, p. 27, 2020/02/24 2020.
- [3] M. D. Allendorf, C. A. Bauer, R. K. Bhakta, and R. J. T. Houk, “Luminescent metal–organic frameworks,” *Chemical Society Reviews*, 10.1039/B802352M vol. 38, no. 5, pp. 1330-1352, 2009.
- [4] C. H. Hendon, D. Tiana, and A. Walsh, “Conductive metal–organic frameworks and networks: fact or fantasy?,” *Physical Chemistry Chemical Physics*, 10.1039/C2CP41099K vol. 14, no. 38, pp. 13120-13132, 2012.
- [5] M. D. Allendorf *et al.*, “Guest-Induced Emergent Properties in Metal–Organic Frameworks,” *The Journal of Physical Chemistry Letters*, vol. 6, no. 7, pp. 1182-1195, 2015/04/02 2015.
- [6] S. Agrawal *et al.*, “Novel semiconducting iron–quinizarin metal–organic framework for application in supercapacitors,” *Molecular Physics*, vol. 117, no. 22, pp. 3424-3433, 2019/11/17 2019.
- [7] B. Liu *et al.*, “Microporous coordination polymers of cobalt(II) and manganese(II) 2,6-naphthalenedicarboxylate: preparations, structures and gas sorptive and

- magnetic properties,” *Microporous and Mesoporous Materials*, vol. 111, pp. 470-477, 04/01 2008.
- [8] Z.-L. Chen *et al.*, “A novel coordination polymer based on 2,6-naphthalenedicarboxylic acid: synthesis, crystal structure and luminescence sensing,” *Transition Metal Chemistry*, vol. 45, no. 2, pp. 121-128, 2020/02/01 2020.
- [9] N. Saffon-Merceron, A. Vigroux, and P. Hoffmann, “Crystal structure of a two-dimensional coordination polymer of formula [Zn(NDC)(DEF)] (H₂ NDC is naphthalene-2,6-dicarboxylic acid and DEF is N, N -diethylformamide),” *Acta Crystallographica Section E Crystallographic Communications*, vol. 75, pp. 1759-1762, 11/01 2019.
- [10] C. G. Silva, A. Corma, and H. García, “Metal–organic frameworks as semiconductors,” *Journal of Materials Chemistry*, 10.1039/B924937K vol. 20, no. 16, pp. 3141-3156, 2010.
- [11] J. I. Feldblyum, A. G. Wong-Foy, and A. J. Matzger, “Non-interpenetrated IRMOF-8: synthesis, activation, and gas sorption,” *Chemical Communications*, 10.1039/C2CC34689C vol. 48, no. 79, pp. 9828-9830, 2012.
- [12] Z. Mai and D. Liu, “Synthesis and Applications of Isorecticular Metal–Organic Frameworks IRMOFs-n (n = 1, 3, 6, 8),” *Crystal Growth & Design*, vol. 19, no. 12, pp. 7439-7462, 2019/12/04 2019.
- [13] D. J. Tranchemontagne, J. R. Hunt, and O. M. Yaghi, “Room temperature synthesis of metal-organic frameworks: MOF-5, MOF-74, MOF-177, MOF-199, and IRMOF-0,” *Tetrahedron*, vol. 64, no. 36, pp. 8553-8557, 2008/09/01/ 2008.

- [14] R. S. Pillai, M. L. Pinto, J. Pires, M. Jorge, and J. R. B. Gomes, "Understanding Gas Adsorption Selectivity in IRMOF-8 Using Molecular Simulation," *ACS Applied Materials & Interfaces*, vol. 7, no. 1, pp. 624-637, 2015/01/14 2015.
- [15] G. Mínguez Espallargas and E. Coronado, "Magnetic functionalities in MOFs: from the framework to the pore," *Chemical Society Reviews*, 10.1039/C7CS00653E vol. 47, no. 2, pp. 533-557, 2018.
- [16] M. Kurmoo, "Magnetic metal-organic frameworks," *Chemical Society Reviews*, 10.1039/B804757J vol. 38, no. 5, pp. 1353-1379, 2009.
- [17] E. Coronado, "Molecular magnetism: from chemical design to spin control in molecules, materials and devices," *Nature Reviews Materials*, vol. 5, no. 2, pp. 87-104, 2020/02/01 2020.
- [18] A. E. Thorarinsdottir and T. D. Harris, "Metal-Organic Framework Magnets," *Chemical Reviews*, 2020/02/11 2020.
- [19] F.-X. Coudert and A. Fuchs, "Computational Characterization and Prediction of Metal-Organic Framework Properties," *Coordination Chemistry Reviews*, vol. 307, 06/26 2015.
- [20] S. Surblé, C. Serre, C. Mellot-Draznieks, F. Millange, and G. Férey, "A new isorecticular class of metal-organic-frameworks with the MIL-88 topology," *Chemical Communications*, 10.1039/B512169H no. 3, pp. 284-286, 2006.
- [21] Y. Li *et al.*, "TiO₂ Nanoparticles Anchored onto the Metal-Organic Framework NH₂-MIL-88B(Fe) as an Adsorptive Photocatalyst with Enhanced Fenton-like Degradation of Organic Pollutants under Visible Light Irradiation," *ACS*

- Sustainable Chemistry & Engineering*, vol. 6, no. 12, pp. 16186-16197, 2018/12/03 2018.
- [22] T. Vu *et al.*, “Highly photocatalytic activity of novel Fe-MIL-88B/GO nanocomposite in the degradation of reactive dye from aqueous solution,” *Materials Research Express*, vol. 4, 02/14 2017.
- [23] W.-T. Xu *et al.*, “Metal–organic frameworks MIL-88A hexagonal microrods as a new photocatalyst for efficient decolorization of methylene blue dye,” *Dalton Transactions*, 10.1039/C3DT52574K vol. 43, no. 9, pp. 3792-3798, 2014.
- [24] B. Xu, H. Yang, Y. Cai, H. Yang, and C. Li, “Preparation and photocatalytic property of spindle-like MIL-88B(Fe) nanoparticles,” *Inorganic Chemistry Communications*, vol. 67, 03/01 2016.
- [25] M. Shen *et al.*, “Antibacterial applications of metal–organic frameworks and their composites,” *Comprehensive Reviews in Food Science and Food Safety*, vol. n/a, no. n/a.
- [26] A. Guo, M. Durymanov, A. Permyakova, S. Sene, C. Serre, and J. Reineke, “Metal Organic Framework (MOF) Particles as Potential Bacteria-Mimicking Delivery Systems for Infectious Diseases: Characterization and Cellular Internalization in Alveolar Macrophages,” *Pharmaceutical Research*, vol. 36, no. 4, p. 53, 2019/02/21 2019.
- [27] G. Wyszogrodzka, B. Marszałek, B. Gil, and P. Dorożyński, “Metal-organic frameworks: mechanisms of antibacterial action and potential applications,” *Drug Discovery Today*, vol. 21, no. 6, pp. 1009-1018, 2016/06/01/ 2016.

- [28] D. Xie *et al.*, “Bifunctional NH₂-MIL-88(Fe) metal–organic framework nanooctahedra for highly sensitive detection and efficient removal of arsenate in aqueous media,” *Journal of Materials Chemistry A*, 10.1039/C7TA07934F vol. 5, no. 45, pp. 23794-23804, 2017.
- [29] S. Hou *et al.*, “Green synthesis and evaluation of an iron-based metal–organic framework MIL-88B for efficient decontamination of arsenate from water,” *Dalton Transactions*, 10.1039/C7DT03775A vol. 47, no. 7, pp. 2222-2231, 2018.
- [30] S. Duan and Y. Huang, “Electrochemical sensor using NH₂-MIL-88(Fe)-rGO composite for trace Cd²⁺, Pb²⁺, and Cu²⁺ detection,” *Journal of Electroanalytical Chemistry*, vol. 807, pp. 253-260, 2017/12/15/ 2017.
- [31] H. Pham *et al.*, “Tuning Crystal Structures of Iron-Based Metal–Organic Frameworks for Drug Delivery Applications,” *ACS Omega*, vol. 5, no. 7, pp. 3418-3427, 2020/02/25 2020.
- [32] A. C. McKinlay *et al.*, “Nitric Oxide Adsorption and Delivery in Flexible MIL-88(Fe) Metal–Organic Frameworks,” *Chemistry of Materials*, vol. 25, no. 9, pp. 1592-1599, 2013/05/14 2013.
- [33] A. Laurikėnas, J. Barkauskas, J. Reklaitis, G. Niaura, D. Baltrūnas, and A. Kareiva, “Formation peculiarities of iron (III) acetate: Potential precursor for iron metal-organic frameworks (MOFs),” *Lithuanian Journal of Physics*, vol. 56, 04/26 2016.
- [34] Y. Guo *et al.*, “Tuning the Luminescence of Metal–Organic Frameworks for Detection of Energetic Heterocyclic Compounds,” *Journal of the American Chemical Society*, vol. 136, no. 44, pp. 15485-15488, 2014/11/05 2014.

- [35] T. Islamoglu *et al.*, “From Transition Metals to Lanthanides to Actinides: Metal-Mediated Tuning of Electronic Properties of Isostructural Metal–Organic Frameworks,” *Inorganic Chemistry*, vol. 57, no. 21, pp. 13246-13251, 2018/11/05 2018.
- [36] M. Hosseini, D. E. P. Vanpoucke, P. Giannozzi, M. Berahman, and N. Hadipour, “Investigation of structural, electronic and magnetic properties of breathing metal–organic framework MIL-47(Mn): a first principles approach,” *RSC Advances*, 10.1039/C9RA09196C vol. 10, no. 8, pp. 4786-4794, 2020.
- [37] Moon, H. R., Kobayashi, N., & Suh, M. P. (2006). Porous Metal– Organic Framework with Coordinatively Unsaturated MnII Sites: Sorption Properties for Various Gases. *Inorganic chemistry*, 45(21), 8672-8676.
- [38] Y.-P. Zhao, H. Yang, F. Wang, and Z.-Y. Du, “A microporous manganese-based metal–organic framework for gas sorption and separation,” *Journal of Molecular Structure*, vol. 1074, pp. 19-21, 2014/09/25/ 2014.
- [39] K. M. L. Taylor, W. J. Rieter, and W. Lin, “Manganese-Based Nanoscale Metal–Organic Frameworks for Magnetic Resonance Imaging,” *Journal of the American Chemical Society*, vol. 130, no. 44, pp. 14358-14359, 2008/11/05 2008.
- [40] T. Ladrak, S. Smulders, O. Roubeau, S. J. Teat, P. Gamez, and J. Reedijk, “Manganese-Based Metal–Organic Frameworks as Heterogeneous Catalysts for the Cyanosilylation of Acetaldehyde,” *European Journal of Inorganic Chemistry*, vol. 2010, no. 24, pp. 3804-3812, 2010.

- [41] Y. Li *et al.*, “A manganese-based metal-organic framework electrochemical sensor for highly sensitive cadmium ions detection,” *Journal of Solid State Chemistry*, vol. 275, pp. 38-42, 2019/07/01/ 2019.
- [42] T. Panda, P. Pachfule, and R. Banerjee, “Template induced structural isomerism and enhancement of porosity in manganese(ii) based metal–organic frameworks (Mn-MOFs),” *Chemical Communications*, 10.1039/C1CC12278A vol. 47, no. 27, pp. 7674-7676, 2011.
- [43] M. A. Nasalevich *et al.*, “Electronic origins of photocatalytic activity in d0 metal organic frameworks,” *Sci Rep*, vol. 6, p. 23676 Accessed on: 2016/03//. doi: 10.1038/srep23676
- [44] S. Dawood, R. Yarbrough, K. Davis, and H. Rathnayake, “Self-assembly and optoelectronic properties of isoreticular MOF nanocrystals,” *Synthetic Metals*, vol. 252, pp. 107-112, 2019/06/01/ 2019.
- [45] C. H. Hendon, A. J. Rieth, M. D. Korzyński, and M. Dincă, “Grand Challenges and Future Opportunities for Metal–Organic Frameworks,” *ACS Central Science*, vol. 3, no. 6, pp. 554-563, 2017/06/28 2017.
- [46] (a) A. M. Ullman *et al.*, “Transforming MOFs for Energy Applications Using the Guest@MOF Concept,” *Inorganic Chemistry*, vol. 55, no. 15, pp. 7233-7249, 2016/08/01 2016. (b) <https://www.ossila.com/pages/iv-curves-measurement>
- [47] N. K. G. Yamoah, “Magnetic Properties of Fe₉₀W₁₀ Powder and Thin Films for Use as Permanent Magnets “ DOCTOR OF PHILOSOPHY Mechanical Engineering North Carolina A&T State University, 2016, 2016.

- [48] A. G. Kolhatkar, A. C. Jamison, D. Litvinov, R. C. Willson, and T. R. Lee, "Tuning the magnetic properties of nanoparticles," (in eng), *International journal of molecular sciences*, vol. 14, no. 8, pp. 15977-16009, 2013.
- [49] G. A. Paterson, X. Zhao, M. Jackson, and D. Heslop, "Measuring, Processing, and Analyzing Hysteresis Data," *Geochemistry, Geophysics, Geosystems*, vol. 19, no. 7, pp. 1925-1945, 2018.
- [50] Kolhatkar, A. G., Jamison, A. C., Litvinov, D., Willson, R. C., & Lee, T. R. (2013). Tuning the magnetic properties of nanoparticles. *International journal of molecular sciences*, 14(8), 15977-16009.
- [51] T. C. C. D. C. (CCDC). [Online]. Available: <https://www.ccdc.cam.ac.uk/>.

CHAPTER IV

EXPERIMENTAL SECTION

4.1 Materials

All the samples used in this research were obtained from commercial providers (such as Sigma-Aldrich, STREM chemicals and Fisher scientific,) and used without any purification. Metal precursors such as Zinc(II)acetate dihydrate, $\text{Zn}(\text{CH}_3\text{CO}_2)_2 \cdot 2\text{H}_2\text{O}$ (> 99.0% pure), Manganese (II) acetate tetrahydrate, $\text{Mn}(\text{CH}_3\text{CO}_2)_2 \cdot 4\text{H}_2\text{O}$ (>99.0% pure) and Iron(III)acetate, anhydrous 97% were purchased from STREM chemicals. Organic linkers such as 1,4-benzene dicarboxylic acid (BDC), 2,6-naphthalene dicarboxylic acid (NDC), and Biphenyl- 4,4'- dicarboxylic acid, were purchased from Sigma Aldrich. Anhydrous Dimethyl formamide (DMF) with 99.8% purity was the solvent of choice purchased from Sigma -Aldrich. Solvents, acetone and 70 % v/v ethanol (EtOH), purchased from Fisher Chemicals were used for washing the samples and for performing spectroscopic analysis in solutions. Chloroform (HPLC grade) used to soak the samples for BET analysis was purchased from Fisher Chemicals.

4.2 Characterization

The XRD analysis of synthesized MOFs was obtained using X ray- powder diffractometer (Agilent technologies Gemini) with copper source (Cu Ka radiation). The surface area and pore volume of synthesized MOFs were obtained using micrometric analyzer with N_2 adsorption-desorption isotherms measured at 77 K prior to degassing of

samples at 150 °C for 6 hours. Thermogravimetric analysis (Q 500) was conducted under nitrogen atmosphere heating the samples up to 700 °C at the increment of 100 °C/ min to determine the thermal stability of MOFs. The Fourier transform infrared spectroscopy (FT-IR Varian 670-IR spectrometer) was recorded in the range of 500-4000 cm⁻¹ to identify the functional groups of MOFs. Further, the surface electronic state and chemical composition of synthesized compounds were obtained using X-ray photon spectroscopy (XPS-Escalab Xi+- Thermos Scientific). A scanning electron microscope (Zeiss Auriga FIB/FESEM) and Transmission electron microscope (TEM Carl Zeiss Libra 120) were used to observe the morphologies of final microstructures.

The absorption and emission spectra were acquired using UV-Vis spectrometer (Varian Cary 6000i) and fluorimeter (Horiba Fluoro-max 4). The electrical properties were determined using Keithley source meter controlled by Photo Emission TEC. INC (PET) I–V test system. E-beam evaporation (Kurt Lesker PVD 75 e-beam evaporator) was used to deposit Cu layer with thickness of 100nm. Thin films were prepared by spin coating the sample onto ozone/UV treated substrates of either quartz plates or ITO coated glass substrates. Ozone/ UV treatment was performed using Bio Force UV/Ozone Pro Cleaner. The Magnetic properties were measured using Vibrating sample magnetometer (VSM) and integral part of Quantum Design Physical property measurement system (PPMS). Excited state lifetime measurements were conducted using 800 nm output from a Coherent Astrella fs amplifier laser which was used to pump a Light Conversion optically parametric oscillator (OPO) laser to generate 340 nm laser light with a bandwidth less than 100 fs.

4.3 Synthesis Procedures

4.3.1 Synthesis Procedure for IRMOF-8A

In this procedure, anhydrous DMF (2 mL) was injected into a 25 mL one-necked round bottom flask and mixture of zinc acetate (100 mg, 0.400 mmol) and 2,6-naphthalene dicarboxylic acid (198 mg, 0.800 mmol) were added. Initially, the reaction mixture was stirred for 15 min at room temperature followed by solvothermal annealing at 260 °C for 7 minutes to yield a white crystalline powder. The end product obtained was washed with cold DMF, followed by acetone, and then it was dried under vacuum to yield pure crystalline product of MOFs. The yield of FT-IR stretching (cm^{-1}); 3158 (broad OH), 1695 (carboxylate carbonyl), 1540-1600 (aromatic C=C bonds), and 1400-1355 (C-O-Zn); XPS composition analysis is presented in the Table 4.1.

Table 4.1

XPS Data Obtained for IRMOF-8A (Zn-MOFs)

Elemental Transition Peak	Energy (eV)	Chemical & Oxidation States	Weight Wt. %
C 1s	284 & 288	C-C & O-C=O	47.63
O1s	531	Zn-O-C	24.81
Zn 2P 2p _{3/2} & 2p _{1/2}	1022.5 & 1045	Zn ⁺²	27.56

4.3.2 Synthesis Procedure for MIL-88B

In a typical process, 1, 4-benzene dicarboxylic acid (50 mg, 0.2 mmol) and Iron (III)acetate (78 mg, 0.4 mmol) were added to anhydrous DMF (2 mL) solution. The

reactants were stirred for 15 minutes at room temperature prior to heating to 260 °C for 7 minutes. The resulting pinkish powder were collected by centrifugation and immediately washed with cold DMF to remove unreacted BDC. The powdered samples were then washed with de-ionized water thrice. Finally, the sample was dried under vacuum at 800 °C for 12 hours for further characterization. FT-IR stretching (cm^{-1}); 3294 (broad OH), 1646 (carboxylate carbonyl), 1497-1584 (aromatic C=C bonds), and 1377 (C-O-Fe); XPS composition analysis is presented in Table 4.2.

Table 4.2

XPS Data Obtained for MIL-88B (Fe-BDC)

Elemental transition peak	Energy (eV)	Chemical and Oxidation States	Weight Wt. %
C1s	283.42 & 286.23	C-C, C-O-C	41.41
O1s	530.19	Fe-O-C	32.73
Fe 2p 2p _{3/2} & 2p _{1/2}	710.83, 715.53 723.78	Fe ⁺² & Fe ⁺³	25.77

4.3.3 Synthesis Procedure for MIL-88C

Light brown pure crystalline product of MIL-88C was prepared using similar method as mentioned above but mixing 2,6-naphthalene dicarboxylic acid (50 mg, 0.2 mmol) and Iron (III) acetate ((78 mg, 0.4 mmol). The samples were washed and dried using above mentioned procedure. FT-IR stretching (cm^{-1}); 3457 (broad OH), 1661 (carboxylate carbonyl), 1586-1600 (aromatic C=C bonds), and 1419 (C-O-Fe); XPS composition analysis is presented in Table 4.3.

Table 4.3

XPS Data Obtained for MIL-88C (Fe-NDC)

Elemental transition peak	Energy (eV)	Chemical & Oxidation State	Weight Wt. %
C1s	284.54 & 287.37	C-C, O-C=O	50.89
O1s	530.28	Fe-O-C	33.05
Fe 2p 2p _{3/2} & 2p _{1/2}	710.83, 715.53, 723.78	Fe ⁺² & Fe ⁺³	14.92

4.3.4 Synthesis Procedure for MIL-126

Dark brown pure crystalline product of MIL-126 was prepared using the same procedure with Biphenyl-4,4'-dicarboxylic acid (50 mg, 0.2 mmol) and Iron (III) acetate (78 mg, 0.4 mmol). The samples were washed and dried using above mentioned procedure. FT-IR stretching (cm⁻¹); 3500 (broad OH), 1670 (carboxylate carbonyl), 1605 (aromatic C=C bonds), and 1400-1355 (C-O-Fe); XPS composition analysis is presented in Table 4.4.

Table 4.4

XPS Data Obtained for MIL-126 (Fe-BPDC)

Elemental Transition Peak	Energy (eV)	Chemical & Oxidation State	Weight Wt. %
C1s	284.1 & 288.2	C-C & O-C=O	50.96
O1s	530.28	Fe-O-C	30.09
Fe 2p 2P _{3/2} & 2P _{1/2}	710.7, 715.5, 7123.84	Fe ⁺² & Fe ⁺³	18.95

4.3.5 Synthesis Procedure for Mn-MOFs (Mn-NDC)

Mn-MOF was prepared using manganese (II) acetate and 2,6-naphthalene dicarboxylic acid as precursors in DMF according to proposed synthesized method. In this procedure, anhydrous DMF (2 mL) was injected into a 25 mL of round bottom- flask and a mixture of manganese acetate (50 mg, 0.27 mmol) and 2,6-naphthalene dicarboxylic acid (88 mg, 0.48 mmol) was added. Initially, the reaction mixture is stirred for 15 minutes at room temperature followed by solvothermal process at 260 °C for 7 minutes to yield a crystalline yellowish powder. The end product obtained was washed with cold DMF, followed by acetone, and then it was dried under vacuum to yield pure crystalline product of MOFs. FT-IR stretching (cm^{-1}); 3369 (broad OH), 1538-1604 (aromatic C=C bonds), and 1394 (C-O-Mn); XPS composition is presented in Table 4.5.

Table 4.5

XPS Data Obtained for Mn-MOF (Mn-NDC)

Elemental Transition Peak	Energy (eV)	Chemical & Oxidation State	Weight Wt.%
C1s	283.52 & 286.61	C-C & O-C=O	56.16
O1s	530.50	Mn-O-C	23.78
Mn 2p 2P _{3/2} & 2P _{1/2}	640.42, 644.4 & 652.15	Mn ⁺² & Mn ⁺³	20.06

CHAPTER V

RESULTS AND DISCUSSION

5.1 Designing and Synthesizing Self-assembled Hierarchical Microstructures of IRMOF-8 to Investigate Optoelectronic Properties of MOF

5.1.1 Introduction

Designing reticular metal-organic framework with desirable properties depends primarily on the synthesis method, choice of the organic linker, and the metal precursor. Typically, solvothermal method and room temperature synthesis methods with a mixture of the organic linker and metal salt in a solvent are used to synthesis MOFs. Recent synthesis methods like microwave, sonochemical, electrochemical, are currently implemented to design MOFs with superior functionalities [1-5]. To date, significant research efforts have been demonstrated to develop isorecticular series (IRMOFs) with chemical formulae $Zn_4O(L)_3$ (where L is a rigid linear dicarboxylates). These MOFs belong to the family IRMOFs, which share similar cubic topological structure as that of prototypical MOF-5, developed from zinc precursor and 1,4 Benzene dicarboxylic acid [6-9]. This family of isorecticular MOFs i.e. IRMOFs-n (n=1-16) gained significant attention in gas storage community due to its high pore volume and surface area. Among the IRMOFs series, IRMOF-8 has been extensively studied for gas adsorption and photoluminescence properties[10-12]. In the area of MOFs, the main desire is to design MOFs with electrically conductive properties and to optimize the charge transport mechanism suitable for developing electronic devices. Numerous applications of MOFs

with different types of synthesis methods are being investigated, but the approach for the preparation of electrically conductive MOFs for electronic devices is still at its infancy stage. The research study conducted in this dissertation work is the first case investigating optical and electrical properties of interpenetrating analogue of IRMOF-8 (INT-IRMOF-8). A modified synthetic strategy is designed by optimizing previously used synthesizing methods discussed in **Chapter 3**. In this method, the parameters like temperature and the amount of solvent used are optimized to obtain highly porous hierarchical structures of INT-IRMOF-8. The synthesis method developed in this work is based on the solvent-driven self-assembly process, which allows tailoring the morphology (IRMOF-8A). This simple and rapid self-assembly process initiates the growth of nanocrystals and self-assembled them into highly crystalline structures of MOFs with promising optoelectronic properties. The chemical composition, solvent-driven morphology analysis, thermal stability, crystallinity and solid-state packing, and optoelectrical properties were investigated [13].

5.1.2 Synthesis and Characterization of IRMOF-8

In the typical synthesis method, a solvent-driven self-assembly followed by the solvothermal method, IRMOF-8A was successfully synthesized by mixing zinc acetate with the organic linker, 2,6-naphthalene dicarboxylic acid by maintaining a molar ratio of 1:4 in a minimum volume of DMF. Then the resulted white slurry paste was subjected to heat in a crucible at 260 °C for 7 minutes, yielding the product as a white crystalline powder. The synthetic scheme for the formation of IRMOF-8A is depicted in Figure 5.1.

The resulted crystalline powder was washed with cold DMF and dried under vacuum to collect highly pure IRMOF-8A as a white crystalline powder.

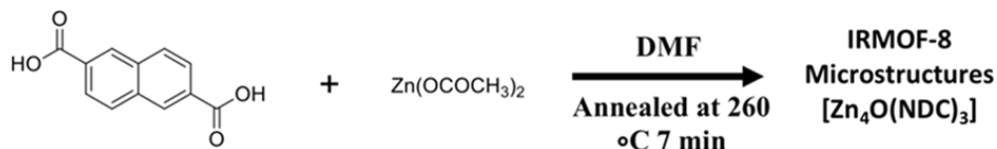


Figure 5.1. Synthetic Route of IRMOF-8A.

Coordination between Zn^{+2} metal ion with carboxylate units of naphthalene moiety was confirmed from FTIR analysis. The FT-IR spectrum shown in Figure 5.2 (a) confirmed the microstructures of IRMOF-8A, showing the stretching at 1685 cm^{-1} which signifies the metal ion coordinated carbonyl stretching of the carboxylate units of naphthalene. Further, it confirms the aromatic $\text{C}=\text{C}$ bond stretching as it is seen in the range of 1540 to 1600 cm^{-1} . The presence of $\text{C}-\text{O}-\text{Zn}$ at 1400 – 1355 cm^{-1} shows the significant co-ordination of 2, 6-naphthalene dicarboxylic acids to Zn^{+2} . Finally, the stretching at 3158 cm^{-1} , which is a broad OH stretching, shows the presence of water in the pores of MOFs [14].

To determine the chemical formulae of the IRMOF-8A and the oxidation states of Zn, XPS was performed. Figure 5.2. (b) shows the XPS spectra of Zn $2p$ containing two sharp distinct peaks at 1022.5 and 1045 eV . XPS analysis reveals the oxidation state of zinc from the binding energy spectrum, which shows binding energies for the typical Zn^{+2} oxidation state with respect to Zn $2\text{P}_{3/2}$ and Zn $2\text{P}_{1/2}$ spin-orbit states centered at 1022.5 eV and 1045.0 eV . The elemental composition analysis confirmed the unit formula of the IRMOF-8A and was found to be $\text{Zn}_4\text{O}(\text{NDC})_3$, which agreed with the

theoretical elemental composition calculated for the unit molecular formula for IRMOF-8A [13].

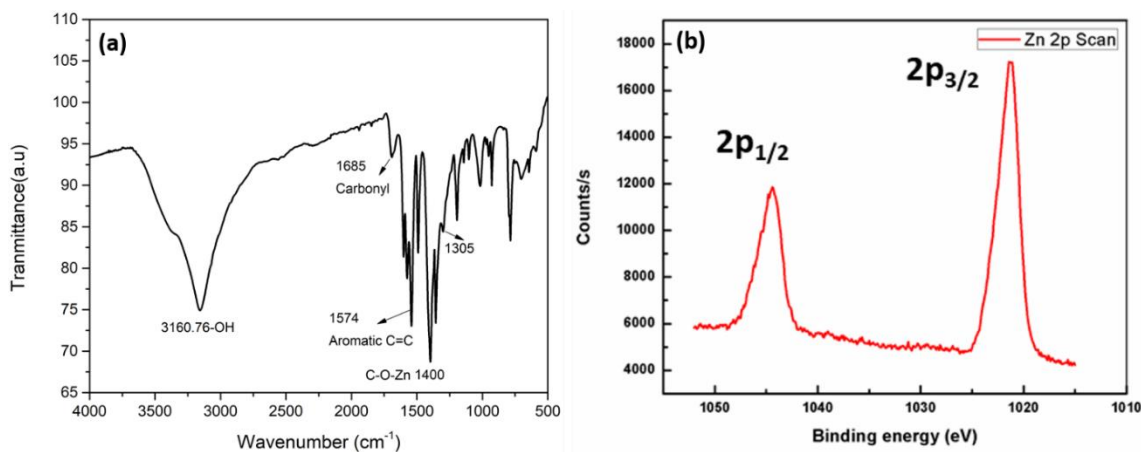


Figure 5.2. (a) FTIR Spectra of IRMOF-8A; (b) XPS of Zn 2P (IRMOF-8A).

The thermal behavior of IRMOF-8A was analyzed by Thermogravimetric analyzer (TGA). The TGA profile was recorded under air from room temperature to 700 °C with a heating rate of 10 °C/min. As depicted in Figure 5.3, the results show that IRMOF-8A structure is stable up to 350 °C. The TGA profile showed three distinct weight losses at 200 °C, 340 °C, and 440 to 500 °C. The initial weight loss of less than 10% at 200 °C could be due to the loss of free and lattice water molecules and solvent molecules (DMF) incorporated into the pores of the MOFs. The second notable weight loss of 40% can be attributed to the removal of carboxylate groups and phenyl rings from organic ligands in the framework. The broader temperature range of 440 - 500 °C is indicative of decomposing residual organic fractions (50% weight loss) and collapsing the framework to form the residual metal oxide [13].

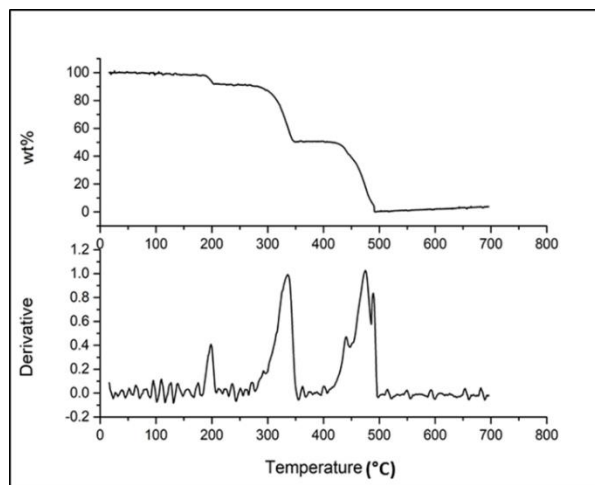


Figure 5.3. TGA Graph of IRMOF-8A.

5.1.2.1 Crystalline Studies

The powder XRD patterns of microstructures (experimental), IRMOF-8 (simulated), and INT-IRMOF-8A (simulated) is shown in Figure 5.4 (a). The powder XRD patterns of the microstructures synthesized using the modified solvothermal method at 260 °C revealed the formation of the product INT-IRMOF-8A when compared with simulated data of IRMOF-8 and INT-IRMOF-8A referred in the literature [15] when compared with simulated data of IRMOF-8 and INT-IRMOF-8A. The simulated data was generated from the acquired crystal structures from Cambridge crystallographic Data Center (CCDC). The experimental pattern was in good agreement with the simulated pattern of INT-IRMOF-8A indicating that unit cell structure and the crystalline phases formed in the experimental microstructures and simulated INT-IRMOF-8A are the same. Figure 5.4 (b) and 5. 4(c) show the crystal structure for IRMOF-8 and INT-IRMOF-8A generated from crystallography data from CCDC [15]. The INT-IRMOF-8A crystallizes

in the primitive cubic topology with the space group P -1 and a lattice parameter of $a = 19.11\text{\AA}$, $b = 23.02\text{\AA}$, and $c = 30.07\text{\AA}$ (CCDC-957268).

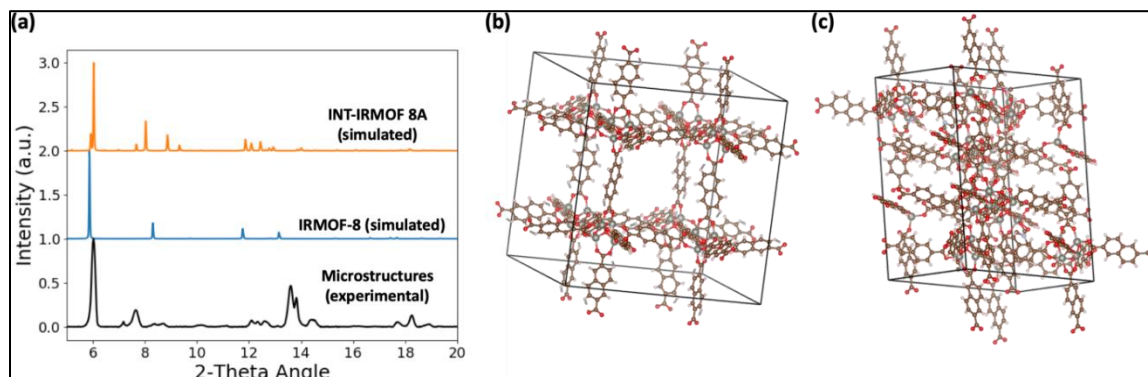


Figure 5.4. (a) The Powder XRD Spectrum of Microstructures and Simulated Powder XRD Spectra of Original IRMOF-8 and Interpenetrated IRMOF-8A; (b) the Crystal Structure Generated from the Originally Reported Crystal Structures of IRMOF-8; (c) the Crystal Structure Generated from the Crystallography Data of INT-IRMOF 8A.

From the crystallographic analyses, it is evident that the packing pattern of microstructures follows the two-fold interpenetrated analogue of IRMOF-8. As it is depicted in Figure 5.5 (a), these are two interpenetrated networks that are constructed from Zn_4O clusters and off-sets layer by layer arrangements of NDC linkers, resulting a primitive cubic (pcu) lattice topology. In the Zn_4O cluster, the oxygen atom which lies in the center of the cluster is coordinated to four Zn atoms. For Zn nodes two types of coordination structures are found. One is tetrahedral and other is octahedral. Three Zn atoms of the cluster ZnO_4 take tetrahedral coordination and the remaining one Zn atom take ZnO_6 octahedral coordination, with additional two oxygen atoms from DMF and water molecules in ZnO_6 . The NDC linkers are bridged to Zn atoms through the oxygen atoms of carboxylate functional groups [15]. Further, the selected area diffraction

(SAED) for a single microstructure of MOF was taken from TEM under dark diffraction by directing the electron beam at 90° angle to one of the microstructure's truncated hexagon faces as depicted in Figure 5.5 (b) [13]. The SAED pattern viewed along the [001] axis supports the *pcu* topology and their interpenetrated layer-by-layer packing pattern. Further, first, second, and third order facets of the nanocrystals along their (100) diffraction planes confirm the off-sets layer by layer packing pattern in the interpenetrated network of IRMOF-8A seen in Figure 5.5 (b)[13].

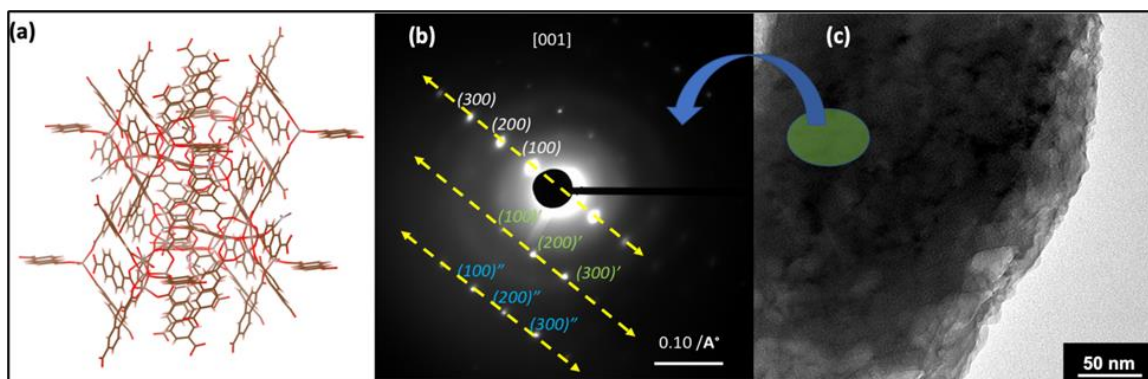


Figure 5.5. (a) A View of Two Identical Interpenetrated Network of IRMOF-8A Crystal Structure Units with Off-sets Layer-by-layer Packing Arrangement; (b) The SAED Pattern of Microstructure Taken from the TEM Under Dark Field Diffraction Mode; and (c) A TEM Image of Microstructures of IRMOF-8A.

5.1.2.2 Solvent-dependent Morphology Studies

The morphology studies of IRMOF-8A were performed by using scanning and transmission electron microscopy. The SEM images in Figure 5.6. showed truncated hexagonal and irregular shaped micro-structures with average widths and lengths are 1–2 μm and 2–4 μm , respectively. It can be inferred from the SEM images that these materials have uniform porous surface morphology with average pore size in the range of

2 nm to 19 nm. Microstructures visualized under TEM reveal that they consisted of hierarchical layers of self-assembled nanocrystals with randomly arranged voids among the nanocrystals as clearly seen in Figure 5.6.

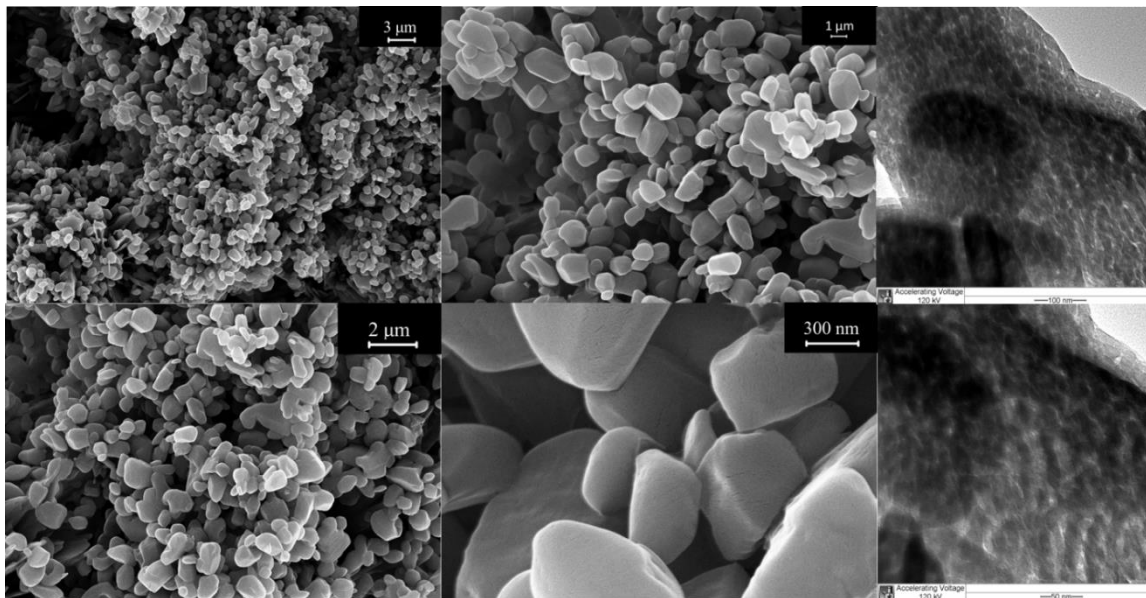


Figure 5.6. SEM and TEM Images of IRMOF-8A.

Further, the morphologies of microstructures of these MOFs were studied in three different solvents, which include butanone, toluene, and the mixture of DMF/Propanol (1:1 v/v). The type of solvent used in the synthesis method has a profound effect on the morphology. From the SEM and TEM images, it is evident that the morphologies of these MOFs changed based on different types of solvents showing that these microstructures were formed from self-assembling nanocrystals. The morphologies formed in butanone and toluene show smooth platelets with no distinct arrangement of nanocrystals or void spaces. The morphology of microstructures in DMF and propanol are thick cubes with smooth surfaces, as shown in Figure 5.7.

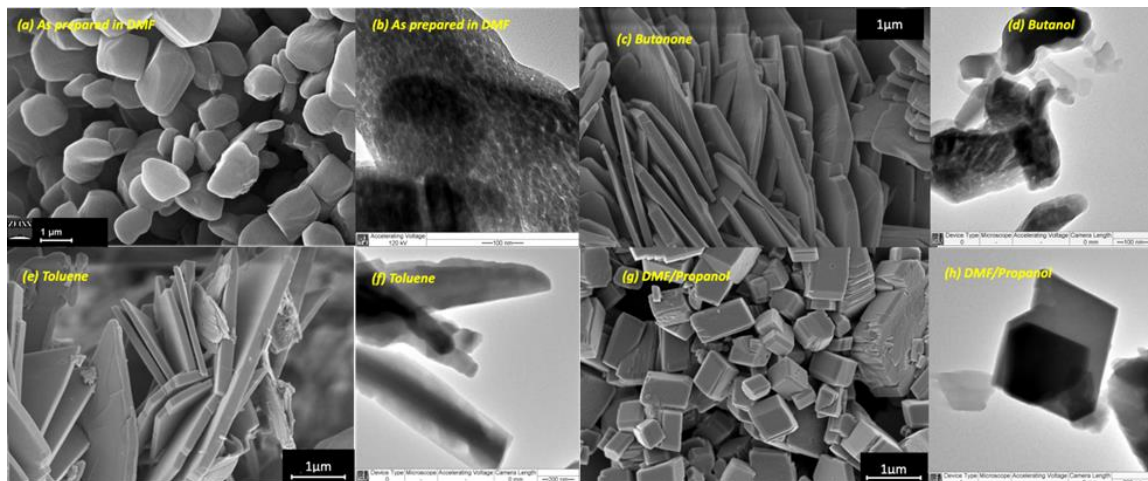


Figure 5.7. SEM and TEM Images of IRMOF-8A in Different Solvents.

5.1.2.3 Optoelectronic Properties of IRMOF-8A

Photophysical properties of IRMOF-8A was studied by acquiring UV-vis and emission spectra in solution and thin films. Zn^{+2} metal ion is an ideal metal center for building MOFs with luminescent properties as it possesses d^{10} electronic configuration. Many MOFs have been developed using 2,6-naphthalene dicarboxylic acid as an organic linker. Hence, the fluorescent properties of microstructure of IRMOF-8A and 2,6-naphthalene dicarboxylic acid in thin film and solution were investigated at room temperature. The absorption spectra of organic ligand in solution shows three pronounced peaks at 216, 284 and 344 nm with a shoulder peak at 246 nm. Similarly, the absorption spectra of IRMOF-8A show peaks at same wavelength as that of organic ligand except a weak absorption peak at 368 nm. The additional peak at longer wavelength 375 nm corresponding to excitonic transition of Zn_4O nodes where a bathochromic shift in UV-Vis absorption maximum is observed for aggregated ZnO particle [13].

In case of thin film, the absorption spectra of MOFs show three characteristics vibronic peaks at 246, 300, 360 nm with a shoulder peak at 384 nm. However, the thin film absorption spectrum of the ligand exhibits three absorption maxima at 218, 300, and 360 nm with a less pronounced shoulder peak at 246 nm as shown in Figure 5.8 (a). Thus, both the thin film absorption spectra for MOF and ligand show ~ 20 nm and 16 nm red shifts respectively, compared to that of in solution phase absorption maxima at 280 and 344 nm. The shift in peak features of thin film compared to solution may be due to intermolecular interaction attributed to the aggregation of MOF and ligand particles in solid state. The presence of high intensity absorption peak set from 220 nm to 360 nm, in the microstructures of MOFs corresponding to vibronic π - π^* absorption transitions of naphthalene core, evidence linker-based absorption favors in both solution and thin films. This behavior evidences the lack of favorable spatial and energetic overlap of the metal and the ligand orbitals.

Further, the optical band gap was calculated, from the on-set of the UV-vis spectra of MOFs and the free ligand. The UV-Vis spectra for both MOFs and free ligand was obtained in solution and thin film. In solution, the optical band gap of 3.20 eV and 3.18 eV was reported for IRMOF-8A and free ligand. Similarly, the optical band gap of 2.82 eV and 2.91 eV for IRMOF-8A and free ligand were obtained for thin films. The obtained optical band gap evidence that the microstructures of IRMOF-8A possess narrow band gap compared to ligand demonstrating the higher electron-donating ability of IRMOF-8A network when compared to free ligand [16, 17]. Thus, the narrow optical band gap evidences semiconducting behavior of IRMOF-8A evidencing strong π - π

interactions due to the interpenetrating arrangement of $\text{Zn}_4\text{O}(\text{NDC})_3$ units in the crystal packing pattern.

To study the luminescence behavior, the fluorescence emission spectra of MOFs and ligand in solution were collected upon excitation at 292 nm and is shown in Figure 5.8 (b). The emission spectrum of the microstructures shows three well-resolved emission bands with peak maxima at 350, 370, and 420 nm. These vibronic transitions are similar to that of a ligand, which further evidence linker-based emission with no indication of additional emissions due to any charge transfer processes from metal ion node to the linker of vice versa. [17, 18].

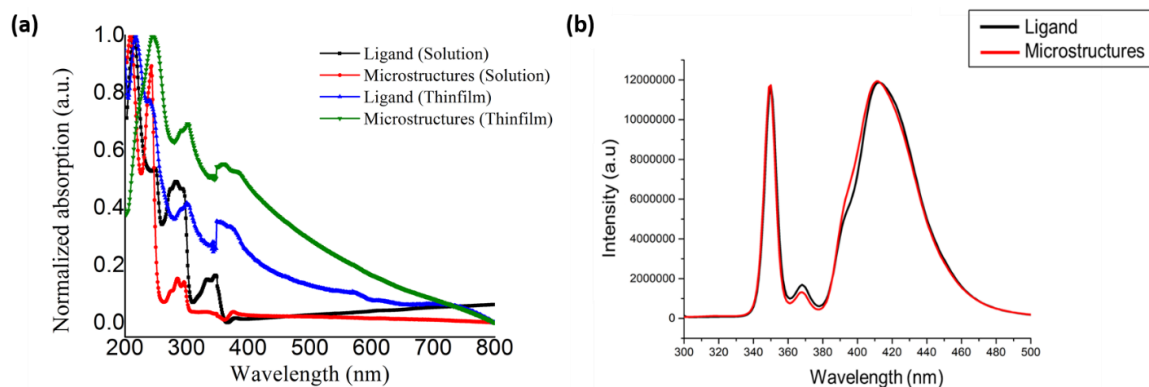


Figure 5.8. (a) UV-Vis Spectra of Microstructures in Solution (Ethanol) and Thin Films; (b) PL Emission Spectra of IRMOF-8A and the Ligand in Solution; (Excitation Wavelength is 292 nm).

The electrical properties of MOF thin films were evaluated using a two-probe technique as shown in Figure 5.9 (b). In order to investigate the conductivity of MOF thin films, we aimed first to fabricate uniform thin film using spin coating. The device was fabricated with MOF thin film using optimized parameters for spin coating and the detailed steps involved for the experimental setup are discussed in **Chapter 3**. The

average electrical conductivity of IRMOF-8A coated thin films, calculated from the slopes of the I-V curves were ranged from 3.98×10^{-2} to 2.16×10^{-2} S cm⁻¹ Figure 5.9 (a). This is the first report of electrically conductive microstructures of isorecticular MOF series. Previously reported isorecticular series IRMOFs developed through solvothermal methods were insulating in nature though they exhibit π -d conjugated structure.

Through the bond, through space and by guest molecules into the framework are three possible pathways for charge transport in the structure MOFs as discussed in **Chapter 2**. Thus the transport of charges could be facilitated by altering or improving the charge transport pathways mentioned above via (a) tailoring covalent bonding interactions between metal nodes and the ligands, (2) introducing organic ligands and metal ion that contain loosely bound electrons, (3) enhancing non-covalent interactions (4) extending the dimensional framework of hierarchical structures or 2D sheets formed by metal ions and the coordinating atoms of the ligands [38–40]. In our case, we believed that the interpenetrated network of two identical networks arising from Zn₄O metal nodes consisting of a layer-by-layer arrangement of NDC linkers in the crystal packing contributes to the electrical conductivity attributing to the π - π stacking in interpenetrated hierarchical structures of IRMOF-8A nanocrystals.

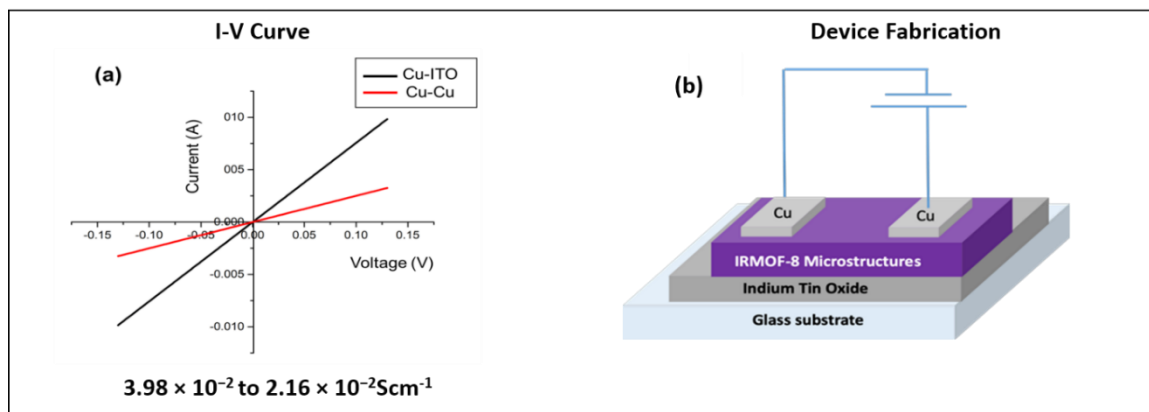


Figure 5.9. (a) I-V Curves of IRMOF-8A; (b) Device Fabricated with Casted Thin Film Microstructures.

5.1.2.4 Summary

In summary, IRMOF-8A was successfully synthesized using a modified solvent driven method thereby reporting the first isorecticular MOF with the incorporation of optoelectronic properties. These properties were investigated using a two-probe technique and absorbance-fluorescence spectroscopy. The synthesis method was rapid with good control over MOFs design achieved in 7-10 minutes which is two orders less when compared to conventional synthesis approaches. X-ray powder diffraction studies and SAED analysis have shown that this synthesis method resulted in the development of self-assembled isorecticular analogue of IRMOF-8 with modified crystalline packing and structural orientation i.e. IRMOF-8A. The TGA profile of IRMOF-8A has shown that this material is stable over the temperature range of 300-350 °C without distorting the framework. The detailed characterization involving composition analysis and morphological studies confirm that they are uniform 3D porous microstructures with the unit formulae of $\text{ZnO}_4(\text{NDC})_3$. A noticeable change in the surface morphology in terms

of pore uniformity, size, and shape of MOFs was observed with the type of solvent used during the synthesis process. The absorption and emission spectra of these robust material evidence ligand base emission in these microstructures. Further, the optical gap obtained from absorption spectra reveals the semiconducting behavior of these MOFs. Thus, the narrow optical bandgap and electrical conductivity observed for the hierarchical microstructure of IRMOF-8A nanocrystals show high potential to be considered as a luminescent semiconducting material for optoelectronic devices.

5.2 To Investigate the Effect of Different Carboxylate Linkers on Magnetic Properties in Fe-MOFs

5.2.1 Introduction

The molecular magnetism has gained significant attention due to its simplicity in molecular approach via self-assembly and its promising applications in the field of electronic industry, including molecular spintronics and quantum technologies [19]. Sharing the similar molecular approach, magnetic metal organic frameworks (MMOFs) emerge within the realm of the molecular magnetism that builds via coordination chemistry between metals and organic ligands. Despite the ability of synthetic programmability and tunability, MOFs could offer superior potential characteristics such as high operating temperature and fascinating multifunctionalities compared to molecular-based magnets [19-22]. In addition, the magnetism in most of the molecular magnets is confined in two dimensions with geometry leading to single domain magnetic states (vertical direction) restricting functionality in three dimensions (3D)[22, 23]. Thus, with advent of new technologies demand for techniques and materials with three-dimension distribution, magnetism is now a hot topic of research.

Taking advantage of structural orientation with building components in the construction of MOFs, magnetic properties could be incorporated and altered based on the desirable applications. In general, magnetism is a cooperative mechanism and it can be incorporated in metal organic framework by right choice of metals, organic linkers, synthesizing method or through incorporation of guest molecule in the pores [24]. The choice of synthesis of MOF not only provides the freedom of chemical tunability but also the ability to engineer the crystalline structure. The rigid frameworks of metal organic framework provide precise position of metal nodes in network that are bridged through organic linkers in the network, providing information about structural and crystalline complexity to understand the origin of magnetism, which is lacking in currently reported intrinsic magnetic materials [25].

The property of magnetism in MOFs is incorporated either intrinsically within the framework or by incorporation of magnetic guest molecules while the framework is non-magnetic. According to literature, majority of magnetic metal organic framework (MMOFs) are derived from paramagnetic metal centers as they exist in different oxidation states allowing the introduction of two major concepts that is spin quantum number and magnetic anisotropy [26]. Among wide range of MOFs, the work described herein is the first case investigating magnetic properties of isorecticular series of MIL-88 with hexagonal and octahedral topology by employing iron precursor and different type of carboxylate linkers i.e. 1, 4-benzene dicarboxylic acid, 2, 6-naphthalene dicarboxylic acid, and Biphenyl-4,4'-dicarboxylic acids. Three different metal carboxylates of MIL-88 with different length of organic linkers, consisting of iron metal precursor is used to

examine and identify the possibility of altering magnetic properties. The incorporation of magnetic properties in isorecticular series of MIL-88 is less explored otherwise it is a potential candidate due to its versatile topology, paramagnetic nature of metal clusters, and crystalline flexibility.

This work targets the role of the linker topology that contribute to the control and optimization of the primary magnetic properties of MOFs; Coercivity (H_C), and blocking temperature (T_B). All three MOFs were synthesized using previously published method, which is a solvent driven self-assembly process followed by solvothermal process. The morphologies, surface composition, textural properties, and magnetic properties of each system were evaluated.

5.2.2 Synthesis and Characterization of MIL-88 Series

5.2.2.1 MIL-88B

In the typical synthesis method, which follows the solvent-driven self-assembly followed by solvothermal method, MIL-88B was successfully synthesized by mixing iron(III)acetate with the organic linker, 1,4-benzene dicarboxylic acid by maintaining the molar ratio at 2:1 in a minimum volume of DMF. Then the resulted light pinkish slurry paste was subjected to heat in a crucible at 260 °C for 7 minutes, yielding the product as light pinkish crystalline powder. The synthetic scheme for the formation of MIL-88B is depicted in Figure 5.10. The crystalline powder prepared in this manner was washed with cold DMF and dried under vacuum to collect highly pure MIL-88B as light pinkish crystalline powder.

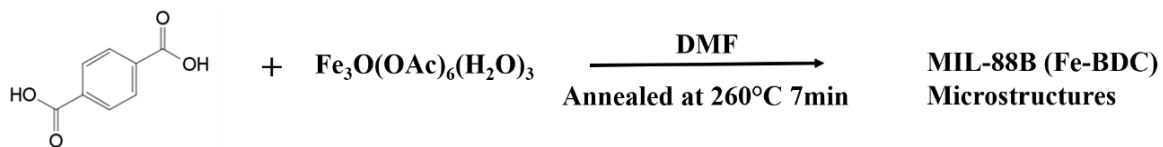


Figure 5.10. Reaction Scheme for MIL-88B.

5.2.2.2 MIL-88C

Following similar synthesis method, light brown crystalline powder of MIL-88C was obtained by mixing iron (III) acetate with the organic linker, 2,6-naphthalene dicarboxylic acid by maintaining the molar ratio of 2:1 in a minimum volume of DMF depicted in Figure 5.11. The samples were washed and dried using above mentioned procedure.

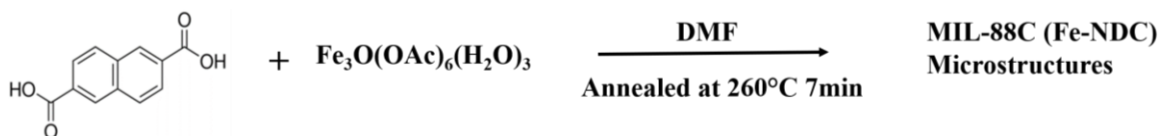


Figure 5.11. Reaction Scheme for MIL-88C.

5.2.2.3 MIL-126

Similarly, dark brown crystalline powder of MIL-126 was obtained by mixing iron (III) acetate with the organic linker, Biphenyl-4,4'-dicarboxylic acid by maintaining the molar ratio of 2:1 in a minimum volume of DMF depicted in Figure 5.12. The samples were washed and dried using above mentioned method.

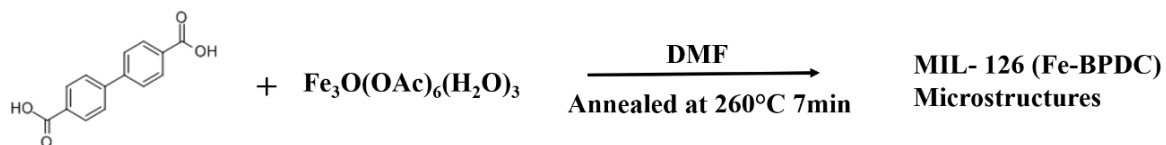


Figure 5.12. Reaction Scheme for MIL-126.

5.2.3 Material Characterization of MIL88 Analogues

The co-ordination of the metal Fe^{+3} to the organic linker of MIL-88B, MIL-88C and MIL-126 were confirmed by Fourier transform infrared spectroscopy (FT-IR). As depicted in Figure 5.13 (a) (b), and (c), the bands at 3254 cm^{-1} , 3270.16 cm^{-1} and 3003.93 cm^{-1} in MIL-88B, MIL-88C and MIL-126 are attributed to the O-H stretching corresponding to adsorbed water in the pores of the MOFs [14]. Further, the vibration in the region of 1586 cm^{-1} , 1567 cm^{-1} and 1537 cm^{-1} for MIL-88B, MIL-88C and MIL-126 corresponds to aromatic C=C bond stretching. The bonds at 1665 cm^{-1} in MIL-88B signifies C=O carbonyl stretching and the presence of C-O-Fe at 1379 cm^{-1} further confirms the significant co-ordination of 1,4-benzene dicarboxylic acid to Fe^{+3} . Similarly, the vibrational bonds at 1661 cm^{-1} and 1666.09 cm^{-1} were identified for MIL-88C and MIL-126 signifying the C=O carbonyl stretching. Further, the coordination of Fe^{+3} with 2,6-naphthalene dicarboxylic acid and Biphenyl-4,4'- dicarboxylic acid in MIL-88C and MIL-126, respectively, was confirmed at 1403.87 and 1394.24 cm^{-1} .

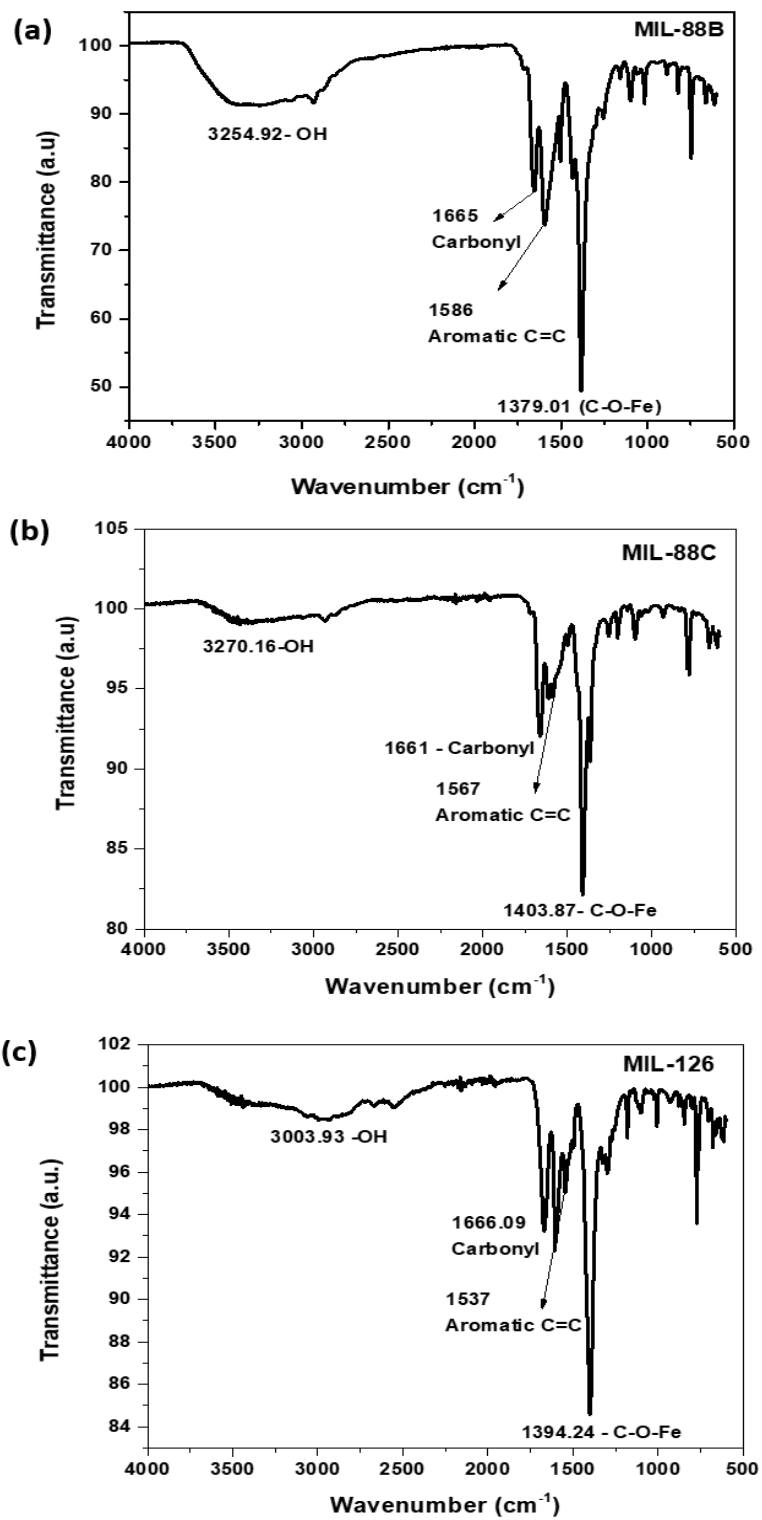


Figure 5.13. (a) FTIR Spectra of MIL-88B; (b) FTIR Spectra of MIL-88C, and (c) FTIR Spectra of MIL-126.

The chemical composition MIL-88B, MIL-88C and MIL-126 was confirmed by XPS analysis as shown in Figure 5.14. In XPS spectra, it is a well-known fact that the binding energy increases with an increase in oxidation states. The XPS survey of all the three samples confirmed the presence of Fe, C and O without any presence of impurities. All the three samples of MIL-88 analogues, i.e., MIL-88B, MIL-88C and MIL-126 showed doublet splitting for Fe $2p$ into Fe $2p_{3/2}$ and Fe $2p_{1/2}$. In all the analyzed samples the Fe $2p_{3/2}$ was observed at 710.83 (MIL-88B & C) and 710.7 (MIL-126) while Fe $2p_{1/2}$ was observed at 723.78 & 723.84 (MIL-88B & MIL-126) and 724.84 (MIL-126) corresponding to α Fe₂O₃ showing Fe⁺³ oxidation state. All the three MIL-88 analogues showed a satellite peak 715.5 eV showing the presence of Fe⁺² oxidation state. Thus, confirming the presence of mixed oxidation states of Fe⁺² and Fe⁺³ in all the three MIL-88 analogues. The C $1s$ spectrum is deconvoluted showing two broad peaks for MIL-88B and MIL-126 with binding energy of 283.42 eV and 286.23 eV and 284.1 eV and 288.2 eV corresponding to C-C and O-C=O, respectively shown in the Figure 5.14. (b&h) [30, 31]. In MIL-88C, the C $1s$ spectrum is deconvoluted showing peaks at 284.54, 287.37 eV assigned to C-C and O-C=O Figure 5.14. (e). The binding energy of the O $1s$ state at 530.2 eV is detected for all the samples, assigned to Fe-O-C showing efficient binding between the metal and the carboxylic group of linkers (metal carbonyl).

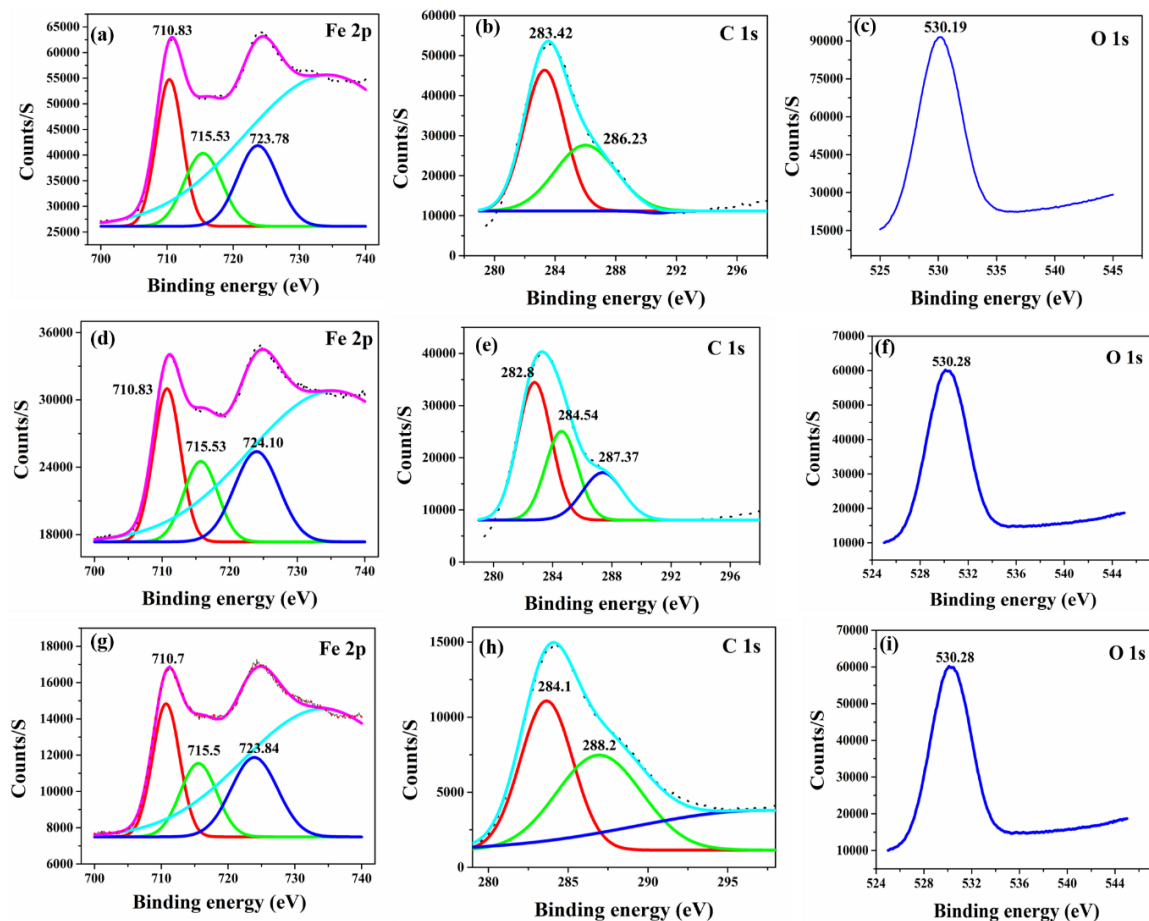


Figure 5.14. (a) Fe2p (b) C1s (c) O1s of MIL-88B; (d) Fe 2p (e) C1s (f) O1s of MIL-88C and (g) (h) and (i) of MIL-126.

5.2.4 Thermal Properties

Thermal stability of MIL-88B, MIL-88C and MIL-126 was analyzed using thermogravimetric analyzer (Figure 5.15). The MIL-88 analogues (MIL-88B, MIL-88C and MIL-126) show three distinct weight losses, initial weight loss of about 10-20 % in the temperature range of 100 °C which could be due to the loss of free solvent molecules (DMF). The second weight loss about 50% is in the temperature range of 100- 250 °C which is attributed to the removal carboxylate groups and phenyl rings present in the

organic linker. The third weight loss in the temperature range of 300 to 350 °C (Figure 5.15) accounts to decomposition of the framework resulting in collapsing of the framework. The thermal stability of MIL-88B, MIL-88C and MIL-126 is about 325 °C, 340 °C and 350 °C, respectively. The thermal stability increases with increase in the size of the linker indicating the rigidity offered by aromatic conjugated systems.

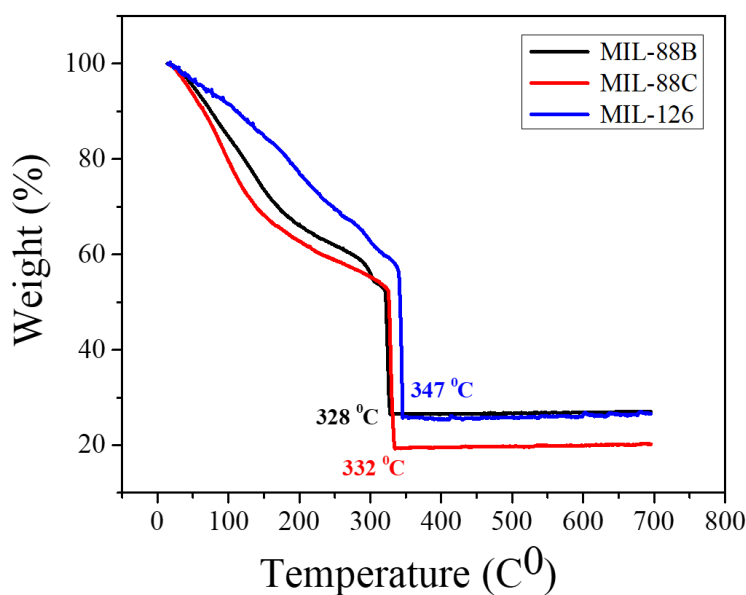


Figure 5.15. TGA of MIL-88B, MIL-88C, and MIL-126.

5.2.5 Crystalline Structure and Packing

The simulated XRD pattern of MIL-88B MIL-88C and MIL-126 was generated from the acquired crystal structures from Cambridge crystallographic Data Center (CCDC).

5.2.5.1 MIL-88B

As shown in the Figure 5.16 a, the powder XRD patterns of the microstructures synthesized using modified solvothermal method at 260°C revealed the formation of the

product MIL-88B when compared with simulated XRD pattern of MIL-88B referred in the literature. When compared, the experimental pattern was in good agreement with simulated pattern of MIL-88B. This indicates that unit cell structure and the crystalline phases formed in the experimental microstructures and simulated MIL-88B are the same. Figure 5.16 (b) show the crystal structure for MIL-88B generated from crystallography data from the CCDC [35].

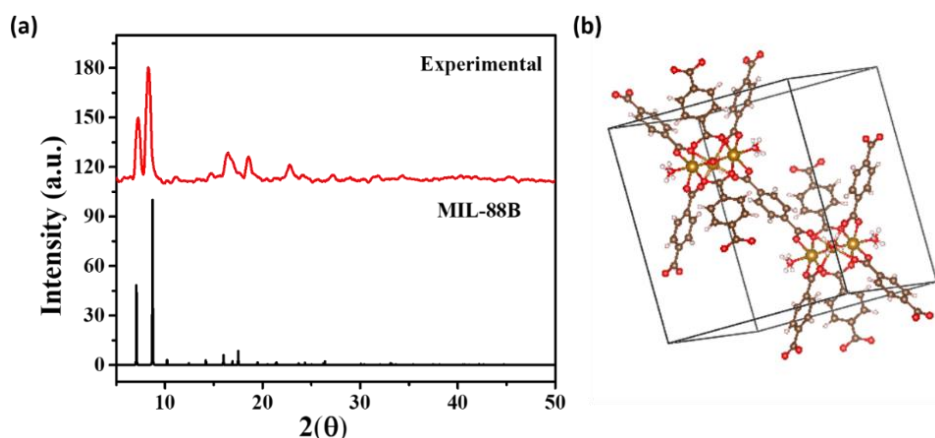


Figure 5.16. (a) XRD Spectrum of Fe-BDC MOFs and Simulated Powder XRD Spectra of Original MIL-88B; (b) the Crystal Structure Generated from the Originally Reported Crystal Structure of MIL-88B.

The MIL-88B crystallizes with lattice parameter of $a = 14.41 \text{ \AA}$ and $c = 17.30 \text{ \AA}$ (CCDC-1415803). From the crystallographic analyses, the packing pattern of microstructures follows the hexagonal symmetry with space group of $P63/mmc$ built from oxo centered trimers of iron (III) acetate units that octahedrally linked together via 1,4-benzene dicarboxylic acid units [35-38]. The simulated diffraction peaks at $2\theta = 7.14^\circ$ and 8.72° with the crystalline phases of (100) and (101) exactly matches the

experimental powder XRD diffraction peaks, confirming the crystal structure of MIL-88B.

5.2.5.2 MIL-88C

As shown in Figure 5.17 (a), the overlapping of the peaks of experimental powder XRD with the simulated XRD peaks confirms the MIL-88C crystal structure. This indicates that unit cell structure and the crystalline phases formed in the experimental microstructures and simulated MIL-88C are the same. Figure 5.17 (b) shows the crystal structure for MIL-88C generated from crystallography data from CCDC [35] [36][39]. The simulated diffraction peaks of MIL-88C (CCDC-285812) at $2\theta = 7.44^\circ$, 10.04° , 10.72° with the crystalline phases of (002) , (100) and (101) exactly matches the experimental powder XRD diffraction peaks confirming the hexagonal symmetry with $P6_2C$ space group built from oxo centered trimers of iron(III)acetate that are octahedrally linked together via 2,6-naphthalene dicarboxylic acid [39].

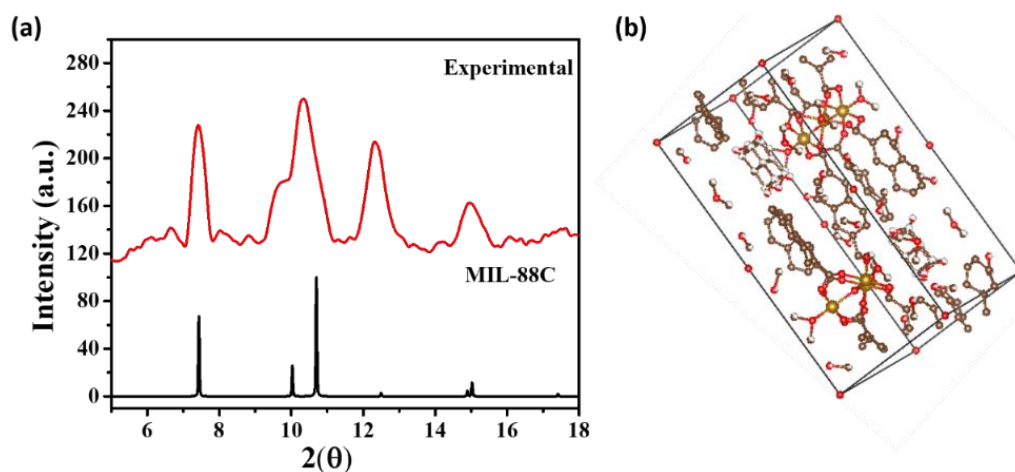


Figure 5.17. (a) XRD Spectra of Experimental and Simulated MIL-88C; (b) the Crystal Structure of MIL-88C Generated from the Originally Reported Crystal Structure of MIL-88C.

5.2.5.3 MIL-126

Similarly, the experimental PXRD pattern obtained for Fe-BPDC MOFs was compared to the simulated powder PXRD data of MIL-126 (cm300450x_si_002) developed from Iron acetate (III) and Biphenyl-4,4'-dicarboxylic acid. When compared, the obtained experimental pattern overlapped with the simulated XRD data shown in Figure 5.18 (a).

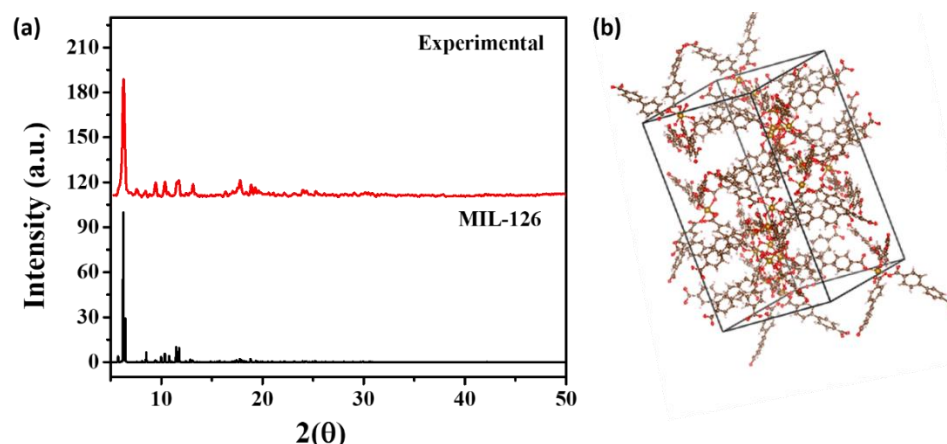


Figure 5.18. (a) XRD Spectrum of Fe-BPDC MOFs and Simulated Powder XRD Spectra of Original MIL-126; (b) the Crystal Structure Generated from the Originally Reported Crystal Structure of MIL-126.

The resulting MIL-126 is the analogue of MIL-88D which is a two-fold interwoven acs network of MIL-88D. The simulated diffraction peaks at $2\theta = 6.42^\circ$ with the crystalline phases of (111) exactly matches the experimental PXRD diffraction peaks confirming the tetragonal symmetry with the space group $P4_32_12$ built from oxo centered trimers of iron acetate (III) that are octahedrally linked together via Biphenyl-4,4'-dicarboxylic acid [29].

In general, the MIL-88 series structures are built from the trimers of Iron acetate (III) octahedrally that share a μ_3 -O oxygen with dicarboxylate forming two types of pores, one is hexagonal and other is bipyramidal cages with the trimers at the vertices. The height of the bipyramid corresponds to the C cell parameters which increases as the length of the linker increases shown in the table 1 which is evident in the synthesized MIL-88 analogues. The MIL-88 structure types are hexagonal with a space group of P-62c or P63/mmc for MIL-88C and MIL-88B and tetragonal with the space group of P4₃2₁2 for MIL-126 [35-38].

Table 5.1

Lattice Parameters of MIL-88B, MIL-88C, and MIL-126

	MIL-88B	MIL-88C	MIL-126
a (Å)	14.41620	10.17510	21.800
c (Å)	17.30400	23.77220	35.4070
V (Å³)	3114.2332	2131.461	16826.822

5.2.6 Morphological Studies of MIL-88 Analogues

In general, the morphology and structures play an important role in defining the properties and applications. The morphology and structure changes based on the composition of metal organic framework. Herein, we report the morphology and structure changes of MIL-88 analogues by varying the length of the linker. The morphological characteristics of synthesized MOFs visualized using SEM and TEM are shown in Figure 5.19. MIL-88B (Fe-BDC) had the appearance of long pyramidal spindle shaped rod with 1.4 μm in length and 0.9 μm in width with uniform size [35]. The appearance of MIL-

MIL-88C follows similar morphology with uneven sizes approximately with 1.3 μm in length and 300 nm in width. Figure 5.19. Further, the TEM images of both MIL-88B (Fe-BDC) and MIL-88C (Fe-NDC) reveals that these are self-assembled microstructures without any void spaces. In case of MIL-126 (Fe-BPDC), the microcrystal was expected to follow MIL-88 topology based on previous literature. A well-faceted large octahedral crystalline structure (Figure 5.19) was observed assuming the formation of MIL-126 MOFs (Interpenetrated structure)[37]. Microstructures visualized under TEM reveal that they are spindle shaped and octahedral shaped microstructures which clearly consists of self-assembled nanoscale crystalline domains with randomly arranged void spaces as seen in Figure 5.19.

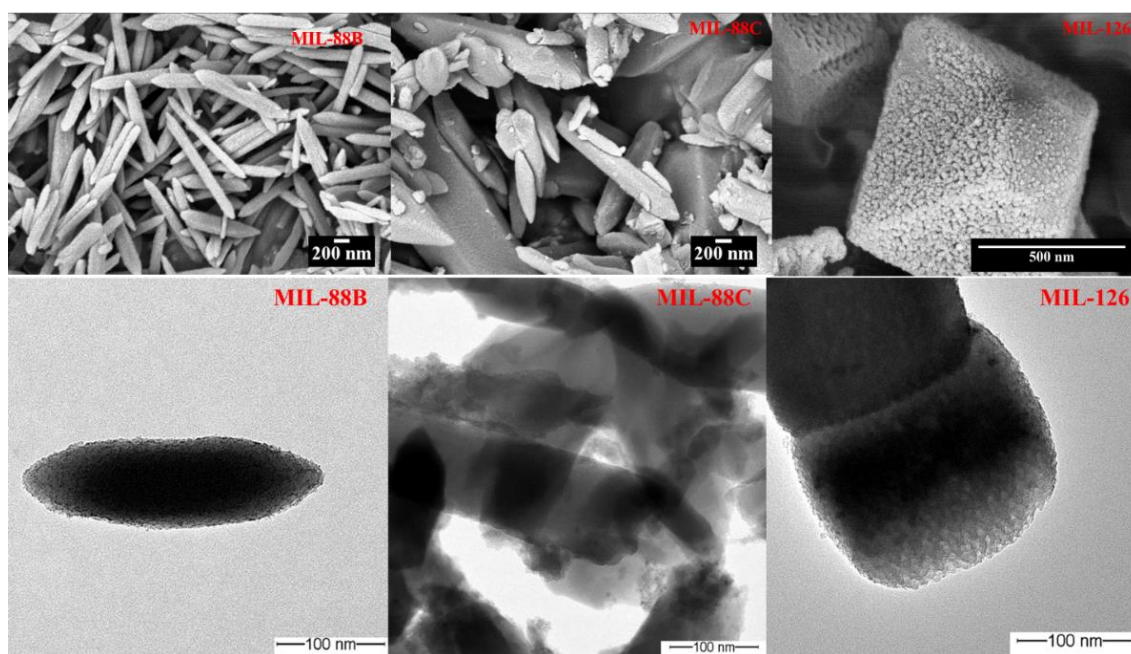


Figure 5.19. SEM and TEM Images of MIL-88B, MIL-88C, and MIL-126.

5.2.7 Textural Properties of MIL-88 Analogues

To confirm that these synthesized materials are indeed porous crystalline MOFs, MIL-88B, MIL-88C and MIL-126 were activated by performing solvent exchange with appropriate volatile solvent (chloroform), followed by heating and drying under vacuum. The isotherms of MIL-88B, MIL-88C and MIL-126 show hysteresis between adsorption/desorption curves that resembles type IV category indicating capillary condensation taking place which is typical for mesoporous materials Figure 5.20 (a) [46]. A similar type of isotherms was reported by other research groups for Fe based materials [47, 48]. The characteristic features of Type IV isotherm are associated with its hysteresis loop, and in this case the adsorption and desorption isotherms of these MOFs are classified into H3 hysteresis based on IUPAC classification [46, 48]. The particles in H3 are plate like forming slit like pores. Figure 5.20 (b) shows BJH pore distribution of all the synthesized MOFs, from which we can observe that MIL-88B, MIL-88C and MIL-126 show mesoporous nature with pore diameter of 3.8 nm, and 3.6 nm. The surface area and pore volume of MIL-88B were found to be 91.52 m²/g and 0.13 cm³/g and 95.5 m²/g, 693 m²/g for MIL-88C and MIL-126 respectively with pore volume of 0.14 cm³/g and 0.448 cm³/g. Among all the MOFs reported, MIL-126 exhibits high surface area due to interpenetrated structure with rigid frameworks that do not collapse on removal of solvent. The total pore volume of the MIL-88 series increases with increase in the length of linker. In contrast, the average pore diameter decreases for MIL-126 when compared to MIL-88B and MIL-88C due to the formation interwoven networking resulting in smaller diameter of pores.

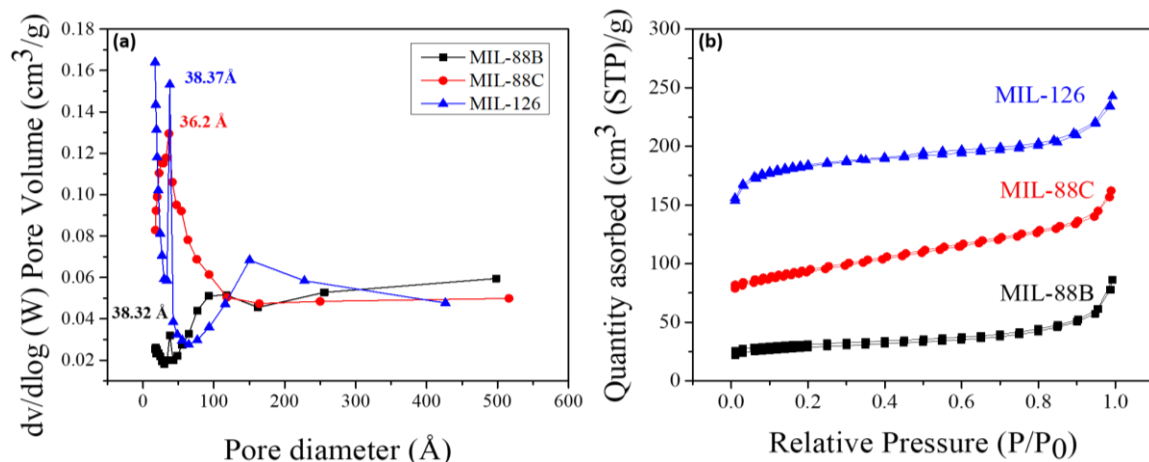


Figure 5.20. (a) N₂ Isotherms of MIL-88B, MIL-88C, and MIL-126; (b) BJH Pore Size Distribution of MIL-88B, MIL-88C, and MIL-126.

5.2.8 Magnetic Properties

5.2.8.1 Magnetization vs. Magnetic Field (M-H Curves)

To determine the magnetic behavior of the synthesized MIL-88 analogues, M-H measurements were performed using PPMS. Figure 5.21 shows the variation of the magnetization with applied magnetic field (M-H curves) at different temperatures about 10 and 300 K, respectively. Notably, at 300 K, the M- H loops for all the analogues of MIL-88 such as MIL-88B, MIL-88C and MIL-126 do not show any measurable values of H_c irrespective of the length of the linkers. This response to the external magnetic field following a sigmoidal curve with no hysteresis indicate superparamagnetic behavior [40, 41]. Upon cooling to 10 K, an increase in coercivity with a finite value and the magnetization was observed.

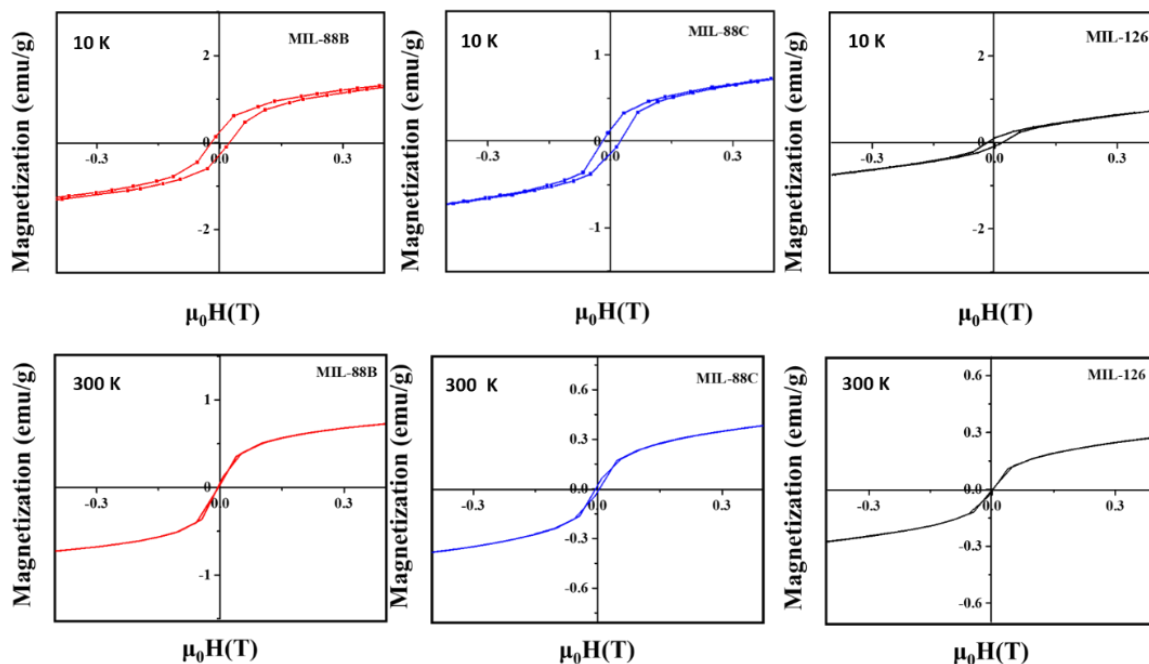


Figure 5.21. M-H Loops for Samples of MIL-88B, MIL-88C, and MIL-126 at 10 K and 300 K.

From the Figure 5. 21, it is evident that at 10K, the finite value of coercivity corresponds to ferromagnetism in which multidomain of the material are aligned due to external magnetic field [42]. The value of the coercivity decreases as the size of the linker increases due to limited communication between the metal clusters that are connected via dicarboxylate linkers. The H_c value is highest (220 G) for the Fe-BDC sample and lowest (180 G) for the Fe-BPDC sample; the H_c value of Fe-NDC sample is 210 G.

5.2.9 Magnetization vs. Temperature (M-T Curves)

In magnetic materials, the magnetic transitions (ferromagnetic and superparamagnetic) at different temperatures is analyzed by measuring the magnetization as the function of temperature in two steps. The first step is called zero-field-cooled (ZFC) and second step is called field cooled (FC). In this case, ZFC measurements were

carried out in which the samples are initially cooled from 300 K to 10 K in the absence of magnetic field. Then a small amount of magnetic field is applied (200 G), and the magnetization is measured as the temperature is increased. The M-T plots for MOF samples with three different linkers are shown in Figure 5.22. Shown in this figure is also the M-T plot for an Fe-acetate precursor sample which do not show any transition displaying paramagnetic behavior. The plots show that the magnetization of all the samples increases moderately as the temperature is increasing from 10 K, reaches a maximum peak (marked by arrows), and then decreases with a further increase in temperature. From Figure 5.22, it is evident that as the temperature increases, thermal energy causes the magnetic moments to align along the direction of magnetic field [30, 43-45].

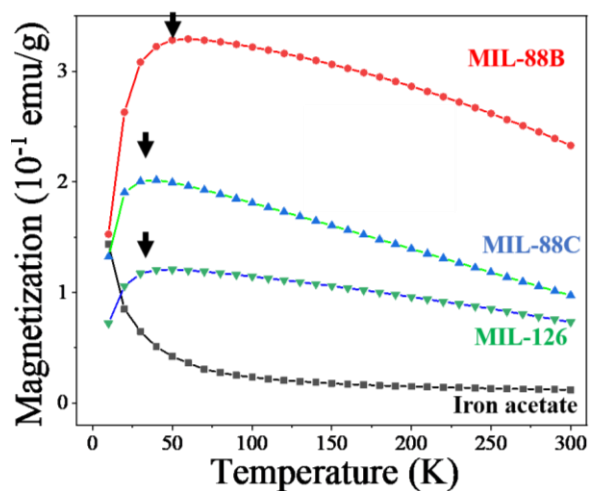


Figure 5.22. Magnetization as a Function of Temperature for MIL-88B, MIL-88C, and MIL-126. The Arrow Indicates the Blocking Temperature T_B of the Respective Sample.

As the temperature increases further the number of magnetic moments aligned increases reaches a maximum peak attributed as the blocking temperature T_B . Further, as

the temperature increases further above T_B , the thermal energy becomes larger than the aligning field causing the magnetic moments to flip resulting in suppression of magnetization. Thus, above the blocking temperature, the ferromagnetic systems display superparamagnetic behavior. It is clear from these plots that all the samples of MIL-88 display superparamagnetic behavior above 100 K. Further, it is evident that T_B of MOF samples decreases with an increase in the length of the linker molecules. For example, the T_B of MIL-88B, MIL-88C, and MIL-126 samples are 60, 50 and 40 K, respectively. This variation in T_B may be attributed to a larger separation, and consequently to a decreasing magnetic coupling between Fe particles at the two ends of a linker molecule. Further when M-H/T plots superimpose to one another, the materials are believed to exist in the superparamagnetic state. It is indeed clear from the plots in Figure 5.23. that all the three MOF samples synthesized in the present work are superparamagnetic above 100 K. In the present study, the Fe particles at the two ends of a shorter linker in case of MIL-88B seem to get coupled with each other. When the linker molecule's length increases, the net enforcement of particle size, and hence, the magnetic coupling between two adjacent Fe particle decreases resulting in the manifestation of smaller coercivity and lower blocking temperatures. In correlation with C axis obtained from crystal structure, the results suggest that the short Fe-Fe distance in C direction with strong spin-orbit coupling contributes to the higher coercivity and blocking temperature for MIL-88B when compared with MIL-126. Thus, our results demonstrate the tunability of the properties of magnetic particles without changing their size with the aid of linker molecules with different length.

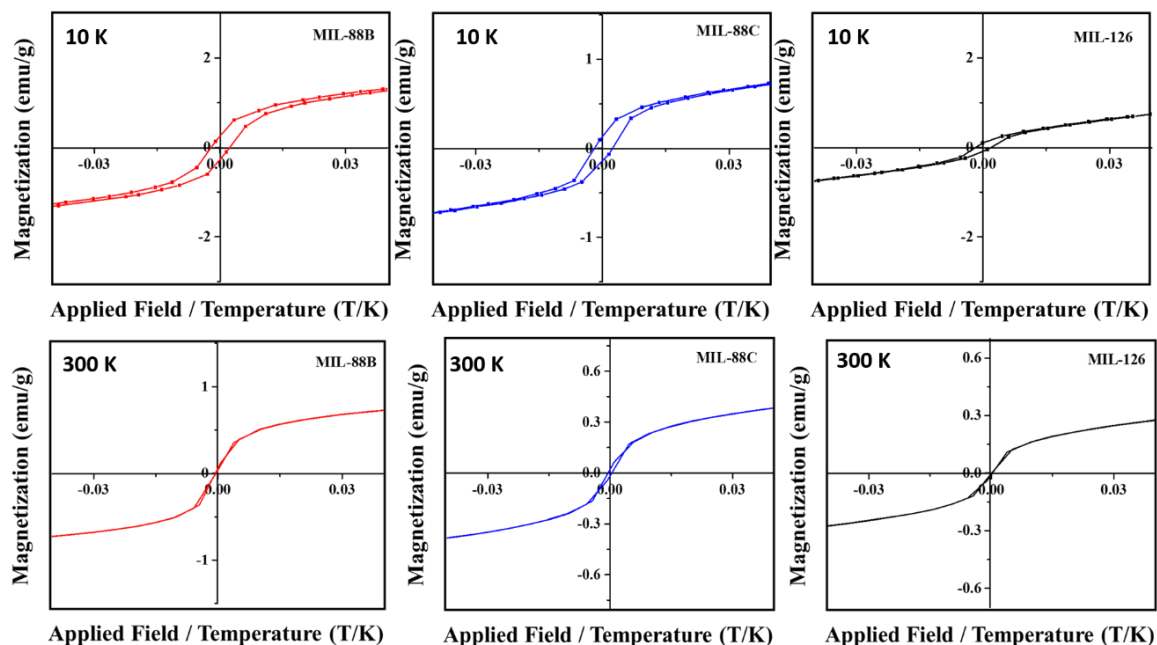


Figure 5.23. M-H/T Loops for MIL-88B, MIL-88C, and MIL-126 at 10 K and 300 K.

5.2.10 Summary

In summary, we have investigated magnetic properties of MIL-88B analogues. Three homologous analogues of MIL-88 such as MIL-88B, MIL-88C and MIL-126 were successfully synthesized using proposed synthetic strategy. The dependence of magnetic nature on the molecular approach is well modulated enabling strong coordination bonding between the Fe metal clusters coupled between the linkers. The detailed analysis of the elemental composition, morphological studies and crystalline packing confirm that the MIL-88 analogues are 3D microstructures with uniform porous morphology. The crystallographic data in Fe-BPDC confirm the synthesis of interpenetrated MIL-88D analogue named as MIL-126. Among three analogues of MIL-88, MIL-126 showed highest surface area due to small pore volume and the formation of interpenetrated

network. The M-H and M-T curves obtained for MIL-88B analogues confirm that they exhibit ferromagnetic behavior at 10 K. High coercivity value was reported for MIL-88B when compared to other analogues such as MIL-88C and MIL-126. The correlation between the C axis of the crystal structure with magnetic properties was well established and evaluated. As the size of the linker increases the value of C axis increases in the crystal structure, therefore providing evidence that the ferromagnetic behavior decreases as the size of the linker increases due to limited communication between the paramagnetic metal clusters via linkers. The potential of the obtained MOFs as ferromagnetic systems was evaluated using M- M-H curves which could be successfully tailored based on the length of the linker. Thus, the magnetic MOFs obtained have great potential to be considered in memory storage devices.

5.3 Investigating Luminescence Properties of Mn-MOF

5.3.1 Introduction

Luminescent materials are an interesting class of materials that have ability to emit light, in response to external stimuli [49] such as exposure to light, temperature and mechanical stimuli [50]. In general, the concept of photoluminescence (response to light) includes fluorescence and phosphorescence depending upon the multiple spin state during the radiative relaxation process [51]. Currently, MOFs have gained significant attention as they offer the flexibility to tune the structural orientation and incorporate physical properties (opto-electronic) based on the preparation and design methodology [51, 52]. The fascinating optoelectronic properties of MOFs have recently stimulated rationally design luminescent metal organic framework (LMOFs) that exhibits longer fluorescent

lifetime by lowering the rate of emission rate or non-radiative decay processes. The photoinduced charge-separation mechanism with the generation of holes and electrons attributed as a transient state (decays typically in the sub-millisecond time scale through charge recombination) could be altered or enhanced through structural orientation of MOFs making them promising candidate for light harvesting and emitting, light scavenging, and applications for photovoltaic devices and optical sensors. [52, 53].

The luminescence property in solid MOFs can originate from various structural building components such as metal node, organic linker, charge transfer mechanism ($d-\pi$ or $\pi-\pi^*$) and by inclusion of guest molecule as discussed in **Chapter 2** (Background). Since MOFs can be synthesized using a wide range of designing strategies, it would be of great interest to identify the molecular approach and establish structural-property relation contributing to the opto-electronic properties. To date, various MOFs have been reported with basic interpretation of photoluminescence and reasoning. Currently, the in-depth understanding of lifetime measurement with the decay and intensity of luminescence is not well explored [17, 54]. The fact that Mn-NDC with the chemical formulae $Mn_3(NDC)_3(DMF)_4$ was widely studied for its gas adsorption properties [13, 55], but the optical properties of these MOFs have not been reported. In this dissertation we explored synthesis, structural characterization and photophysical characterization of a $[Mn(NDC)(DMF)]_n$ MOF constructed from the 2,6-naphthalene dicarboxylic acid (H_2NDC) and Mn^{+2} ions. The work demonstrated herein is the first case investigating excited state lifetime measurements and the luminescence behavior of Mn (NDC). The effect of coordination of the organic ligand in the MOF structure was investigated and compared

with the free organic ligand. A MOF consisting of luminescence properties was designed by optimizing previously used synthesizing method.[56]. The chemical composition, morphology analysis, thermal stability, crystallinity, solid-state packing, textural and optoelectronic properties were investigated.

5.3.2 Synthesis and Characterization

Following the previously developed synthesis method, Mn-MOF was successfully synthesized from manganese (II) acetate and 2,6-naphthalene dicarboxylic acid by maintaining the molar ratio at 2:1 in a minimum volume of DMF. Then the resulted light-yellow slurry paste was subjected to heat in a crucible at 260 °C for 7 minutes, yielding to a light-yellow crystalline powder. The synthetic scheme for the formation of Mn-NDC MOF is depicted in Figure 5.24. The crystalline powder was washed with cold DMF and dried under vacuum to collect highly pure Mn-NDC MOF as light-yellow crystalline powder.

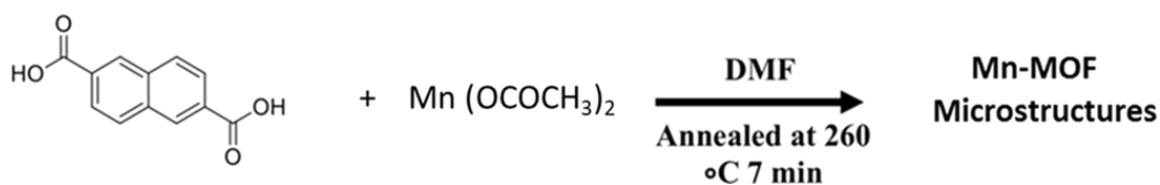


Figure 5.24. Reaction Scheme for the Synthesis of Mn-NDC MOFs.

The coordination of Mn^{+2} metal to carboxylate groups of 2,6-naphthalene dicarboxylic acid was confirmed by Fourier transform infrared spectroscopy (FTIR) and is shown in Figure 5.25. The aromatic stretching was observed at 1538.93 cm^{-1} confirming the aromatic C=C bond stretching.

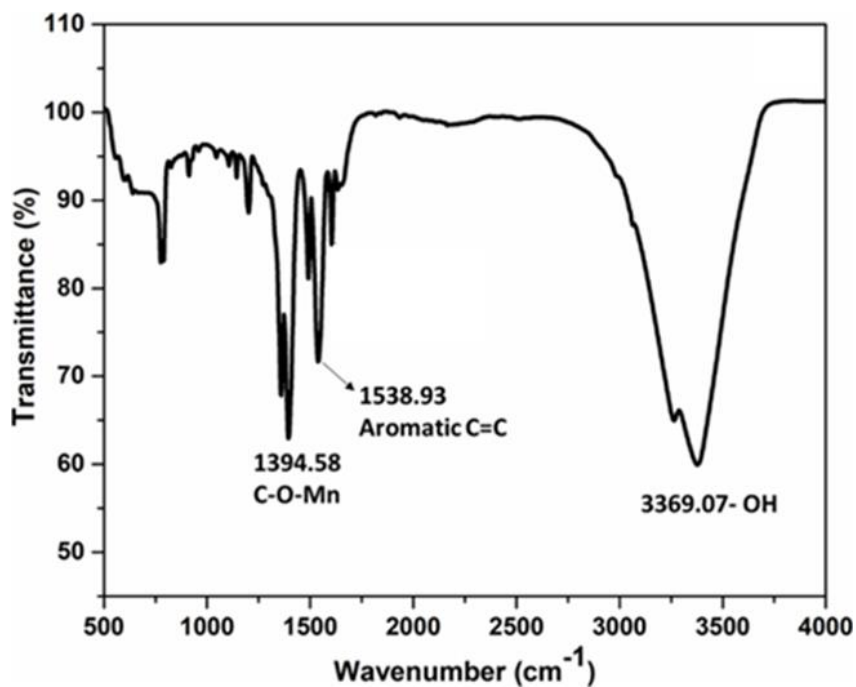


Figure 5.25. FTIR Spectra of Mn-NDC MOFs.

Further, the presence of C-O-Mn at 1395.58 cm⁻¹ proves that Mn⁺² has been successfully coordinated with the carboxylate group of 2,6-naphthalene dicarboxylic acid linker [56]. The peak at 3369 cm⁻¹ belongs to (OH) in Mn-MOF is assigned to physisorption of water molecules in the microstructures of Mn-MOF [57]. The composition analysis by X-ray photoelectron spectroscopy confirms that as synthesized Mn-MOFs are composed of Mn, O and C without any impurity elements shown in Figure 5.26.

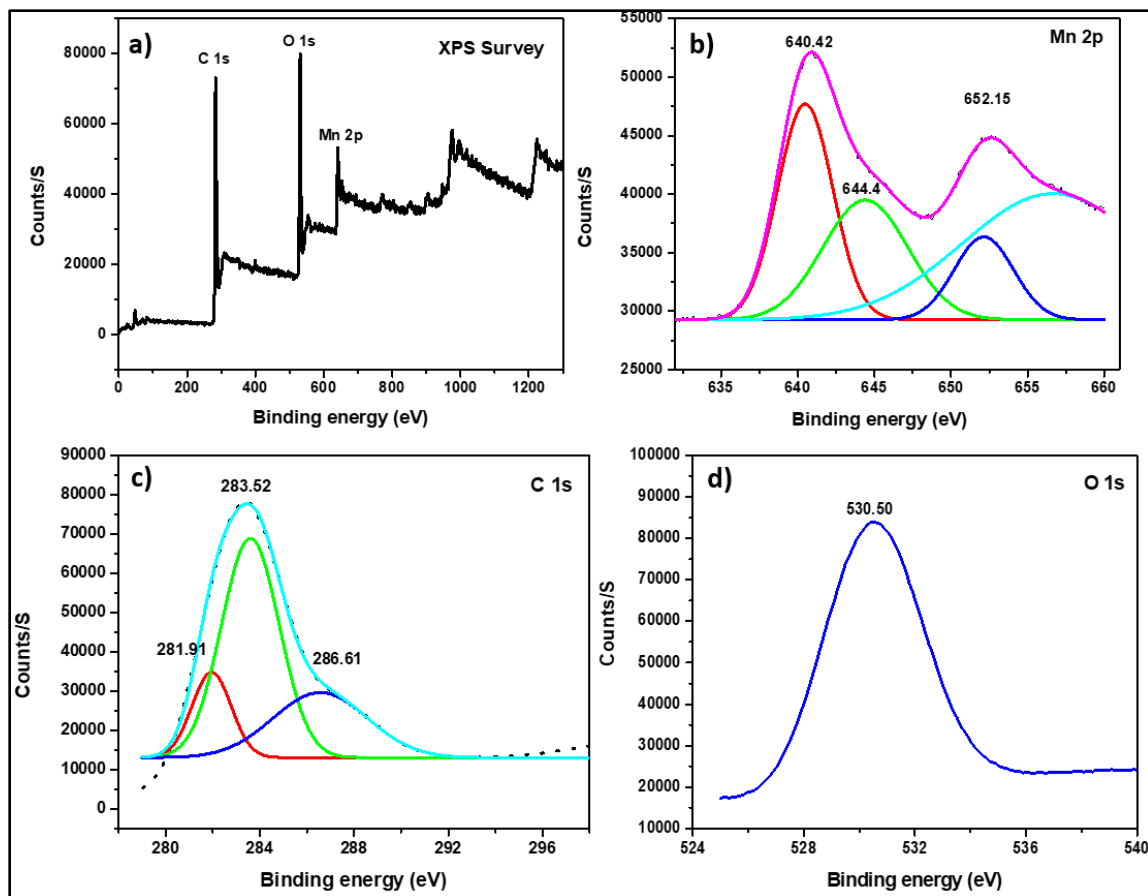


Figure 5.26. The XPS Analysis of the Mn-NDC MOFs; (a) XPS Survey; (b) Mn 2p; (c) C1s; (d) O1s.

The Mn 2p spectra show two major peaks of 640.8 eV and 652.15 eV attributed to the binding energy of Mn $2p_{3/2}$ and Mn $2p_{1/2}$, respectively. The Mn $2p_{3/2}$ is deconvoluted into two fine doublets implying the presence of multivalence states such as Mn²⁺ at 640.42 eV and Mn⁺³ 644.4 eV. The Mn 2p spectrum of Mn-MOFs consists of spin orbit split between Mn $2p_{1/2}$ and Mn $2p_{3/2}$ of 12 eV confirming the presence Mn⁺³ oxidation state. Thus, demonstrating the existence of Mn in two oxidation states i.e. +2, and +3. C 1s peak shows deconvoluted three peaks attributing to three series of carbon oxidized as C-C, C-O-C and O-C=O at 281.91eV, 283.52eV and 286.61 eV, respectively. Moreover,

the O 1s peak at 530.50 eV can be assigned to normal Mn-C-O coordination bonding in Mn-MOFs [64-68][55].

The thermogravimetric analyses (TGA) experiment was conducted to investigate the thermal stability of Mn-MOF. The TGA analysis shows three distinct weight losses at 190 °C, 350 °C, and 400 °C as shown in the Figure 5.27. The initial weight loss at 190 °C could be ascribed to the loss of coordinated DMF molecules, further supporting the presence of trace amount of DMF on the surface of MOF and perhaps in the crystal structure. No weight loss was observed until 350 °C that is attributed to the decomposition of aromatic rings in the organic linker. The third weight loss of at 390 °C represents the collapsing of the framework and no further weight loss is identified. Thus the TGA analysis shows that synthesized Mn-MOFs are stable up to 390 °C, above which the decomposition of dicarboxylate linkers takes place [56-58].

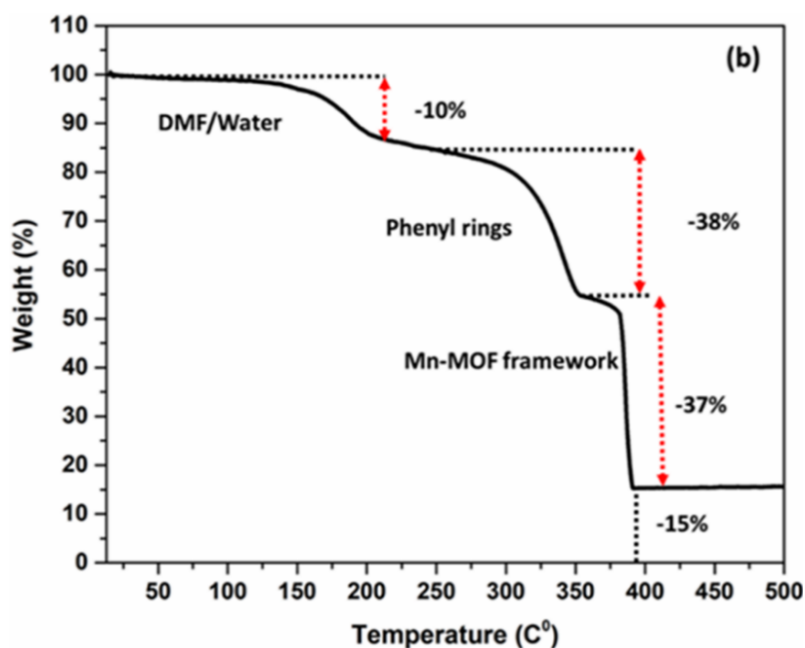


Figure 5.27. TGA of Mn-NDC MOF.

5.3.2.1 Powder X-ray Diffraction Analysis

The experimental powder XRD pattern and the simulated pattern of $\text{Mn}_3(\text{NDC})_3(\text{DMF})_4$ MOF (simulated) are shown in Figure 5.28. The simulated data was generated from the acquired crystal structures from Cambridge crystallographic Data Center (CCDC). The experimental pattern was in good agreement with the simulated pattern indicating that unit cell structure and the crystalline phases formed in the experimental microstructures and simulated Mn (NDC) MOF (CCDC-639914) are the same. These microstructures of Mn (NDC) crystallizes in a monoclinic system with space group $C2/c$.

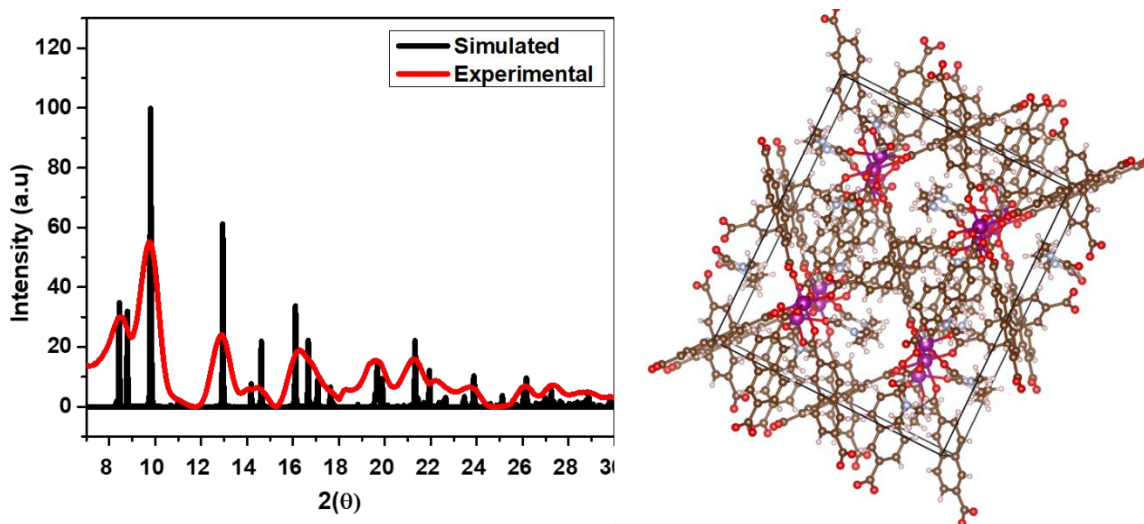


Figure 5.28. Left: Powder XRD Spectrum of Mn-NDC MOFs and Simulated Powder XRD Spectra of Original Mn-NDC MOFs; Right: The Crystal Structure Generated from the Originally Reported Crystal Structure.

However, the powder X-ray diffractogram of the synthesized Mn-NDC did not show well resolved diffraction peaks. Instead of two sharp diffraction peaks at $2\theta = 8.44^\circ$ (002) and 8.83° (111) in the simulated pattern, the experimentally obtained pattern

shows a single broad peak. From the crystallographic analyses, the packing pattern of microstructure follows three-dimensional network as the trimeric Mn_3 units are linked via six carboxylate groups of 2,6-naphthalene dicarboxylic acid. The Mn_3 units consisting of Mn^{+2} as a central atom is coordinated octahedrally by six carboxylate oxygen atoms. The other two metal atoms present on both the sides are coordinated to four oxygen carboxylate atoms and two DMF molecules in distorted octahedral geometry, respectively. Thus, the crosslinking of building units through naphthalene linkers result in 3D network group as depicted in the crystal structure shown in Figure 5.28 [55, 59, 60][55].

The morphological studies of synthesized 3D Mn-MOF was investigated through SEM and TEM (Figure 5.29 (a, b)). The SEM images show a cluster of densely packed uniformly shaped self-assembled MOF microstructures, where the individual microstructures were about 40-75 μ m in size. It is evident that the proposed synthetic strategy as discussed in **Chapter 3**, favors the controlled homogenous dispersion with the uniform shape of the microcrystals. Figure 5.29 (c) – (e) shows the Transmission electron microscopy (TEM) images with the detailed structure of Mn-NDC MOFs, which shows self-assembled microcrystals with void spaces. It is worthy to note that crystals developed through the proposed synthetic strategy allows crystals of about 75 μ m, while it was reported about 200 μ m in size for the $Mn_3(NDC)_3(DMF)_4$ prepared in the literature using the traditional solvothermal method [55].

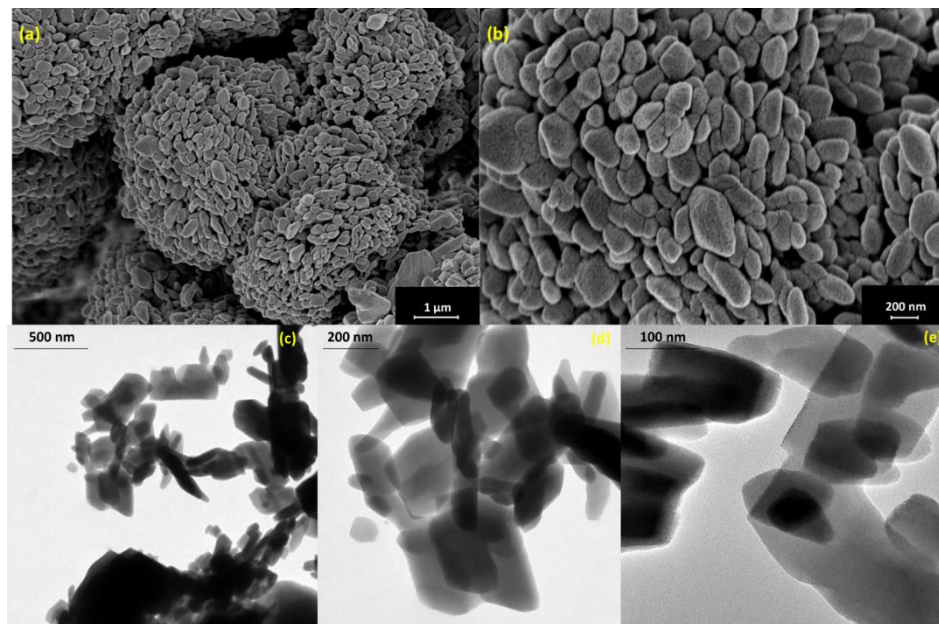


Figure 5.29. SEM and TEM Images of Mn-NDC MOFs.

The textural properties such as specific surface area, pore size, pore volume and porosity were obtained from nitrogen gas adsorption isotherm studies using BET (Brunauer- Emmett-Teller) equation in the relative pressure P/P_0 range of 0.05-0.3. Initially, the samples were activated by performing solvent exchange with an appropriate volatile solvent (chloroform), followed by heating, and drying under vacuum. The average surface area calculated from the nitrogen gas adsorption isotherm data is about $18 \text{ m}^2\text{g}^{-1}$ which is similar to $\text{Mn}_3(\text{NDC})_3(\text{DMF})_4$ MOF crystals obtained using solvothermal synthesis [47, 55]. The isotherm shows hysteresis between adsorption/desorption curves representing type IV isotherm based on IUPAC classification (Figure 5.30 a) that are indicative of mesoporous materials. The sharp N_2 -adsorption at elevated relative pressures in the range of 0.9-1 with a very small hysteresis is attributed to capillary condensation of nitrogen into the pores of these mesoporous materials. A

similar type of isotherms was reported by other research groups for Fe based materials [48]. According to the IUPAC classification of sorption isotherms, these adsorption/desorption isotherms are classified into the H3 isotherm. The BJH pore distribution shows mesoporous nature with two pore distribution ranging from 2 nm to 30 nm (Figure 5.30 b).

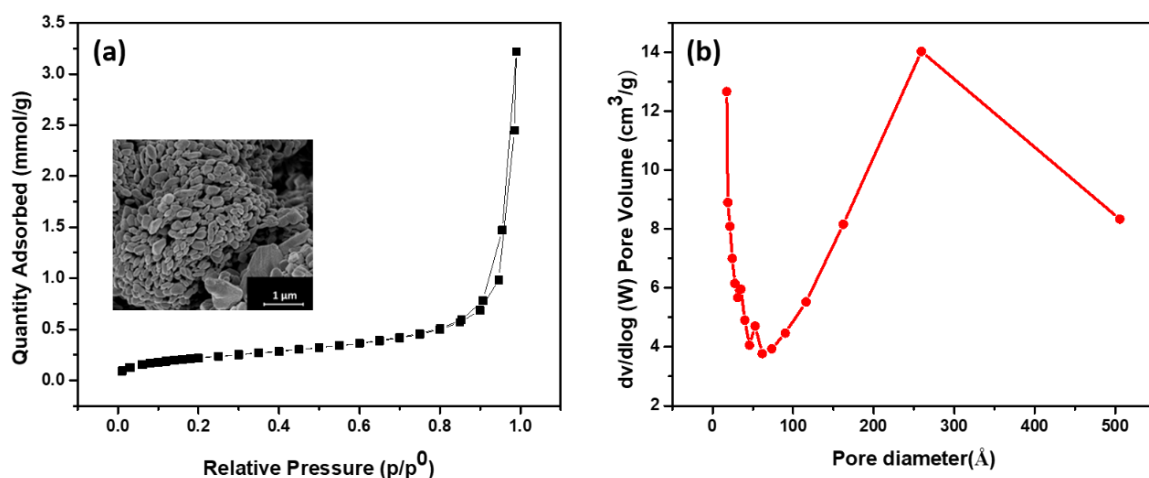


Figure 5.30. (a) N₂ Isotherms for Mn-NDC MOFs at 77K; (b) BJH Pore Size Distribution of Plots of Mn-NDC MOFs.

5.3.2.2 Luminescent Properties

Photophysical properties of Mn-NDC MOFs was studied by acquiring UV-vis and emission spectra in solution. Using Mn (II) as a metal center for building MOFs with luminescent properties offers advantage of multiple coordination modes as it possesses more than one oxidation states. Many MOFs have been developed using 2,6-naphthalene dicarboxylic acid as an organic linker. Hence the fluorescent properties of microstructure of Mn-NDC and 2,6-naphthalene dicarboxylic acid in solution were investigated at room temperature. The UV-Vis spectrum of 2,6- naphthalene organic linker consists of three

distinct regions at 220 ,290 and 344 nm. Similarly, the absorption spectra of Mn-NDC MOF show similar peaks at similar wavelength as that of organic ligand absorption shown in Figure 5.31 (a).

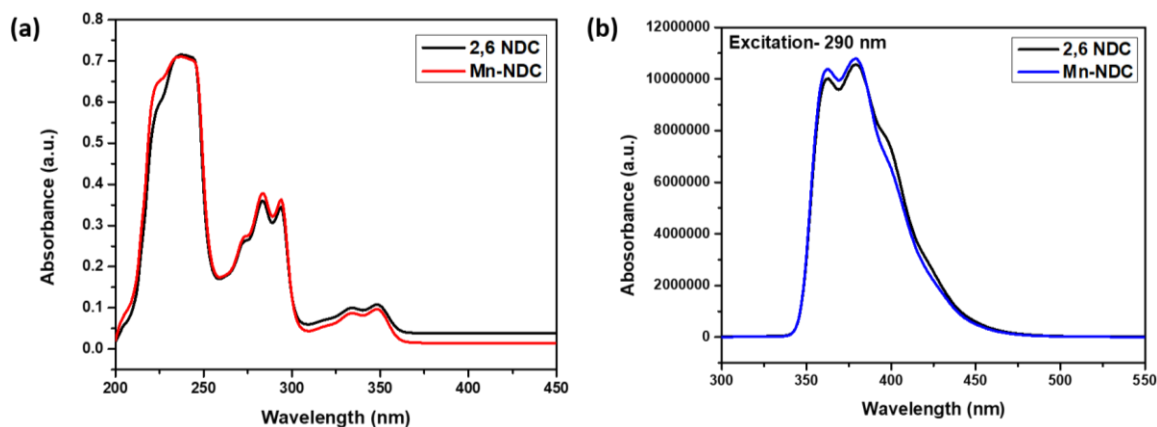


Figure 5.31. (a) UV-Vis Absorption Spectra of 2,6 NDC and Mn-NDC MOFs; (b) PL Spectra of 2,6 NDC and Mn-NDC MOFs.

In general MOFs with fluorescent linker, the optical properties of the MOF structure depend upon the ligand-local environment. In our results, both the materials exhibit similar shape and vibronic peaks set from 220 nm to 360 nm corresponding to π - π^* absorption transitions of naphthalene core. These similarities evidence linker- base absorption with no contribution of the metal cluster consisting of Mn^{+2} and Mn^{+3} oxidation state (confirmed in XPS data) in the network of Mn-NDC MOFs. The luminescence properties were investigated using PL emission spectra shown in Figure 5.31(b) with excitation wavelength of 290 nm for both organic ligand and Mn-NDC MOF. The emission spectrum of the linker exhibits a broad band in 350 nm- 450 nm, with a maximum peak at 378 nm which could be attributed to the π - π^* transitions in the

ligand. Similarly, the emission spectrum of Mn-NDC MOF shows similar broad band with slight blue shift (2-3 nm) with increase in the luminescence property signifying ligand-based emission[61]. Thus, there is no charge transfer mechanism occurring between metal ion and organic ligand.

The photophysical properties (PL emission) was further complemented by transient absorption spectroscopy (TAS) Figure 5.32. Nanosecond transient absorption (nsTA) spectroscopy was used as an additional tool to further investigate the excited state photo physics of 2,6-NDC and Mn-NDC. Using this technique, radiative relaxation of excited singlet state that typically occurs on nanosecond time scale can be investigated. In this case, the transient decay curves with respect to time was measured at excitation wavelength of 290 nm. In general, this curve gives information about number of decay processes and how fast or slow the decay processes take place. The nsTA spectra of both NDC linker and Mn-NDC were measured in 70% ethanol solution. The kinetics obtained from the Nanosecond TAS data for NDC linker and Mn-NDC at 290 nm wavelength show single -exponential decay with a lifetime of 14.22 ns and 5.58 ns, respectively. The measured lifetime of NDC linker free in solution is approximately 2.5 times greater than that of Mn-NDC MOFs. In general, it is expected that emissive rate and/or non-radiative decay rate decreases favoring the increase in lifetime of NDC linker which functions as a backbone in the overall construction of 3D Mn-NDC MOF. However, in this case the lifetime of Mn-NDC was found to be shorter when compared to free linker NDC due to quick quenching of exciton [62-64] [65, 66].

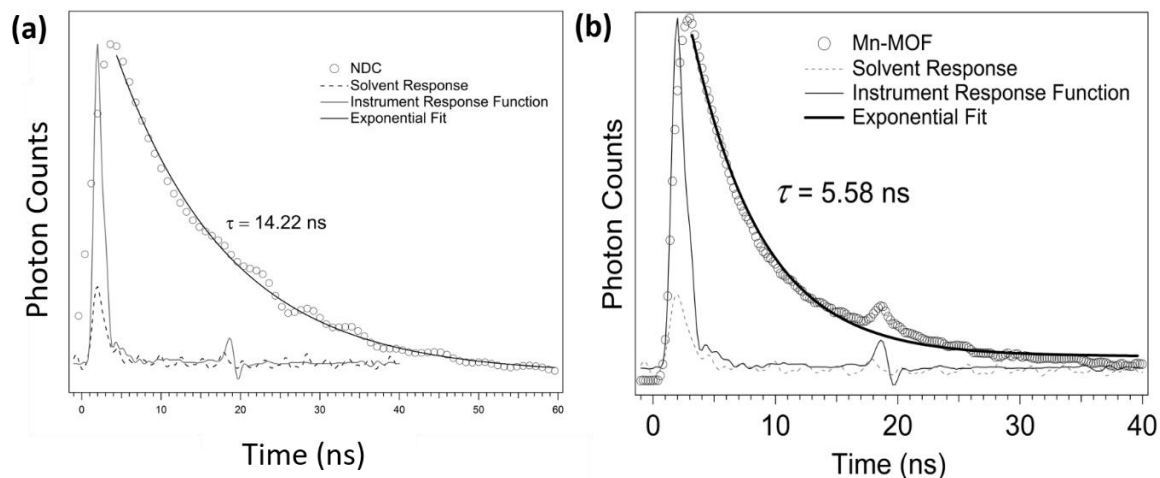


Figure 5.32. Transient Absorption Data for (a) 2,6 Naphthalene Dicarboxylic Acid; (b) Mn-NDC MOF.

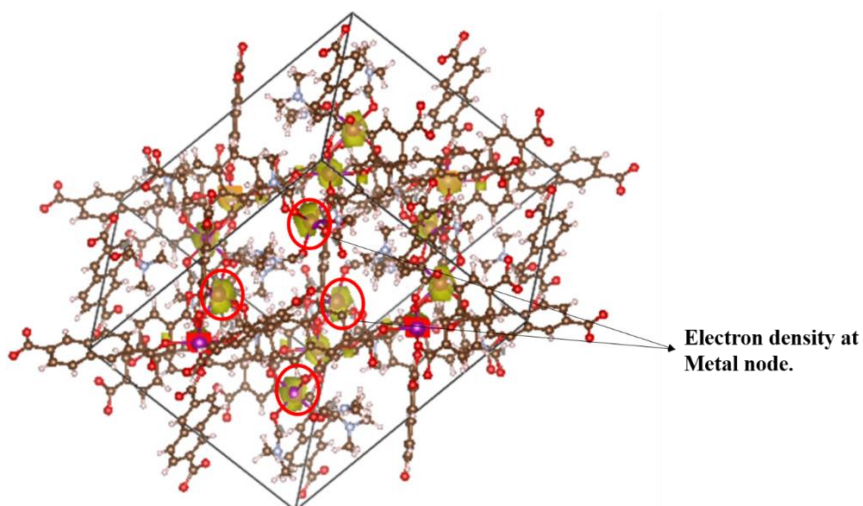


Figure 5.33. Simulated Crystalline Structure of Mn-NDC MOFs (CCDC-639914) Showing Electron Densities at the Metal Node.

In our results, the 2,6-naphthalene dicarboxylic acid which is an electron-rich π -conjugated system showed excited lifetime of about 14.22 ns. While 2,6-naphthalene dicarboxylic acid coordinated with Mn^{+2} shows the excited lifetime of 5.58 ns attributing to the quick quenching of exciton. The shortening of excited lifetime in Mn-MOFs could

be due to absence of HOMO-LUMO energy levels in the naphthalene core. This was confirmed by electron density mapping in simulated structure of Mn-NDC (Vesta), which shows no electron density in the aromatic rings of naphthalene linker while significant distribution of electron density at Manganese nodes. Thus, photophysical properties evaluated using both optical measurements confirm ligand centered emission without charge transfer mechanism between metal ions and organic clusters.

5.3.2.3 Summary

In summary, the photophysical properties of the synthesized Mn- NDC MOFs were investigated using time resolved transient spectroscopic technique and fluorescence spectroscopy. The Mn-NDC MOFs were developed using the proposed synthetic strategy with 2,6-naphthalene dicarboxylic acid as an organic linker. The detailed composition analysis, morphological studies and crystalline packing confirm that they are 3D-dimensional porous uniform microstructures. The absorption and desorption curves confirm the mesoporous nature with a pore diameter of 2-30 nm. From the fluorescence spectroscopy, it was observed that though the PL emission spectra show similar spectral features for both NDC and Mn-NDC when excited at 290 nm. Thus, the nanosecond transient absorption decays showed that the lifetime of the MOF (>2.5 times) is relatively shorter than that of the organic ligand. Further, optical emission and nanosecond transient absorption spectroscopy measurements evidence ligand base emission otherwise the spin-orbit coupling in the building blocks of Mn-NDC may increase the excited lifetime showing potential in photovoltaic applications. However, the shorter lifetime of NDC

linker after coordination with Mn^{+2} ion shows great potential to be considered as a sensor for detecting transition metal ions.

5.4 References

- [1] J. I. Feldblyum, A. G. Wong-Foy, and A. J. Matzger, “Non-interpenetrated IRMOF-8: synthesis, activation, and gas sorption,” *Chemical Communications*, 10.1039/C2CC34689C vol. 48, no. 79, pp. 9828-9830, 2012.
- [2] L. G. Qiu *et al.*, “Hierarchically micro- and mesoporous metal-organic frameworks with tunable porosity,” (in eng), *Angewandte Chemie (International ed. in English)*, vol. 47, no. 49, pp. 9487-91, 2008.
- [3] S. H. Jung, J.-H. Lee, J. W. Yoon, C. Serre, G. Férey, and J.-S. Chang, “Microwave Synthesis of Chromium Terephthalate MIL-101 and Its Benzene Sorption Ability,” *Advanced Materials*, vol. 19, no. 1, pp. 121-124, 2007.
- [4] L. Peng *et al.*, “Highly mesoporous metal-organic framework assembled in a switchable solvent,” (in eng), *Nat Commun*, vol. 5, p. 4465, Jul 22 2014.
- [5] Y. Zhao, J. Zhang, B. Han, J. Song, J. Li, and Q. Wang, “Metal-organic framework nanospheres with well-ordered mesopores synthesized in an ionic liquid/CO₂/surfactant system,” (in eng), *Angewandte Chemie (International ed. in English)*, vol. 50, no. 3, pp. 636-9, Jan 17 2011.
- [6] E. Castaldelli *et al.*, “Electrical semiconduction modulated by light in a cobalt and naphthalene diimide metal-organic framework,” *Nature Communications*, vol. 8, no. 1, p. 2139, 2017/12/15 2017.

- [7] N. Stock and S. Biswas, "Synthesis of Metal-Organic Frameworks (MOFs): Routes to Various MOF Topologies, Morphologies, and Composites," *Chemical Reviews*, vol. 112, no. 2, pp. 933-969, 2012/02/08 2012.
- [8] L. Sun, M. G. Campbell, and M. Dincă, "Electrically Conductive Porous Metal-Organic Frameworks," (in eng), *Angewandte Chemie (International ed. in English)*, vol. 55, no. 11, pp. 3566-79, Mar 7 2016.
- [9] H. Furukawa, K. E. Cordova, M. O'Keeffe, and O. M. Yaghi, "The chemistry and applications of metal-organic frameworks," (in eng), *Science*, vol. 341, no. 6149, p. 1230444, Aug 30 2013.
- [10] H. E. Li, M.; O'Keeffe, M.; Yaghi, O. M, "Design and synthesis of an exceptionally stable and highly porous metal-organic framework," 1999.
- [11] M. Eddaoudi *et al.*, "Systematic design of pore size and functionality in isorecticular MOFs and their application in methane storage," (in eng), *Science*, vol. 295, no. 5554, pp. 469-72, Jan 18 2002.
- [12] J. L. C. Rowsell, A. R. Millward, K. S. Park, and O. M. Yaghi, "Hydrogen Sorption in Functionalized Metal-Organic Frameworks," *Journal of the American Chemical Society*, vol. 126, no. 18, pp. 5666-5667, 2004/05/01 2004.
- [13] S. Dawood, R. Yarbrough, K. Davis, and H. Rathnayake, "Self-assembly and optoelectronic properties of isorecticular MOF nanocrystals," *Synthetic Metals*, vol. 252, pp. 107-112, 2019/06/01/ 2019.

- [14] Z. Mai and D. Liu, "Synthesis and Applications of Isoreticular Metal–Organic Frameworks IRMOFs-n (n = 1, 3, 6, 8)," *Crystal Growth & Design*, vol. 19, no. 12, pp. 7439-7462, 2019/12/04 2019.
- [15] J.-H. Cho *et al.*, "Structural Transformation and Gas Adsorption Properties of Interpenetrated IRMOF-8," *Bulletin of the Korean Chemical Society*, vol. 35, 03/20 2014.
- [16] L. Spanhel and M. A. Anderson, "Semiconductor clusters in the sol-gel process: quantized aggregation, gelation, and crystal growth in concentrated zinc oxide colloids," *Journal of the American Chemical Society*, vol. 113, no. 8, pp. 2826-2833, 1991/04/01 1991.
- [17] M. D. Allendorf, C. A. Bauer, R. K. Bhakta, and R. J. T. Houk, "Luminescent metal–organic frameworks," *Chemical Society Reviews*, 10.1039/B802352M vol. 38, no. 5, pp. 1330-1352, 2009.
- [18] W. Dong *et al.*, "Synthesis, crystal structures and luminescent properties of two supramolecular assemblies containing [Au(CN)₂]⁻ building block," *New Journal of Chemistry*, 10.1039/B403329A vol. 28, no. 11, pp. 1347-1351, 2004.
- [19] E. Coronado, "Molecular magnetism: from chemical design to spin control in molecules, materials and devices," *Nature Reviews Materials*, vol. 5, no. 2, pp. 87-104, 2020/02/01 2020.
- [20] A. E. Thorarinsdottir and T. D. Harris, "Metal–Organic Framework Magnets," *Chemical Reviews*, 2020/02/11 2020.

- [21] X.-L. Tong, H.-L. Lin, J.-H. Xin, F. Liu, M. Li, and X.-P. Zhu, "Recent Advances as Materials of Functional Metal-Organic Frameworks," *Journal of Nanomaterials*, vol. 2013, p. 616501, 2013/05/07 2013.
- [22] C. Yang *et al.*, "A semiconducting layered metal-organic framework magnet," (in eng), *Nature communications*, vol. 10, no. 1, pp. 3260-3260, 2019.
- [23] A. Fernández-Pacheco, R. Streubel, O. Fruchart, R. Hertel, P. Fischer, and R. P. Cowburn, "Three-dimensional nanomagnetism," *Nature Communications*, vol. 8, no. 1, p. 15756, 2017/06/09 2017.
- [24] M. Shen *et al.*, "Antibacterial applications of metal–organic frameworks and their composites," *Comprehensive Reviews in Food Science and Food Safety*, 01/07 2020.
- [25] A. Guo, M. Durymanov, A. Permyakova, S. Sene, C. Serre, and J. Reineke, "Metal Organic Framework (MOF) Particles as Potential Bacteria-Mimicking Delivery Systems for Infectious Diseases: Characterization and Cellular Internalization in Alveolar Macrophages," (in eng), *Pharm Res*, vol. 36, no. 4, p. 53, Feb 21 2019.
- [26] M. Kurmoo, "Magnetic metal–organic frameworks," *Chemical Society Reviews*, 10.1039/B804757J vol. 38, no. 5, pp. 1353-1379, 2009.
- [27] M. Ma, A. Bétard, I. Weber, N. S. Al-Hokbany, R. A. Fischer, and N. Metzler-Nolte, "Iron-Based Metal–Organic Frameworks MIL-88B and NH₂-MIL-88B: High Quality Microwave Synthesis and Solvent-Induced Lattice "Breathing", *Crystal Growth & Design*, vol. 13, no. 6, pp. 2286-2291, 2013/06/05 2013.

- [28] Y. Wu, H. Luo, and H. Wang, "Synthesis of iron(iii)-based metal–organic framework/graphene oxide composites with increased photocatalytic performance for dye degradation," *RSC Advances*, 10.1039/C4RA07566H vol. 4, no. 76, pp. 40435-40438, 2014.
- [29] M. Dan-Hardi *et al.*, "How Interpenetration Ensures Rigidity and Permanent Porosity in a Highly Flexible Hybrid Solid," *Chemistry of Materials*, vol. 24, no. 13, pp. 2486-2492, 2012/07/10 2012.
- [30] A. G. Kolhatkar, A. C. Jamison, D. Litvinov, R. C. Willson, and T. R. Lee, "Tuning the magnetic properties of nanoparticles," (in eng), *International journal of molecular sciences*, vol. 14, no. 8, pp. 15977-16009, 2013.
- [31] A. Sharma, S. Mohan, and S. Suwas, "Evidence of adaptive modulation and magnetic field induced reorientation of variants in epitaxially grown Ni-Mn-Ga thin film on Al₂O₃ (112̄0) substrate," *Materials Science and Engineering: B*, vol. 242, pp. 6-16, 2019/03/01/ 2019.
- [32] J. Sui, L. Wang, W. Zhao, and J. Hao, "Iron–naphthalenedicarboxylic acid gels and their high efficiency in removing arsenic(v)," *Chemical Communications*, 10.1039/C6CC01621A vol. 52, no. 43, pp. 6993-6996, 2016.
- [33] P. Li, E. Y. Jiang, and H. L. Bai, "Fabrication of ultrathin epitaxial γ -Fe₂O₃ films by reactive sputtering," *Journal of Physics D: Applied Physics*, vol. 44, no. 7, p. 075003, 2011/02/02 2011.

- [34] K. Djebaili, Z. Mekhalif, A. Boumaza, and A. Djelloul, "XPS, FTIR, EDX, and XRD Analysis of Al Scales Grown on PM2000 Alloy," *Journal of Spectroscopy*, vol. 2015, p. 868109, 2015/03/25 2015.
- [35] Y.-S. Wei *et al.*, "Coordination templated [2+2+2] cyclotrimerization in a porous coordination framework," (in eng), *Nature communications*, vol. 6, pp. 8348-8348, 2015.
- [36] S. Surblé, C. Serre, C. Mellot-Draznieks, F. Millange, and G. Férey, "A new isorecticular class of metal-organic-frameworks with the MIL-88 topology," *Chemical Communications*, 10.1039/B512169H no. 3, pp. 284-286, 2006.
- [37] C. Serre, C. Mellot-Draznieks, S. Surblé, N. Audebrand, Y. Filinchuk, and G. Férey, "Role of Solvent-Host Interactions That Lead to Very Large Swelling of Hybrid Frameworks," *Science*, vol. 315, no. 5820, p. 1828, 2007.
- [38] P. Horcajada *et al.*, "How Linker's Modification Controls Swelling Properties of Highly Flexible Iron(III) Dicarboxylates MIL-88," *Journal of the American Chemical Society*, vol. 133, no. 44, pp. 17839-17847, 2011/11/09 2011.
- [39] A. J. Rondinone, A. C. S. Samia, and Z. J. Zhang, "Superparamagnetic Relaxation and Magnetic Anisotropy Energy Distribution in CoFe₂O₄ Spinel Ferrite Nanocrystallites," *The Journal of Physical Chemistry B*, vol. 103, no. 33, pp. 6876-6880, 1999/08/01 1999.
- [40] J. Abiade, G. X. Miao, A. Gupta, A. Gapud, and D. Kumar, "Corrigendum to "Structural and magnetic properties of self-assembled nickel nanoparticles in a

- yttria stabilized zirconia matrix” (DOI:10.1016/j.tsf.2007.10.103),” *Thin Solid Films*, vol. 516, pp. 2082-2086, 02/01 2008.
- [41] D. Kumar, S. Yarmolenko, J. Sankar, J. Narayan, H. Zhou, and A. Tiwari, “Pulsed laser deposition assisted novel synthesis of self-assembled magnetic nanoparticles,” *Composites Part B: Engineering*, vol. 35, no. 2, pp. 149-155, 2004/03/01/ 2004.
- [42] G. Barrera *et al.*, “Magnetic Properties of Nanocomposites,” *Applied Sciences*, vol. 9, p. 212, 01/09 2019.
- [43] S. Shaji, N. R. Mucha, P. Giri, C. Binek, and D. Kumar, “Magnetic and magnetocaloric properties of Fe₂Ta thin films,” *AIP Advances*, vol. 10, no. 2, p. 025222, 2020/02/01 2020.
- [44] D. Kumar *et al.*, “Improved magnetic properties of self-assembled epitaxial nickel nanocrystallites in thin-film ceramic matrix,” *Journal of Materials Research*, vol. 17, no. 4, pp. 738-742, 2002.
- [45] A. K. Singh, S. Mallik, S. Bedanta, and A. Perumal, “Spacer layer and temperature driven magnetic properties in multilayer structured FeTaC thin films,” *Journal of Physics D: Applied Physics*, vol. 46, no. 44, p. 445005, 2013/10/17 2013.
- [46] K. S. W. Sing, “Reporting physisorption data for gas/solid systems with special reference to the determination of surface area and porosity (Recommendations 1984),” (in English), vol. 57, no. 4, p. 603, 1985.
- [47] M. Ahmad, X. Quan, and H. Yu, “Tuning Lewis acidity of MIL-88B-Fe with mixed-valence coordinatively unsaturated iron centers on ultrathin Ti₃C₂ nanosheets for

- efficient photo-Fenton reaction,” *Applied Catalysis B Environmental*, vol. 264, p. 118534, 12/19 2019.
- [48] S. K. Maji, N. Mukherjee, A. Mondal, and B. Adhikary, “Synthesis, characterization and photocatalytic activity of α -Fe₂O₃ nanoparticles,” *Polyhedron*, vol. 33, no. 1, pp. 145-149, 2012/02/09/ 2012.
- [49] A. Z. M. S. Rahman, “Solid State Luminescent Materials: Applications,” in *Reference Module in Materials Science and Materials Engineering*: Elsevier, 2016.
- [50] F. Rouhani, A. Morsali, and P. Retailleau, “Simple One-Pot Preparation of a Rapid Response AIE Fluorescent Metal–Organic Framework,” *ACS Applied Materials & Interfaces*, vol. 10, no. 42, pp. 36259-36266, 2018/10/24 2018.
- [51] J. Dong, D. Zhao, Y. Lu, and W.-Y. Sun, “Photoluminescent metal–organic frameworks and their application for sensing biomolecules,” *Journal of Materials Chemistry A*, 10.1039/C9TA07022B vol. 7, no. 40, pp. 22744-22767, 2019.
- [52] J. Lakowicz, *Lakowicz JR (2006) Principles of fluorescence spectroscopy, 3rd edn. Springer, New York, 2006.* 2006.
- [53] T. Duchanois *et al.*, “An Iron-Based Photosensitizer with Extended Excited-State Lifetime: Photophysical and Photovoltaic Properties: An Iron-Based Photosensitizer with Extended Excited-State Lifetime,” *European Journal of Inorganic Chemistry*, vol. 2015, 04/14 2015.
- [54] J. G. Santaclara, F. Kapteijn, J. Gascon, and M. A. van der Veen, “Understanding metal–organic frameworks for photocatalytic solar fuel production,” *CrystEngComm*, 10.1039/C7CE00006E vol. 19, no. 29, pp. 4118-4125, 2017.

- [55] L. Nguyen, C. Nguyen, D. Giao, and K. Le, "Towards applications of metal–organic frameworks in catalysis: Friedel–Crafts acylation reaction over IRMOF-8 as an efficient heterogeneous catalyst," *Journal of Molecular Catalysis A: Chemical*, vol. 349, pp. 28–35, 10/01 2011.
- [56] S. Maiti, A. Pramanik, U. Manju, and S. Mahanty, "Reversible Lithium Storage in Manganese 1,3,5-Benzenetricarboxylate Metal–Organic Framework with High Capacity and Rate Performance," *ACS Applied Materials & Interfaces*, vol. 7, no. 30, pp. 16357-16363, 2015/08/05 2015.
- [57] D. Mukherjee, B. Govinda Rao, and B. Reddy, "CO and soot oxidation activity of doped ceria: Influence of dopants," *Applied Catalysis B: Environmental*, vol. 197, 03/01 2016.
- [58] Y. Song *et al.*, "Ferromagnetic and Transport Properties of Mn-Doped ZnO," *Journal of The Korean Physical Society - J KOREAN PHYS SOC*, vol. 52, 01/15 2008.
- [59] Z. Jiang, "Trinuclear Manganese Metal-Organic Frameworks Based on 2,6-Naphthalenedicarboxylic Acid," *Asian Journal of Chemistry*, vol. 25, pp. 2347-2348, 04/01 2013.
- [60] I. Senkovska, J. Fritsch, and S. Kaskel, "New Polymorphs of Magnesium-Based Metal–Organic Frameworks $Mg_3(ndc)_3$ ($ndc = 2,6$ -Naphthalenedicarboxylate)," *European Journal of Inorganic Chemistry*, vol. 2007, no. 35, pp. 5475-5479, 2007/12/01 2007.

- [61] B. Liu *et al.*, “Microporous coordination polymers of cobalt(II) and manganese(II) 2,6-naphthalenedicarboxylate: preparations, structures and gas sorptive and magnetic properties,” *Microporous and Mesoporous Materials*, vol. 111, no. 1, pp. 470-477, 2008/04/15/ 2008.
- [62] R. Berera, R. van Grondelle, and J. T. M. Kennis, “Ultrafast transient absorption spectroscopy: principles and application to photosynthetic systems,” *Photosynthesis Research*, vol. 101, no. 2, pp. 105-118, 2009/09/01 2009.
- [63] Shaunak M. Shaikh, A. Chakraborty, J. Alatis, M. Cai, E. Danilov, and A. J. Morris, “Light harvesting and energy transfer in a porphyrin-based metal organic framework,” *Faraday Discussions*, 10.1039/C8FD00194D vol. 216, no. 0, pp. 174-190, 2019.
- [64] C. A. Bauer *et al.*, “Influence of Connectivity and Porosity on Ligand-Based Luminescence in Zinc Metal–Organic Frameworks,” *Journal of the American Chemical Society*, vol. 129, no. 22, pp. 7136-7144, 2007/06/06 2007.
- [65] R.-X. Yao, X. Cui, X.-X. Jia, F.-Q. Zhang, and X.-M. Zhang, “A Luminescent Zinc(II) Metal–Organic Framework (MOF) with Conjugated π -Electron Ligand for High Iodine Capture and Nitro-Explosive Detection,” *Inorganic Chemistry*, vol. 55, no. 18, pp. 9270-9275, 2016/09/19 2016.
- [66] C. Wang *et al.*, “Increasing the triplet lifetime and extending the ground-state absorption of biscyclometalated Ir(III) complexes for reverse saturable absorption and photodynamic therapy applications,” *Dalton Transactions*, 10.1039/C6DT02416E vol. 45, no. 41, pp. 16366-16378, 2016.

CHAPTER VI

CONCLUSIONS AND FUTURE DIRECTIONS

6.1 Conclusions

The primary goal of this research within the thesis was to develop a novel synthetic strategy that could offer the following possibilities.

- To introduce electronic characteristics such as electrical, optical, and magnetic in the MOFs via manipulating the structural orientation and crystalline packing.
- To understand the influence of structure- property relationship in providing crucial intrinsic details necessary to understand their solid-state properties (electronic characteristics).

Due to lack of understanding of structural-property relationship and suitable synthetic conditions, MOFs with electronic characteristics were rarely reported. This is why the major focus of this thesis was aimed at optimizing the synthesis process in terms of its physical structure (size, crystallinity, etc.) and designing robust MOFs with electronic properties. The optimization of the synthesis conditions and precise control over its physical characteristics make the novel synthetic approach introduced here for developing MOFs with promising electronic characteristics. The successful demonstration of a synthetic approach that incorporates electronic characteristics was achieved in three stages: the choice of the material (isoreticular system), self-assembly

process, characterization, and the evaluation of the properties discussed in **Chapters 3** and **5** in three specific aims, respectively. The major challenges were achieving MOFs with the electronic characteristics and finding implementation in device fabrication. The summary of the dissertation research findings of MOFs (IRMOF-8, MIL-88, and Mn-MOF) are summarized below.

Aim 1 of the dissertation research work was to develop a rapid synthetic approach to design isorecticular series of IRMOF-8 with promising optoelectronic properties. Interpenetrated INT-IRMOF-8A an analogue of IRMOF-8 could be produced in a very short period of time, enabling a significant improvement compared to traditional solvothermal synthetic approaches developed in the past. The resulting IRMOF-8 nanocrystals were self- assembled by a solvent-polarity driven method from Zinc metal ions and 2,6-naphthalene dicarboxylic acid, yielding 3D-MOFs. The solvent-driven self-assembly to yield variety of morphologies was further confirmed via solvent studies in which the morphology of the 3D MOFs changes based on the nature of the solvent. The nanocrystal orientation depending upon the solvent polarity, where solvent molecules act as surfactant absorbing to crystal facets yielded interpenetrated network, which greatly affected the size, shape, and crystallinity, and consequently the functional performance of the material. Further, these MOFs are thermally stable up to 400-550°C owing to the rigidity offered by the interpenetrated framework.

The structure of INT-IRMOF-8A was confirmed via a detailed analysis of the structural orientation and crystallinity from the powder X-ray diffraction studies and selected area diffraction (SAED) using TEM. The off-sets layer-by layer arrangement of

the NDC linkers in the network of IRMOF-8A contributes significantly in the origin of optoelectronic properties.

The electrical conductivity measurements and optical band gap of the reported INT-IRMOF-8 was found to be about 3.86×10^{-2} S/cm and 2.84 eV, respectively. In our findings, the charge transport pathway in these frameworks is through space containing extensive π - π stacking. The transport of electrons is the result of closer contact distance via stacking. Further, the ligand centered emission analyzed from absorption and emission spectroscopy further evidences no charge transfer between the metal node and the orbital ligand. The optical band gap obtained for these MOFs displays semiconducting behavior. Thus, proposed synthetic strategy offer structural tunability and control over transport properties in MOFs offering great potential to be considered in electronic industry.

Aim 2 targeted at investigating the role of the linker topology on the primary magnetic properties of MOFs such as Coercivity (HC) and blocking temperature (TB). 3D MIL-88B, MIL-88C and MIL-126 an interpenetrated analogue of MIL-88D were developed. The detailed composition analysis, morphology, and crystalline packing confirms the formation of three homologous analogues of MIL-88 such as MIL-88B, MIL-88C and MIL-126. The crystalline packing reveals hexagonal symmetry for MIL-88B, MIL-88C and tetragonal symmetry for MIL-126.

MOFs with magnetic properties are very less explored due to the most MOFs are inherently non-magnetic. The incorporation of magnetic behavior depends on various factors such as choice of the metal, the topology of the linker, and synthetic approach that

could facilitate interaction between metal nodes. The topology of the linker plays a significant role in offering structural tunability and control over magnetic properties. The M-H and M-T measurements confirm that the reported MIL-88 analogues display ferromagnetic behavior at 10 K. The length of the linkers demonstrates the advantage of tailoring the ferromagnetic behavior. The highest ferromagnetic behavior was displayed by MIL-88B, which consists of the shortest linker, 1,4-BDC compared to MIL-126, having the longest linker, i.e. biphenyl units. The temperature dependent magnetic behavior analysis provides evidence that the shortest organic linker unit length promotes effective interaction between the metal nodes displaying ferromagnetic behavior.

The variation of the linker length not only provided the feasibility of altering the magnetic properties but also displayed interesting results regarding textural, morphological, and thermal properties. The morphological studies analyzed via SEM and TEM confirm the self-assembly of nanocrystals forming spindle shaped and octahedral shaped microstructures for MIL-88B, MIL-88C, and MIL-126, respectively. The thermal stability of all three MOFs developed was in the range of 350°C and above framework of MOF collapses. It was also observed that the thermal stability of the MIL-88 series increases with increase in length of the linker attributing to the rigidity offered by aromatic conjugated systems. Further, the adsorption and desorption isotherms reveal mesoporous nature of MIL-88 analogues with average pore diameter of 3.8 nm and 3.6 nm for MIL-88B, MIL-88C, and MIL-126, respectively. The physical properties such as porosity and magnetic properties are two inimical properties such as the porosity of MOF increases with increase in the length of the linker whereas the magnetic properties

decrease with the increase in the length of the linker. Based on structural requirements, it is difficult to design MOFs with porosity and magnetic properties. In our findings, we were able to design MOFs with both porosity and magnetic properties that could be altered based on the length of the linker.

Aim 3 focused on investigating the luminescence properties of Mn-NDC MOFs. Significant research related to optical properties of MOFs have been reported as discussed in **Chapter 3** and **4**. The luminescent optical behavior of MOFs depends on various factors such as choice of the metal, linker and interaction (covalent or non-covalent) between them. The choice of metal plays a significant role in offering structural tunability and control over optical properties due to its coordination environment. This study was targeted to understand the role of the coordination geometry of metal node (multiple oxidation state) that could contribute controlling and optimization of the optical properties of MOFs.

An isorecticular series of Mn- NDC MOF was chosen to investigate their optical and excited lifetime behavior. The structure of Mn-MOF was confirmed through a detailed analysis of the structural orientation and crystallinity via diffraction patterns from XRD. The details material composition and morphological studies reveal that these MOFs are 3D structures. The adsorption and desorption isotherm shows mesoporous nature with pore diameter of 2-30 nm. The absorption and emission spectrum confirm that the reported Mn-MOF show ligand centered emission with little or no influence of metal clusters. Further, the transient absorption lifetime measurement of 2,6 NDC in

solution displays a lifetime approximately 2.5 times greater than that of Mn-NDC MOFs attributing to quick quenching of the exciton.

6.2 Recommendations for Future Research

The research presented in this dissertation leaves many promising avenues open for future research. This section emphasizes some of the future directions in implementing these MOFs in electronic devices. Magnetic, electrical, and optical properties of MOFs have started to be exploited recently for potential applications in the electronic industry[1].

6.2.1 The Electrical Conductivity of INT-IRMOF-8A

The conductive IRMOF-8A may provide great prospects for their applications as conducting channels in construction of the field effect transistors (FETs). These MOFs can also be employed as a semiconducting channel in the construction of FETs via two possibilities: altering the band gap with chemical modification and by incorporation of guest molecule in the pores of the framework. The major challenge towards accomplishing this would be the thin-film preparation of conductive IRMOF-8A. There are various methods like spin coating and layer-by-layer self-assembly, but the air-liquid interfacial self-assembly process reported by Gang Xu and his coworkers would be recommended [2]. They have successfully demonstrated the semi conductive MOF membrane as an active channel in the construction of field effect transistors[2]. Thus, the future work based off of this study may easily target the fabrication of single microstructure-based miniature field effect transistors.

6.2.2 Magnetic Properties of MIL-88 Analogues (MIL-88B, MIL-88C and MIL-126)

In this work, isoreticular analogues of MIL-88 (MIL-88B, MIL-88C and MIL-126) displayed ferromagnetic behavior at 10 K. The ferromagnetic behavior of these MOFs may yield prospective applications in memory storage devices. In general, ferromagnets capable of room temperature functionality are preferred. The ferromagnetic behavior of the aforementioned MOFs could be altered by the incorporation of short linkers using the synthetic strategy similar to the one proposed in this work so that the distance between the two metal nodes is shorter facilitating effective cooperative magnetism.

Currently, the incorporation of ferromagnetism in semiconductors has great potential for the development of spintronic applications. Herein we reported the ferromagnetic behavior (M-H curves) of the analogues of MIL-88 of which MIL-88B showed highest coercivity and the MIL-126 with the lowest. Thus, these materials could be a potential candidate in the development of spintronic devices. However, further experiments are required to improve crystallinity and obtain MOFs with ferromagnetic behavior at room temperature. Advanced characterization tools to exclude the magnetic secondary phase such as superparamagnetism [3] are also necessary. Our work demonstrates successful incorporation of magnetism in 3D MIL-88 analogues and encourages research on conducting properties for potential applications in spintronic devices.

6.2.3 Optical Behavior of Mn-NDC

The luminescent properties obtained for Mn-MOFs have a great potential to be considered for light harvesting and photovoltaic applications. However, in depth understanding of excited lifetime is necessary to rationally design luminescent MOFs for specific applications.

6.3 References

- [1] G. Mínguez Espallargas and E. Coronado, “Magnetic functionalities in MOFs: from the framework to the pore,” *Chemical Society Reviews*, 10.1039/C7CS00653E vol. 47, no. 2, pp. 533-557, 2018.
- [2] G. Wu, J. Huang, Y. Zang, J. He, and G. Xu, “Porous Field-Effect Transistors Based on a Semiconductive Metal–Organic Framework,” *Journal of the American Chemical Society*, vol. 139, no. 4, pp. 1360-1363, 2017/02/01 2017.
- [3] C. Yang *et al.*, “A semiconducting layered metal-organic framework magnet,” *Nature Communications*, vol. 10, no. 1, p. 3260, 2019/07/22 2019.